The Physical and Chemical Evolution of Star Forming Regions

A Thesis submitted for the Degree

of

Doctor of Philosophy of the University of London

by

Deborah Patricia Ruffle

Department of Physics & Astronomy

University College London

University of London

September 1998

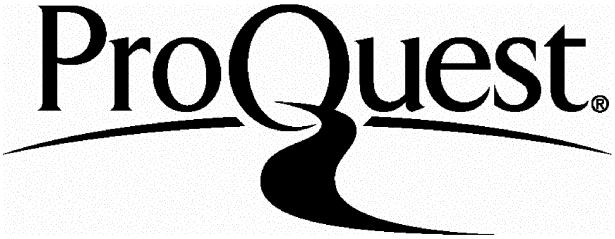

Abstract

A wide variety of molecular species are observed in regions of star formation. The chemistry is measured to change between different sources; analysis of these observed chemical changes provides a probe of the physical and chemical mechanisms occurring within different regions. Of particular importance is the gas–dust interaction, which affects the physical and chemical properties of interstellar gas.

In this thesis, theoretical models of the physics and chemistry in star forming regions are applied to existing observational data, in attempts to deduce the evolutionary history and physical conditions of such regions. In some cases, the models are used to suggest other species that could be observed to further explore the dominant mechanisms occurring in different regions.

An investigation into the initial support and collapse of diffuse clumps to form dense cores suggests that a clump may require a minimum column density for star formation to occur. For the first time the chemical evolution of a cloud that is initially magnetically supported against collapse perpendicular to the field lines, but is collapsing along the field lines, up to an unknown but critical density is explored. It is shown that observations may reveal the value of the critical density.

Study is made of the gas–dust interaction. Some molecular species which have been used as signposts of cloud evolution are demonstrated to be indicative of both early and late times; implications of this are discussed. The sulphur depletion problem is explored; a simple model is suggested where S^+ is accreted rapidly onto dust grains. In addition, the elemental depletions in star-forming cores are examined with reference to the use of species to search for signatures of infall.

Finally, it is established that low temperature homonuclear diatomic molecules, which are thought to be unobservable, should be detectable in cold interstellar clouds.

Contents

List of Tables

List of Figures

Chapter 1

Introduction

Over the last quarter of a century observations of interstellar molecular emissions have permitted the determination of the physical and chemical properties of star forming regions within the Galaxy, and a basic picture of how stars form has been developed. Giant Molecular Clouds, containing up to about 10^6 $M_\odot$ are sites of stellar birth and contain translucent clumps with masses ranging from of the order of 10 $M_\odot$ to 10^3 $M_\odot$ (Williams, Blitz & Stark 1995). The translucent clumps possess superthermal turbulence that probably consists of a superposition of Alfvén waves (Arons & Max 1975). The clumps are supported against gravitationally driven collapse by the turbulence and by the large-scale magnetic field. As described in section 2.4, the decay rate of the turbulence due to ion-neutral friction and the evolution of the large-scale magnetic field depend on the ionization structure, which is governed by the chemistry. The eventual collapse of a translucent clump leads to the formation of dense objects called dense cores. The thermal structure of material in translucent clumps and in the dense cores is determined by molecular processes. Thus, the evolution of translucent clumps and dense cores leading to star formation is controlled by, as well as traced through, chemical processes.

In this thesis we describe original work aimed at the exploitation of molecular diagnostics of star forming regions, to elucidate the roles of chemistry in controlling star formation. Particular emphasis is placed on the role of the gas–dust interaction in affecting the chemical and physical properties of interstellar gas. We begin below by presenting an overview of a scenario for star formation and the physical and

chemical mechanisms of importance in it.

1.1 Overview

Gas and dust are the main constituents of interstellar clouds. (Dust contains roughly 1% of the mass.) In Table 1.1 we provide a list of all the interstellar molecular species detected in the gas phase (van Dishoeck 1998; NRAO list 1998). These species have been observed in absorption lines against background stars and through their emission lines at millimetre wavelengths (van Dishoeck & Blake 1998; van Dishoeck 1998). The presence of interstellar dust grains is inferred from several observational results, including the reddening of starlight (see the review by Williams & Taylor 1996). From the observations of dust we can gain information on its properties, such as grain size and composition, which we discuss further in section 2.5.1.

The gas is greatly modified through interactions with the dust grains. The grain surfaces provide sites for the formation of molecules. Indeed, molecular hydrogen must be produced on grain surfaces in order for its observed high abundance to obtain (Williams & Taylor 1996). Gas phase species can accrete onto grain surfaces; these molecules are adsorbed to the surface, which leads to their depletion from the gas phase as they are now frozen-out onto the grain. We can measure the extent to which species are depleted from the gas phase, as described in section 2.2.

Species that have frozen-out onto a dust grain form an icy mantle around the grain core. We can observe molecules that are trapped in icy mantles and in Table 1.2 we give a list of these species (van Dishoeck & Blake 1998; Tielens & Whittet 1997). The molecules in ices are observed through the absorption of radiation from background stars. Once a species is frozen-out onto a grain's surface it can be ejected back into the gas phase via desorption processes. Several possible desorption mechanisms exist and these include chemical, radiative and high energy cosmic ray processes (Williams & Taylor 1996; see section 2.5.1).

A measure of the quantity of dust along a line of sight or in a cloud is the visual extinction, A_V, measured in magnitudes. The visual extinction equals 1.086 times the optical depth at the wavelength 5550 Å, due to both scattering and absorption by

Table 1.1: Table of observed interstellar and circumstellar molecules. We also denote the wavelength ranges of the detections if they are not made at millimetre wavelengths. From van Dishoeck (1998), NRAO list (1998).

Molecules with Two Atoms					
AlF	AlCl	$C_2^{\dagger}$(IR)	CH	CH^+(VIS)	$CN^{\dagger}$
$CO^{\dagger}$	$CO^{+\dagger}$	CP*	$CS^{\dagger}$	CSi*	HCl
H_2(IR)	KCl	NH(UV)	NO	NS	NaCl
$OH^{\dagger}$	PN	$SO^{\dagger}$	SO^+	SiN*	SiO
SiS	HF				
Molecules with Three Atoms					
$C_3^{\dagger}$(IR,UV)	C_2H	C_2O	C_2S	CH_2	$HCN^{\dagger}$
HCO	$HCO^{+\dagger}$	HCS^+	HOC^+	$H_2O^{\dagger}$	$H_2S^{\dagger}$
$HNC^{\dagger}$	HNO	MgCN	MgNC	N_2H^+	N_2O
NaCN	$OCS^{\dagger}$	$SO_2^{\dagger}$	c-SiC_2	$CO_2^{\dagger}$	$NH_2^{\dagger}$
H_3^+(IR)					
Molecules with Four Atoms					
c-C_3H	l-C_3H	C_3N	C_3O	C_3S	$C_2H_2^{\dagger}$(IR)
CH_2D^+?	HCCN*	HCNH+	$HNCO^{\dagger}$	HNCS	$HOCO^+$
H_2CO	H_2CN	$H_2CS^{\dagger}$	$H_3O^{+\dagger}$	$NH_3^{\dagger}$	
Molecules with Five Atoms					
C_5^*(IR)	C_4H	C_4Si	l-C_3H_2	c-C_3H_2	CH_2CN
$CH_4^{\dagger}$(IR)	HC_3N	HC_2NC	$HCOOH^{\dagger}$	H_2CHN	H_2C_2O
H_2NCN	HNC_3	SiH_4^*(IR)	H_2COH^+		
Molecules with Six Atoms					
C_5H	C_5O	$C_2H_4^*$(IR)	$CH_3CN^{\dagger}$	CH_3NC	$CH_3OH^{\dagger}$
CH_3SH	HC_3NH^+	HC_2CHO	$HCONH_2$	l-H_2C_4	
Molecules with Seven Atoms					
C_6H	CH_2CHCN	CH_3C_2H	HC_5N	$HCOCH_3$	NH_2CH_3
c-C_2H_4O					
Molecules with Eight Atoms					
CH_3C_3N	$HCOOCH_3^{\dagger}$	CH_3COOH?	C_7H	H_2C_6	
Molecules with Nine Atoms					
CH_3C_4H	CH_3CH_2CN	$(CH_3)_2O$	CH_3CH_2OH	HC_7N	C_8H
Molecules with Ten Atoms					
CH_3C_5N?	$(CH_3)_2CO$	NH_2CH_2COOH?			
Molecules with Eleven Atoms					
HC_9N					
Molecules with Thirteen Atoms					
$HC_{11}N$					

* represents species observed only in circumstellar environments.
† represents species also observed in comet Hale-Bopp.
? indicates that the identification is unconfirmed.
The prefixes 'l-' and 'c-' refers to the linear and cyclic forms of a species.

dust. The value of A_V of a cloud is important in determining the physical conditions within the cloud, as we describe below.

The major classes of interstellar clouds that this work deals with are 'translucent clumps' and 'dense cores'. We can measure how dense the different types of clouds are, and define their number densities of H nuclei, $n_{\rm H}$, as

$$n_{\rm H} = n({\rm H}) + 2n({\rm H_2}) \tag{1.1}$$

where n(H) and $n(H_2)$ are the number densities of hydrogen atoms and molecules respectively. Diffuse clouds have the lowest number densities, typically of the order of $n(H_2)$>10 cm^{-3}, and low visual extinctions ($A_V \sim 1$ mag). Translucent clumps have number densities of the order of $n(H_2) \sim 10^2$–10^3 cm^{-3} and visual extinctions in the range of 2 to 5 mag. Dense cores have number densities of $n(H_2) \sim 10^4$–10^6 cm^{-3} and much higher visual extinctions of A_V>5 mag.

Radiation from stars passes through the interstellar medium and can interact with the gas and dust. A mean interstellar radiation field intensity was determined by Draine (1978). Interstellar radiation can easily penetrate the diffuse clouds and translucent clumps, as these have low visual extinctions. However, dense cores have much greater visual extinctions, and due to the increased scattering and absorption by grains their interiors are shielded from the radiation. When radiation can penetrate a cloud it can ionize atoms and molecules, in addition to dissociating molecules. It is for this reason that only a limited set of molecules are observed in diffuse clouds and translucent clumps (such as CO, CN, CH, CH^+, H_2 and OH), as the presence of the radiation inhibits the formation of complex species. On the

Table 1.2: Table of observed species in interstellar ices. Those in the second row only have upper limits on their abundances. From van Dishoeck & Blake (1998) and Tielens & Whittet (1997).

H_2O	CO	CO_2	OCS	CH_4	CH_3OH	XCN*	
H_2CO	HCOOH	NH_3	HCN	SO_2	H_2S	C_2H_2	C_2H_6

* The X does not stand for Halogen; it is used to indicate that the exact carrier of the band near 4.62 μm is not known, although laboratory studies suggest an origin in a nitrile or isonitrile compound. Schutte & Greenberg (1997) have suggested assignment of the band to OCN^-.

other hand, in dense cores we observe many different complex species. In addition to the interstellar radiation field, cosmic rays (energetic protons) are another source of ionization which contribute to the ionization in diffuse clouds and are the major source in dense cores. In dense cores the cosmic rays can directly interact with species to ionize and dissociate, in addition to inducing photons which can then destroy species. The cosmic ray ionization of H_2 results in an energetic electron which then collides with and excites H_2. When the excited hydrogen molecule relaxes it produces ultraviolet photons (Prasad & Tarafdar 1983; Gredel et al. 1989). The direct cosmic ray ionization rate is lower than that of the interstellar radiation field, although its exact value is not clear as we discuss in section 2.4. The exact ionization level or 'structure' in a cloud is determined by the chemistry, as we also describe in section 2.4.

The temperatures of diffuse clouds, translucent clumps and dense cores also differ. Typically, the temperature in a diffuse cloud is approximately 100 K and in a translucent clump or a dense core it is around 10–30 K. The temperature that obtains is the result of a balance between the heating and cooling mechanisms that operate in a cloud. UV radiation and cosmic rays can heat a cloud by the ionization of species. The ionizing source imparts energy to the gas as the ejected electron carries away excess energy. Photons, including those produced as a consequence of cosmic-ray induced ionization, provide an additional heating source.

The gas is cooled when radiation is emitted by the atoms and molecules that comprise the gas. Recombination of an atomic or molecular ion with an electron results in the emission of a photon, which can then escape from the gas; energy is lost from the system and the gas is cooled. The collisional excitement of an atom or a molecule also results in the emission of a photon, as the excited species decays back to the ground state. Both of these cooling mechanisms depend on the number density to the power of two, which results in dense regions tending to be cooler than more diffuse environments. An additional loss mechanism is provided by the grains, which are heated when they absorb radiation. The grains then radiate this energy in the infrared, which can then escape from the cloud. The dominant coolant in both translucent clumps and dense cores is CO. It can be excited at gas temperatures of

only a few Kelvins. However, its effectiveness is reduced as its abundance rises in denser clouds since the radiation emitted by one CO molecule can be absorbed by another. This is a process called radiation trapping.

An important point to note is that in dense cores the cosmic rays cannot maintain the temperatures that are measured, when the cooling mechanisms are accounted for. Another heating process is needed. A potential source is some form of dynamical heating where movements within the gas produce frictional heating.

Once we have determined the temperature and number density of a cloud we can consider its thermal pressure. Diffuse clouds and translucent clumps have low thermal pressures unlike dense cores which have thermal pressures around a hundred times greater. The material between clumps and dense cores is referred to as the interclump medium. The properties of the interclump medium are poorly understood but its total pressure must be comparable to that of a translucent clump. (Contributions to the total pressure include the thermal, turbulent and magnetic pressures.) Pressure equilibrium between a translucent clump and the interclump medium should be established on roughly the timescale for a fast-mode magnetic wave to cross the clump; for an assumed fast-mode speed of 3 km s^{-1}, this is 10^6 years for a clump that is 3 pc across.

We now discuss how the gas is supported against collapse. We regard translucent clumps and dense cores as representing two different stages of star formation: the translucent clumps collapse to form dense cores. Dense cores are identified as the direct progenitors of stars. Investigation into the star formation process is conventionally divided into considerations of low-mass and high-mass star formation separately. Stars of low-mass (with masses less than 4 $M_\odot$) are thought to form as a result of a gradual weakening of the magnetic fields. However, higher mass stars are believed to form because the ratio of the magnetic flux to the clumps mass is too small for the magnetic field to prevent collapse when the pressure external to the clump is increased above a critical value (e.g. Mouschovias 1987). High-mass star formation can therefore be triggered by increases in the pressure of the interclump medium. Potential catalysts include winds and the supernovae of other high-mass stars (e.g. Elmegreen & Lada 1977; Mouschovias 1987). In this work we are con-

cerned with the formation of low-mass stars. Hence, all further descriptions, unless stated otherwise, refer to low-mass star formation only.

The gas in translucent clumps is confined by the pressure exerted by the warm, tenuous interclump medium as these objects are not gravitationally bound. They are believed to be supported against collapse by magnetic fields and magnetohydrodynamic (MHD) waves which comprise the turbulence (e.g. Mouschovias 1987; Shu, Adams & Lizano 1987). We describe the evidence for turbulence in section 1.2. The MHD waves can be dissipated, and the damping rate depends inversely on the ion number density. The ionization structure of a cloud is determined by the chemistry (see section 2.4). Hence, as the fractional ionization drops, the rate of wave damping increases and the clump will begin to collapse along the magnetic field lines. (In Chapter 3 we investigate the nature of decreases in the fractional ionization.) The collapse of a translucent clump by this process leads to the formation of a dense core.

By contrast, dense cores are supported by thermal pressure and magnetic pressure. Waves are not important for their support (see Chapter 3). Their further collapse is governed by ambipolar diffusion, the drift of the neutral component of the gas relative to the charged component. The charged component of the gas consists of ions and electrons, and the grains which carry one negative charge (Draine & Sutin 1987). The magnetic field acts on the charged components and tends to push particles out of the cloud. The magnetic force does not act directly on the neutral component. Gravity acts to pull the neutral component inward. The relative motions produce friction between the neutral and charged components which acts to reduce their relative velocities. The friction therefore leads to the 'magnetic retardation' of collapse (and may provide the additional heating source that is required in order for dense cores to have their observed temperatures, as mentioned above, and as described by Scalo 1987). The time for which the collapse of a cloud remains magnetically retarded is the time required for the neutrals to drift through the charged particles due to gravity. This is the ambipolar diffusion timescale. In Table 1.3 we give approximate expressions for this and some of the other important timescales in star forming regions.

Table 1.3: Some important timescales. From Hartquist & Williams 1998.

Timescale	Process	Years
Collapse	Gravity	$10^8/n_{\rm H}{}^{1/2}$
Cooling	Radiation	3×10^5 (for 10 K)
Freeze-out	Gas grain collisions	$3\times10^9/n_{\rm H}S$
Ion-molecule chemistry	Cosmic Ray ionization	3×10^5
Ambipolar Diffusion	Ion-neutral drift	$4\times10^5 x(i)/10^{-8}$
Desorption	Chemically driven*	$3\times10^5[x({\rm CO})/10^{-4}][1{\rm cm}^{-3}/n({\rm H})]$

$n_{\rm H}=n({\rm H})+2n({\rm H_2})$; $x({\rm CO})=n({\rm CO})/n_{\rm H}$; $x(i)=n({\rm ions})/n_{\rm H}$

* by H_2 formation; S is the sticking probability.

The collapse of clumps probably occurs via free fall, and we can compare the free fall collapse timescale to some of the other timescales given in Table 1.3. With $n_{\rm H}$ of 10^4 cm^{-3} we obtain a free fall timescale of $\sim10^6$ yrs. Compare this to the ion-molecule chemistry timescale, which is the timescale on which the nature of the chemistry can be entirely changed (the time to ionize an amount of H_2 that equals the C and O gas phase abundance). This is about 3×10^5 yrs and is independent of $n_{\rm H}$. Consequently, it is possible that dynamical changes can occur rapidly enough so that some signatures of the past physical conditions remains in the observable chemistry. The freeze-out timescale (cf. section 2.5.1) for 10^4 cm^{-3} is 3×10^5 yrs for standard assumptions, but may be larger, and this is less than the free fall timescale. So molecules may be lost from the gas quickly compared to the collapse timescale, unless desorption is also occuring.

The remainder of the chapter provides a more detailed introduction to the problems that are the concern of the following work. In section 1.2 we provide a more complete introduction to the structures of Giant Molecular Cloud complexes, which contain many of the Galaxy's star forming regions. Each giant molecular cloud is gravitationally self-bound and is likely to have been formed from the collision and subsequent merging of clouds that were initially diffuse. Each contains structures on several scales. Most of the mass is contained in translucent clumps. We will consider the initial support and collapse of one of these clumps leading to the formation of dense cores, which can be identified as the progenitors of stars. These dense cores are *sometimes* seen to exist together in what is known as a 'core cluster'. This is a

collection of several cores, which are close enough to one another that the birth of even a low-mass star in one of the cores may then regulate the further evolution of the other cores within the cluster. In section 1.3 we discuss the possible scenarios for the development of core clusters, in which low-mass stars form. Another core cluster, TMC-1, which is one of the closest and most thoroughly observed, is the topic of section 1.4. TMC-1 consists of several dense cores which lie in a ridge in the vicinity of a recently formed low-mass star. A chemical gradient is observed along the ridge and is used to infer information on the dynamical properties of the source. In section 1.5 we examine the observational studies of dense core collapse which leads to the formation of stars. Finally in section 1.6 we treat the theoretical studies of the collapse of dense cores. Section 1.7 is a summary, and also sets out the content of the thesis.

1.2 Clumpy Giant Molecular Cloud complexes

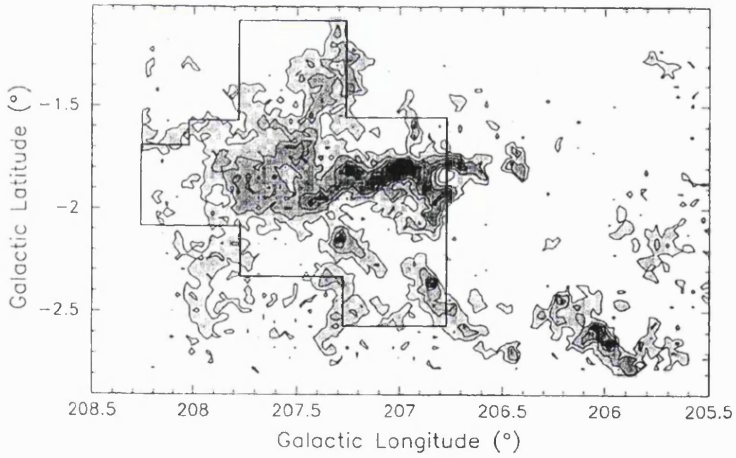

Figure 1.1: Map of the Rosette Molecular Cloud in ^{12}CO(J=1-0) emission. 1° ≈ 28 pc. From Williams, Blitz & Stark (1995).

In the Milky Way the majority of the molecular matter exists in Giant Molecular Cloud (GMC) complexes. These have masses which are typically in the range of 10^4 to 10^6 $M_\odot$ and have linear extents of about 30 to 100 pc. One such GMC is the Rosette Molecular Cloud (RMC), which is at a distance of 1600 pc. Figure 1.1 shows

the integrated ^{12}CO (J=1–0) emission line map of the RMC. The ^{12}CO (J=1–0) and ^{13}CO (J=1–0) emission maps of the RMC have been analyzed in detail by Williams, Blitz & Stark (1995). Their work has provided information on the structure of this particular GMC complex. The projected cross section of the RMC is about 2200 pc^2, it has a mass of about 1–2$\times10^5$ M$_\odot$, a mean H_2 column density of 4×10^{21} cm^{-2} and a mean H_2 number density of 30 cm^{-3}. Much of the molecular material in the RMC exists in approximately 70 clumps which have masses between about 30 and 2500 M$_\odot$; the number of clumps with masses between M and M+dM scales as $M^{-1.27}$ dM. Less massive clumps may also exist within the complex, but only a few were detected at the limit of the sensitivity of the observations.

The clumps which have been identified occupy only approximately eight percent of the volume of the RMC. In most clumps $n(H_2)\approx200$ cm^{-3}; a variation of about a factor of 4 in this value is found, but the measured variation may be more limited than the real variation in density because CO is a poor tracer of denser gas. This is due to the small dipole moment of CO resulting in the CO rotational level population distribution becoming thermalized at values of $n(H_2)$ of several hundred cm^{-3}. The peak ^{13}CO column density through a clump scales roughly as $M^{0.63}$ and is about 10^{16} cm^{-2} for M=10^3 M$_\odot$; the H_2 column density is assumed to be a factor of 5×10^5 larger. There are seven embedded stars which exist in the three most massive and the fifth, seventh, eleventh, and eighteenth most massive clumps. The clumps that contain stars are all amongst the 16 clumps having the highest ^{13}CO column densities of about 10^{16} cm^{-2} and more.

For a feature formed in an individual clump the line of sight full width at half maximum lies in the range of about 0.9 to 3.3 km s^{-1}. For comparison, the value for ^{13}CO that is thermally broadened only and is at 30 K (which is roughly the maximum temperature obtaining in the clumps) is only 0.22 km s^{-1}. It has been inferred that about half of the clumps are not bound by their own gravitational fields, from the comparison of the velocity dispersion with the escape velocity estimated from the mass and radius of each clump. This is a result that appears to also apply to clumps in other GMCs (Bertoldi & McKee 1992). A clump that is not bound by its own gravity must be bound by the pressure of an interclump medium, which

may consist primarily of gas at about 10^4 K.

The clumps have magnetic fields which are important for their support (e.g. Mouschovias 1987). Turbulent pressure, which is associated with the broad lines that are observed, is important for clump support and acts along the magnetic field lines. The form of the turbulence is a superposition of Alfvén waves (Arons & Max 1975; Mouschovias & Psaltis 1995).

In Chapter 3 we examine the collapse of a clump to form a dense core. We argue that collapse may begin if a critical column density is exceeded, and that this is directly related to the extent of turbulent support in a clump.

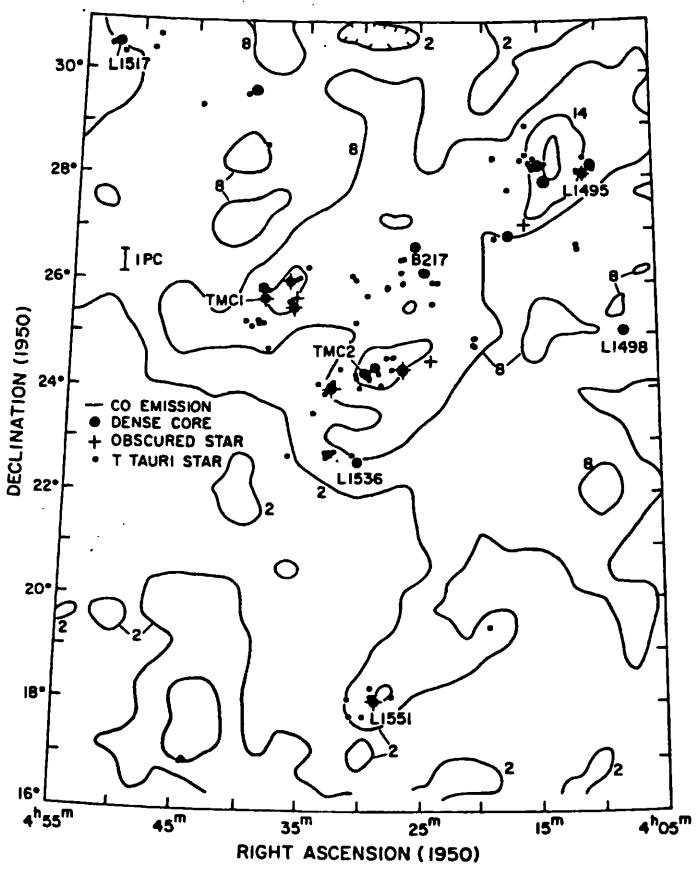

Figure 1.2: The distribution of dark cores and low-mass stars in the Taurus – Auriga complex. From Myers (1986).

1.3 Low-mass star formation in a cluster of dense cores

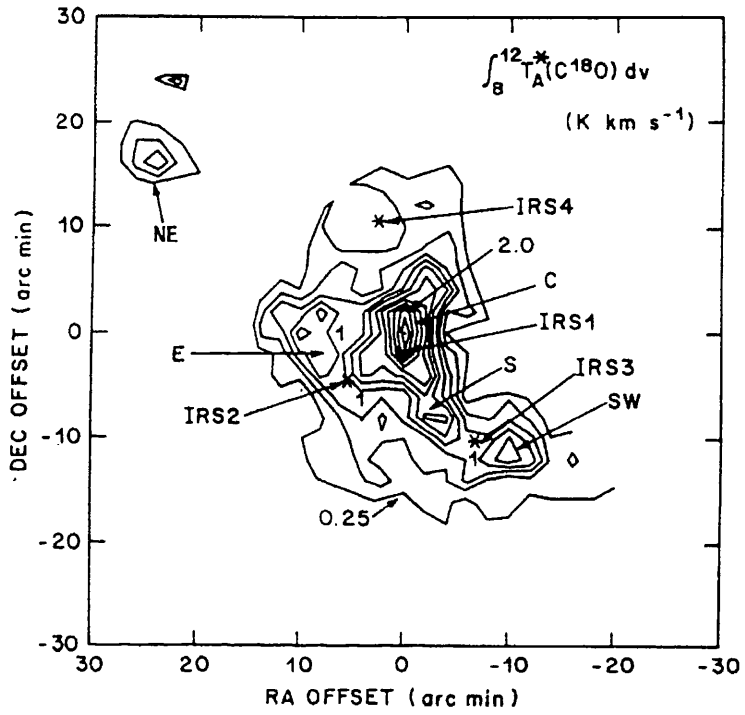

Figure 1.3: $C^{18}O$ contour map of B5. The positions of four infrared sources (IRS1–4) associated with young stars are shown. From Goldsmith, Langer & Wilson (1986).

When a clump like one of those observed in the RMC collapses, it fragments and objects known as dense cores form (e.g. Myers 1990). Ammonia emission has been used to map many of the dense cores (e.g. Benson & Myers 1989). Dense cores typically have masses of one to several tens of solar masses each, number densities $n(H_2) \approx 10^4 - 10^5$ cm^{-3} and temperatures of $\approx$10–30 K. However, some dense cores are observed to have number densities of up to roughly 10^7 cm^{-3} and masses of more than one hundred solar masses, particularly in regions where massive stars form. In Fig. 1.2 the dense core distribution in the Taurus – Auriga complex is shown. Approximately half of all dense cores are associated with young low-mass stars. Dense cores are considered to be the direct progenitors of protostars.

Figure 1.2 shows that many (but not all) of the dense cores are near other dense cores. Barnard 5 (B5) contains a cluster of five dense cores and four young low-

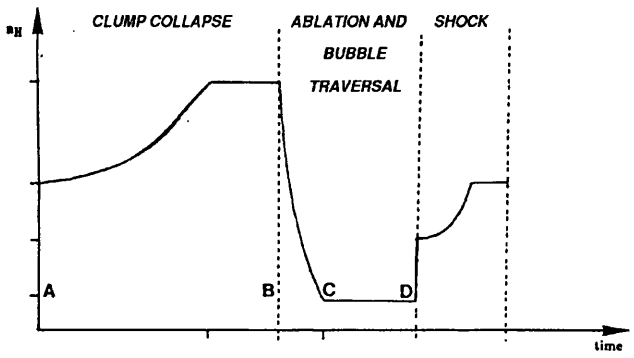

Figure 1.4: The evolution of $n_{\rm H}$ for a parcel of gas in a cyclic model. At point A collapse of the interclump medium begins; the collapse continues until a more slowly evolving core is formed. At point B the parcel is ablated from the dense core by a stellar wind. H^+ and He^+ are assumed to mix from the wind into the ablated gas as it is accelerated. At point C the ablated gas is fully incorporated into the wind. The ablated gas–stellar wind mixture expands freely until at point D it passes through a termination shock inside the interface of the mixture and the ambient intercore medium. The density of the decelerated mixture increases as it cools; after cooling is complete the mixture becomes part of the cool phase of the ambient intercore medium. The parcel of gas may then pass through a qualitatively similar cycle again. Adapted from Charnley et al. (1988). Note the time axis is not to scale.

mass stars. Figure 1.3 shows a $C^{18}O$ emission line map of B5. The gravitationally induced collapse of a core is an important step in the formation of a star, but once young stars have formed in a region their winds may affect the collapse of the neighbouring cores. In Fig. 1.4 we present an illustration of a model of cyclic clump evolution, which is a modified version of one developed by Norman & Silk (1980). In this scenario, a core is ablated by the supersonic wind of a nearby young low-mass star, to create a stellar wind-ablated material mixture. This mixture then moves supersonically until it collides with the similarly mass-loaded winds of the other nearby stars, where it is decelerated and passes through a shock. The shocked gas is then radiatively cooled leading to the formation of irregular shells separating the winds of different stars. As a result, an intercore medium of regions of supersonic wind-ablated material mixtures and shells of decelerated mixtures is produced. The formation of subsequent generations of cores could occur if the shells fragment. Alternatively, core ablation may be so inefficient that nearly all cores simply collapse

to form stars, before they can be significantly eroded. The material that was in a core but does not go into a star may then be blown to a large enough distance from the cluster of cores, by the stellar winds, such that it cannot be considered to be associated with the cluster.

1.4 TMC-1

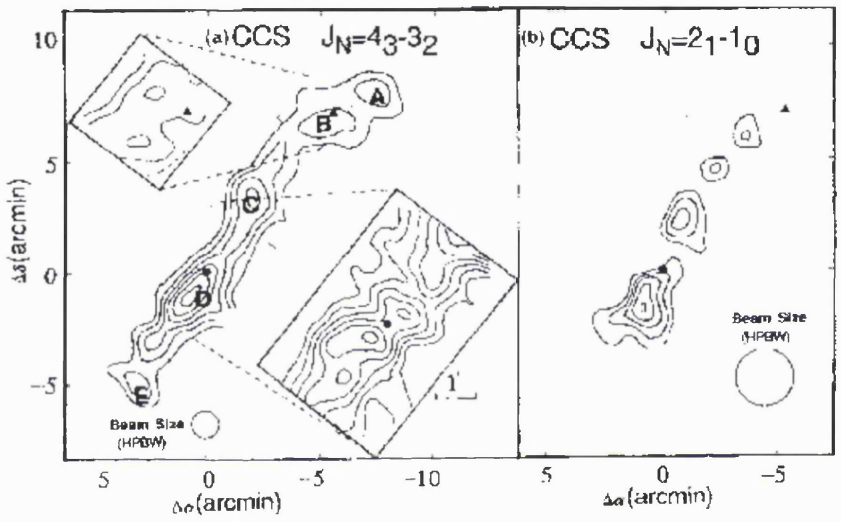

Figure 1.5: Contour map of the CCS emission from TMC-1. The filled triangle and circle represent the positions of the ammonia and cyanopolyyne peaks respectively. From Hirahara et al. (1992).

TMC-1 (Taurus Molecular Cloud-1) is one of the most thoroughly observed dense core sources. It is located within the Taurus – Auriga complex (see Fig. 1.2), at a distance of 140 pc. Figure 1.5, a map of CCS emission, shows that TMC-1 is a ridge which contains 5 dense cores that are aligned on the plane of the sky, which are labelled A to E (Hirahara et al. 1992). There is a sixth core that lies to the side of the Northern most core, core X which contains a star (its position is given in Fig. 1.6). TMC-1 has an estimated mass of approximately 10 $M_\odot$ and an average temperature of about 10 K, in addition to being the site where some of the largest detected molecules (HC_9N, $HC_{11}N$) have been found.

Figures 1.6 and 1.7 show maps of the NH_3 (J,K)=(1,1) inversion emission and

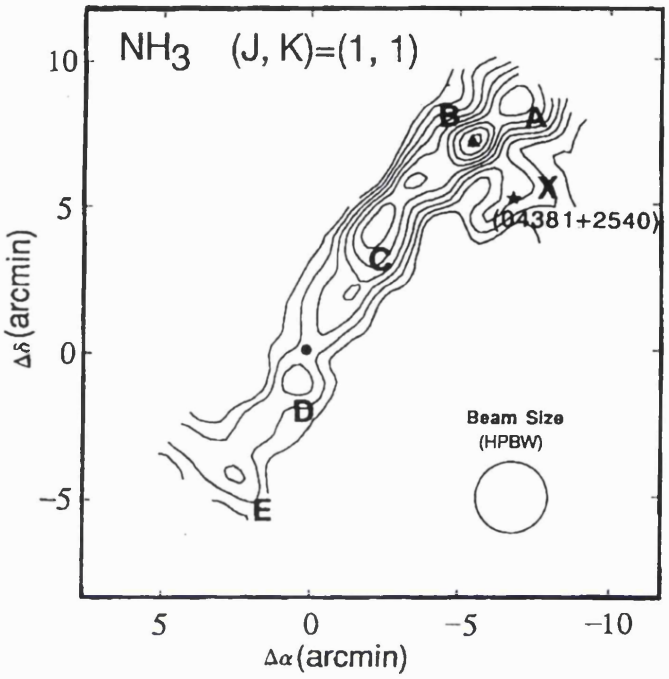

Figure 1.6: Contour map of the NH_3 emission from TMC-1. The location of a star is indicated. From Hirahara et al. (1992).

HC_3N J=5–4 emission (Hirahara et al. 1992). One can see that core B is the site of the peak in the NH_3 emission, whilst the cyanopolyyne emission peaks at core D. Hirahara et al. (1992) have estimated the densities of the various cores from single-dish observations of $C^{34}S$ (J=1–0 and 2–1) and C_2S (J_N=4_3–3_2 and 2_1–1_0) emissions and found $n(H_2)\approx 4\times10^4$ cm^{-3}, 2.4×10^5 cm^{-3}, and 4×10^5 cm^{-3} in cores D, C and B respectively. From interferometric studies of core D using C_2S emission, Langer et al. (1995) found core D to be fragmented, with $n(H_2)$ ranging from roughly 3 to 8×10^4 cm^{-3} in the largest fragments, to 10^6 cm^{-3} in the smallest.

An understanding of the chemical variations along TMC-1 would lead to insight into how TMC-1 has reached its present physical state and, more generally, into dense core formation and evolution during the process of stellar birth. There are several different ways in which the variations of the HC_3N fractional abundance along TMC-1 might have arisen. In Chapter 4 we examine in detail the many different explanations for the observed chemical gradient along TMC-1 and the assumption that some observed molecules are indicative of a specific epoch of cloud evolution.

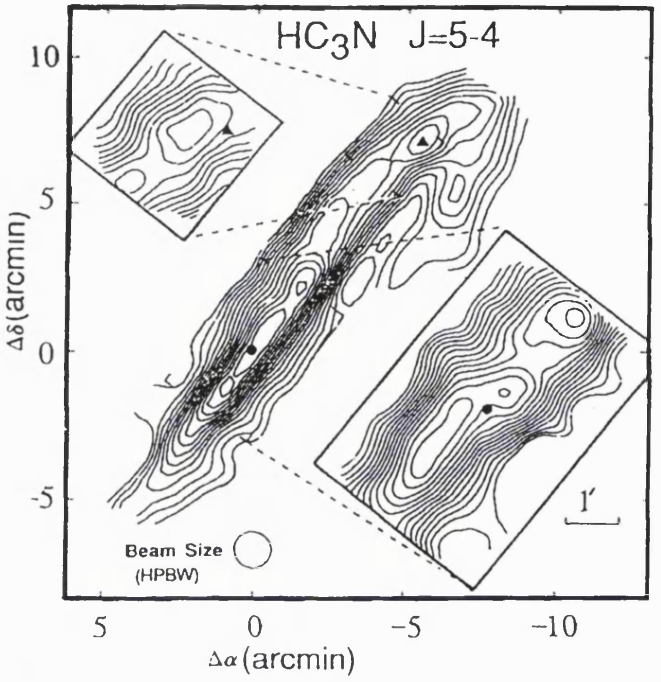

Figure 1.7: Contour map of HC_3N emission from TMC-1. From Hirahara et al. (1992).

Then in Chapter 5 we explore whether it may be possible to observe molecular nitrogen and oxygen in such regions, and thereby provide a direct measure of the nitrogen and oxygen budgets in star forming regions and a limit on the theoretical chemical models.

1.5 Collapse of dense cores in regions of low-mass star formation

As described previously, dense cores are thought to be the immediate progenitors of protostars, which has fueled efforts to detect signatures in molecular emission line profiles of the collapse of such cores. In the search for evidence of collapse, comparisons are normally made between line profiles from both optically thick and thin lines. The optically thin lines probe higher density and temperature regions and as a result are broadened (transitions between higher rotational levels are needed). The optically thin lines are symmetric and have a single peak. Therefore, such lines do not necessarily indicate that infall is occurring. The optically thick lines are

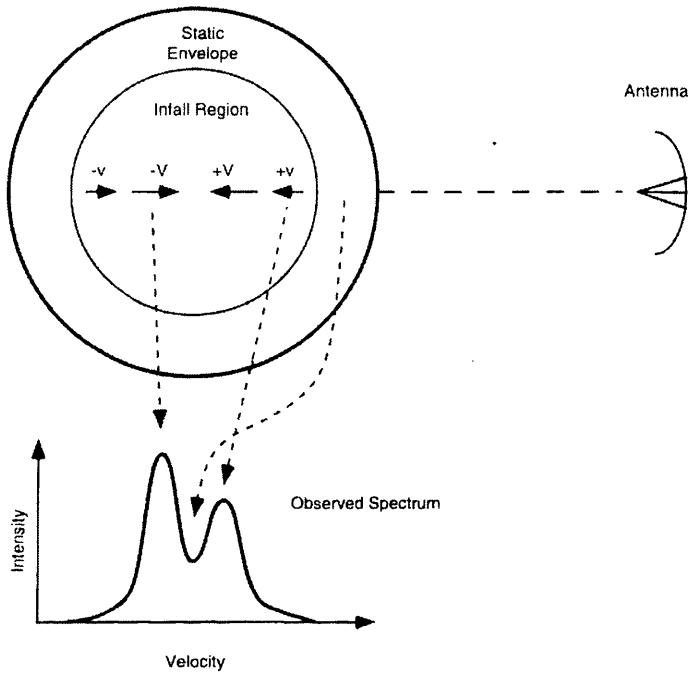

Figure 1.8: Collapse signatures: the formation of asymmetric, double-peaked, self-absorption line profiles in optically thick lines. From Rawlings (1996).

used to search for the infall signatures. The signatures that observers search for are asymmetric, narrow and double-peaked line profiles. Figure 1.8 depicts how the characteristic infall signature is produced (Rawlings 1996). As the line is optically thick we preferentially 'see' emission from the parts of the blue-shifted and red-shifted hemispheres that are closest to us. In the red-shifted case, this emission will be from the outer part of the infall region, which is cooler and has a low infall velocity. However, the blue-shifted part of the emission comes from a more central region of the infall, which will be moving faster than the outer regions, and will also be denser and hotter; consequently this emission is brighter than that produced in the red-shifted hemisphere. The surrounding envelope of material, which is static, absorbs some of the emission and hence a self-absorption dip at the center of the profile is produced.

The requirements to produce such asymmetric line profiles are that i) the line is optically thick in both hemispheres of emission; ii) a velocity gradient is present in the part of the core where lines are formed (the rate of infall increases towards

the core centre); iii) the observed species is also present in the static outer envelope; and iv) a positive temperature gradient towards the cloud centre exists.

Observational detections of this sort of blue-red asymmetric self-absorption were made for a number of clouds in CO emission line profiles by Snell & Loren (1976), but these results were challenged by Leung & Brown (1977) who argued that the infall explanation for the origin of the asymmetric features was not unique. (Turbulence, rotation and outflows also produce double-peaked profiles. However, as described by Zhou (1997), these motions should produce equal amounts of blue-shifted and red-shifted emission.) Walker et al. (1986) reported the detection of infall in IRAS 16293-2422 using a CS emission line study. However, Menten et al. (1987) showed that the observed line profiles could be explained using a model in which the emission from a rapidly rotating core undergoes foreground absorption.

In an attempt to establish more thoroughly what the characteristics of spectral line profiles formed in collapse models are, Zhou (1992) performed radiative transfer calculations based on simplifying approximations. One particular collapse model that Zhou (1992) used is one studied analytically by Shu (1977). Shu (1977) showed that an initially static, singular isothermal sphere (with $n \sim r^{-2}$) will undergo self-similar collapse with the collapse wave propagating out from the centre where the collapse velocity and the density are infinite. Collapse in which the infall speed decreases with radius and the outer radius of the collapsing region, $r_{\rm out}$, increases with time has come to be known as "inside-out" collapse. Computations like those of Zhou (1992) and the more accurate Monte-Carlo calculations of Choi et al. (1995) give results that imply that for cores undergoing inside-out collapse and in which the temperature decreases with radius:

1. optically thick lines show the blue-red self-absorption asymmetry,

2. for fixed angular resolution and equal optical depths the width of a line of a transition for which the critical density is large is greater than the width of a line of a transition for which the critical density is small,

3. the self-absorption and linewidth of a line appear to increase with increasing angular resolution of the central parts of a core.

Table 1.4: Table of infall candidates.

Collapse Candidates	Authors
B335	Zhou et al. (1993); Choi et al. (1995)
CB3, CB54, CB244	Wang et al. (1995)
HH 25MMS, IRAS 20050	Gregersen et al. (1997)
IRAS 16293-2422	Walker et al. (1986); Zhou (1995); Mardones et al. (1997)
IRAS 03256+3055	Mardones et al. (1997)
IRAS 13036-7644	Lehtinen (1997); Mardones et al. (1997)
L483	Myers et al. (1995)
L1157	Gueth et al. (1997); Mardones et al. (1997)
L1251	Myers et al. (1996); Mardones et al. (1997)
L1527	Myers et al. (1995); Zhou et al. (1996)
L1544	Myers et al. (1996)
NGC 1333 IRAS 2	Ward-Thompson et al. (1996)
NGC 1333 IRAS 4A/4B	Gregersen et al. (1997); Mardones et al. (1997)
S68N	Hurt et al. (1996); Mardones et al. (1997)
Serpens SMM4	Hurt et al. (1996); Gregersen et al. (1997); Mardones et al. (1997)
Serpens SMM5	Mardones et al. (1997)
VLA 1623	Mardones et al. (1997)
WL22	Mardones et al. (1997)

With these three points in mind, Zhou et al. (1993) demonstrated that H_2CO and CS emission profiles (both are optically thick) originating in B335 show the characteristic shapes associated with infall. B335 is a low-mass star forming core with an embedded 3 $L_\odot$ infrared source and a collimated outflow. High resolution (3″ to 5″) aperture synthesis maps of ^{13}CO and $C^{18}O$ emissions also support the hypothesis that B335 is still undergoing collapse (Chandler & Sargent 1993).

In order to confirm these initial encouraging results there is a need to:

a) observe more molecules and transitions

b) consider the effects of the outflow on the profiles

c) detect outflows in more sources.

Many attempts to address points (a) and (c) have recently been made by Zhou

et al. (1994), Mardones et al. (1994), Myers et al. (1995), Velusamy et al. (1995), Wang et al. (1995), Zhou et al. (1996), Myers et al. (1996), Gregersen et al. (1997) and Mardones et al. (1997). Many new infall candidates have been discovered and are listed in Table 1.4. The characteristic infall signatures have been observed in a variety of molecular lines: $C^{18}O$ (2–1), C_3H_2 ($2_{1,2}$–$1_{0,1}$), C_2S (2_1–1_0), HCO^+, ^{13}CO and HCN, besides H_2CO and CS. However, point (b) is a difficult one to address because it further complicates already sophisticated models. Myers et al. (1996) have developed a simple analytic model of radiative transfer in which the contribution of outflowing gas to spectral line profiles from contracting clouds is also considered. This model provides a simple way to quantify characteristic infall speeds, and its use to interpret data strongly suggests that the inward motions derived from the line profiles are gravitational in origin.

One way to avoid complications due to the presence of stellar outflows is to observe starless cores which, presumably, do not have outflows. Some of these objects may be collapsing, yet are starless due to insufficient development time. To date, only one starless core L1544 has shown evidence of infall asymmetry profiles which strongly suggest infall motions (Myers et al. 1996; Tafalla et al. 1998). The measured linewidths in L1544 are extremely small ($\sim$0.3 km s^{-1}) and imply that thermal pressure is playing an important role in the dynamics. In addition, it is one of the most opaque cores in the Taurus Molecular Cloud, suggesting the presence of high column densities. Myers and collaborators have therefore defined L1544 as the *most evolved starless core*. L1498 is another interesting starless core which shows an intriguing double-peaked CS feature with the blue peak stronger than the red peak (Lemme et al. 1995). However, L1498 has a complicated physical and chemical structure which hinders an easy interpretation of observational data (see Kuiper, Langer & Velusamy 1996). Figure 1.9 shows the shape of an NH_3 emission line feature arising in the dense core L1498 (Myers & Benson 1983). As the source was observed in two separate lines a temperature could be derived. The NH_3 emission profile shows very little deviation from that expected from a static core with very subsonic turbulence. There are no broad wings like those that might be expected to arise, during some stages of the gravitationally induced collapse of a core in which

magnetic effects are negligible, in the fastest (supersonically) infalling material.

High sensitivity and high spectral resolution interferometric observations are providing a new window to the innermost parts of low-mass star forming cores, and are helping to establish infall from outflow motions (e.g. Ohashi et al. 1997). Interferometers are also needed to identify which part of the cloud is traced by the chosen molecular species. For example, C_2S in B335 is tracing the outer parts of the collapsing envelope of the core (Velusamy et al. 1995), whereas H_2CO and CS emission is coming from deeper regions. A similar result has been found from high resolution observations toward L1498 (Kuiper et al. 1996). This starless core shows a chemically differentiated onion-shell structure, with the NH_3 in the inner and the C_2S in the outer part of the core; the CS and C_3H_2 emission seems to lie between these. The chemical and physical properties of L1498 have been interpreted by Kuiper et al. in terms of a "slowly contracting" dense core in which the outer envelope is still growing.

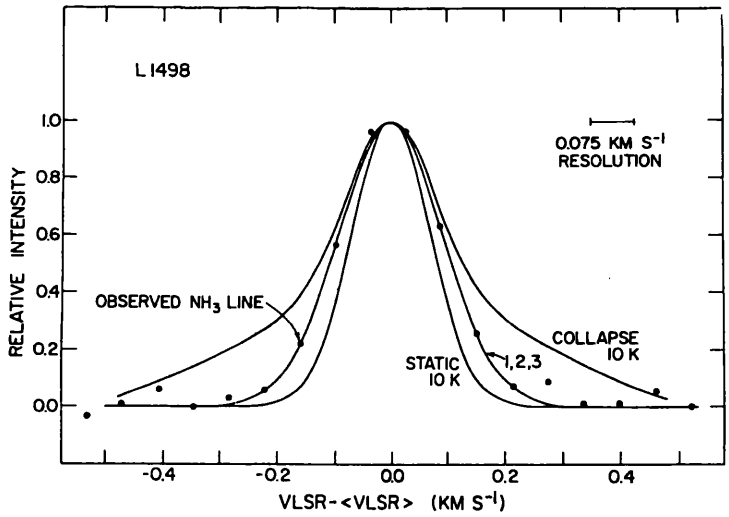

Figure 1.9: The NH_3 line profile of L1498. The curve associated with the dots is the observed profile. That marked static is the one expected from 10K gas that is not turbulent and experiences no systemic motion. The curve marked collapse is the profile expected if the fractional abundance of NH_3 is constant and the core is undergoing collapse governed by a particular solution of the class that Shu (1977) investigated. From Myers & Benson (1983).

Some questions arise from the above summary of observational evidence of dark cloud core collapse:

1. How deeply in the core are infalling motions traced by H_2CO and CS observations? These are the species used most for this kind of study.

2. How strongly do stellar outflows affect the abundance and the excitation of the above molecular species?

3. Why does NH_3 not reveal infall signatures?

4. Why do CS and C_2S seem to trace "envelope" material, even though they are both high density tracers? They should trace densities higher than NH_3 but their emission seems to be external to ammonia emission.

5. What is happening to molecular material in a region immediately surrounding the accreting young star, and can depletion onto grains occur in spite of the proximity of a central source?

More high sensitivity and high resolution observations are required to answer these questions, to better understand the physics of gravitational collapse in cloud cores, and the chemical processes in star forming regions.

1.6 Theoretical studies of the chemistry of dense core collapse in regions of low-mass star formation

Analysis of dense cores have revealed variations in their chemical composition and these have effects on the profiles of lines observed to study core collapse. In order to obtain the maximum information from the profiles about the dynamics of core collapse, the observed variations in chemical composition must be understood theoretically so that their effects on the profiles can be reliably deconvolved from those of the dynamics.

As mentioned in the previous section, a key problem associated with dense core observations is the absence of infall signatures in NH_3 line profiles. Menten et al. (1984) suggested that depletion in the infalling gas may be so high that NH_3

is not observable in it. This suggestion was taken by Rawlings et al. (1992) to be the starting point for a theoretical examination of chemistry in dense core collapse. Hartquist & Williams (1989) argued that for some ranges of depletion, some species should have gas phase fractional abundances that increase as depletion occurs (see Chapter 4). Following these findings of Hartquist & Williams (1989), Rawlings et al. (1992) attempted to identify gas phase species that have non-diminishing or at most slowly diminishing fractional abundances during some stages of depletion. The proposal by Rawlings et al. (1992) was that the lines of such species would be the most suitable ones to observe when attempting to discover unambiguous spectral signatures of ongoing collapse, such efforts having been unsuccessful up to that time.

The model of collapse adopted was that of the inside-out collapse of a singular isothermal sphere due to Shu (1977), as described in 1.5. Rawlings et al. (1992) calculated time-varying profiles for optically thin lines of a number of species. The line profiles were calculated for angular resolutions obtainable with existing single dish telescopes and for an object at the distance of L1498. Species found to have noticeably broader line profiles than NH_3 included HCO, HNO, N_2H^+, HCO^+, HS, CH and H_2S. For a number of these species the primary cause for their greater widths was that as depletion occurs the reduction of the high gas phase H_2O fractional abundance (which was an artifact of the initial conditions used in the model) decreases the rate of the primary removal mechanism of the species itself or a species that is a progenitor of it. It was concluded that the suggestion of Menten et al. (1984) is plausible, and that the proposal may be further tested by study of the line profiles of the additional species listed above.

Unfortunately, Rawlings et al. (1992) did not follow the behaviour of CS. The behaviour of the sulphur depletion is a key unanswered question in star formation. Sulphur is observed to be practically undepleted in diffuse clouds, yet it is heavily depleted in dense cores even when carbon, nitrogen and oxygen are not (Taylor et al. 1996). It is not known whether the depletion of S increases where C and O depletions are more substantial, but it is apparent that S depletes in a very different way to C, N and O. In Chapter 6 we investigate the sulphur depletion problem in

detail and propose a potential mechanism to explain the unusual behaviour of S.

Various models of the ways in which magnetic fields and ambipolar diffusion affect dense core collapse exist (e.g. Ciolek & Mouschovias 1995). It is sometimes valuable to adopt a simple description of the dynamics or even assume a fixed density to explore the effects of depletions in models with varying initial conditions, rather than performing complex calculations for detailed dynamical models. Nejad, Hartquist & Williams (1994) studied the chemical evolution in a single parcel of gas undergoing cycling in one cyclic model. Species found to have fractional abundances increasing with time or at least remaining fairly level with time included CH, OH, C_2H, H_2CO, HCN, HNC and CN, for model times when some important TMC-1 fractional abundances were reasonably well matched by the model fractional abundances. These species might be good candidates to observe in studies of infall, as H_2CO has, in fact, proven to be (Zhou et al. 1993). We investigate the dependences of the fractional abundances of a number of species on the selective depletions of elemental carbon, nitrogen, oxygen and sulphur, as well as metals in Chapter 7.

1.7 Summary

In the previous sections we have outlined some fundamental questions that inhibit our understanding of the star formation process. In the following chapters we examine these problems in detail.

In Chapter 2 we discuss further the chemistry and physics of star forming regions, and provide an introduction to the model which is employed in the remaining chapters. We investigate the initial support and collapse of translucent clumps to form dense cores in Chapter 3. In Chapter 4 we study the effects that the gas grain interaction has on observable molecular species and the assumption that certain types of molecules are indicative of a specific evolutionary epoch in a clouds lifetime.

In an attempt to test the accuracy of the models that we use, we examine the feasibility of a novel proposal to observe molecular nitrogen in a dark, dense core in Chapter 5. We study in Chapter 6 the long standing sulphur depletion problem:

why is S observed to be much more depleted in dense cores than carbon, nitrogen and oxygen are? In Chapter 7 we investigate the suitability of different molecular species for use in attempts to observe regions of infall.

Finally in Chapter 8 we summarise the results presented in the preceeding chapters and explore the future avenues of research that the work presented here indicates.

Chapter 2

Chemistry and physics of collapsing interstellar clouds

In this chapter we provide an introduction to the chemical and dynamical modelling employed in this work. In section 2.1 we describe the basic chemical reactions that occur in both the gas phase and grain surface production schemes. Section 2.2 concerns the relative abundances of the elements, values of which need to specified in a model. In section 2.3 we examine the chemical networks for a few selected elements and in section 2.4 we discuss how the ionization structure is determined by the chemistry. We summarise the physics that is involved in the model in section 2.5. Finally in section 2.6 we describe in detail the method of using the model and producing values for the evolution with time of the abundances of species in the model.

2.1 Chemical reactions

Many different models have been used in attempts to explain the observed interstellar molecular species and their abundances. There are two basic schemes for the formation of molecules that have been established. The first scheme involves reactions taking place in the gas phase (Bates & Spitzer 1951; Herbst & Klemperer 1973; Black & Dalgarno 1973), and the second involves reactions on interstellar grain surfaces (Hollenbach & Salpeter 1971; Tielens & Hagen 1971). It has become apparent

from recent observations of an increasing number of molecular species that both gas phase and grain surface production of molecules must be included into models (e.g. Williams & Taylor 1996; Crawford & Williams 1997). We examine these different schemes in turn.

2.1.1 Gas phase chemistry

Molecules can be formed via ion-molecule or neutral-neutral reactions. The rates of these reactions are given by $kn(\mathrm{X})n(\mathrm{Y})$ in $\mathrm{cm}^{-3}\ \mathrm{s}^{-1}$, where k is the reaction rate coefficient (in $\mathrm{cm}^3\ \mathrm{s}^{-1}$) and n is the number density of the species (in cm^{-3}). The reactants X and Y could be any of the following: atoms, molecules, atomic ions or molecular ions.

Ion-molecule reactions are particularly effective in forming increasingly complex species, and the reactions are rapid even at the low temperature conditions of interstellar clouds. If the reaction is exothermic then from Langevin theory the reaction rate coefficient will be independent of temperature, and will depend only on the reduced mass of the system and the polarizability of the molecule. Rate coefficients for ion-molecule reactions are typically of the order of $\sim 10^{-9}\ \mathrm{cm}^{-3}\ \mathrm{s}^{-1}$. However, if the molecule has a permanent dipole (e.g. H_2O), then the enhanced long range attraction leads to rate coefficients of between ten to a hundred times larger.

Both an ion and a molecule are required to initiate this chemistry. The starting molecule is H_2, and when H_2 is present the effectiveness of ion-molecule chemistry is directly related to the ion formation rate. Ionization can be induced by ultraviolet radiation or cosmic rays (cf. section 1.1).

Various loss mechanisms exist to hinder the build up of complex species. These include dissociative recombination of molecular ions and radiative recombination of atomic ions. Both of these processes also control the ionization level within a cloud. Photodissociation of molecules is another destructive mechanism. This last process can be caused by photons from the background interstellar radiation field or by photons which are generated as a result of cosmic ray ionization (see section 1.1).

Neutral-neutral reactions can also occur. Neutral exchanges are the most important form of these reactions (e.g. $\mathrm{CH+O \rightarrow CO+H}$). If the two reactants are

atoms then they are more likely to bounce off one another than form a molecule and reach stability by the emission of a photon. This is known as radiative association. However, if at least one of the reactants is a molecule a nonradiative reaction may be possible. Many of these reactions have activation energy barriers. On the other hand, there are some reactions that are measured to be very rapid, even at the low temperature conditions of the interstellar medium. Some are only a factor of $\sim$5 slower than ion-molecule reactions (Sims & Smith 1995; Smith 1997). The types of neutral-neutral reactions that are found to be rapid involve two radicals (e.g. CN+O_2), a radical and an unsaturated molecule (e.g. CN+C_2H_2) and even a radical and a saturated molecule (e.g. CN+C_2H_6). Also reactions of some radicals with atoms having non zero angular momentum (e.g. OH+O($^3P_2$)) are rapid.

2.1.2 Grain surface production

Dust grain surfaces provide sites for the formation of molecules. Two atoms A and B may rarely combine in the gas as the time of the collision is so short and radiative association is slow. However, on a surface there are sites to which A and B are drawn and held long enough for a reaction to occur. In such cases some of the excess energy produced by the reaction goes into the grain. The observed abundance of molecular hydrogen in the interstellar medium cannot be explained by gas phase production routes. The formation of H_2 on dust grain surfaces has therefore been invoked (e.g. Williams & Taylor 1996). The first H atom collides with the grain surface and is weakly bound. The second H atom arrives at the grain and finds the first H atom and combines with it to form the molecule. The recent observations of NH in diffuse clouds apparently requires that it too is formed on grains (Meyer & Roth 1991; Crawford & Williams 1997).

The dust temperature is low, at around 10 K (e.g. Williams & Taylor 1996), so molecules tend to stick to the surface when they collide with the grains. By this process icy mantles covering the grain surface are produced. Atoms including O, C and N can also stick to the grains. These are probably converted via hydrogen addition into water, methane and ammonia. Such icy mantles have been detected (as indicated in section 1.1, Table 1.2).

Many different molecular species may be created in the icy mantles (Williams & Taylor 1996). These molecular species can then be returned to the gas phase via one or more of the various desorption processes, which may occur sporadically or constantly with time (sections 1.1, 2.5.1).

2.2 Elemental abundances

The relative abundances of the elements are key to the chemistry in a model as these will greatly influence the relative importance of reactions in the chemical network. Table 2.1 gives the solar elemental abundances relative to hydrogen. These are derived from photospheric and meteoritic studies (Grevesse & Noels 1993). However these values for the relative elemental abundances are not representative of those in the interstellar medium. It is observed that the abundances of the elements are depleted relative to the solar values. Table 2.1 provides a comparison of the measured solar values to those obtained towards ζ Ophiuchi. ζ Oph is a bright star which is about 130 pc distant from the Sun. Absorption of visible and ultraviolet light from the spectrum is due to the presence of a low density cloud which contains a variety of different atomic and molecular species. The table also gives the calculated values of the logarithmic depletions, $D_{\rm X}$, where

$$D_{\rm X} = \log\left[\frac{N({\rm X})}{N({\rm H})}\right] - \log\left[\frac{N({\rm X})}{N({\rm H})}\right]_{\odot} \qquad (2.1)$$

where N(X) and N(H) are the column densities of elements X and H respectively. Typically, oxygen and carbon are reduced by $\sim$30% (Meyer 1997) and large fractions of the heavier elements, which have high condensation temperatures (e.g. Si, Mg and Fe), are incorporated into dust grains (Jenkins 1987; also see Fig. 6.1 in Chapter 6). It should be noted that Snow & Witt (1995) suggested that the solar abundances may not be representative of the interstellar medium, as they appear to be richer in heavy elements. However, we shall still use the solar abundances as the baseline for comparison. In the models of chemistry that we utilize, we incorporate the following elements: H, He, C, N, O, S, Na, Mg and Si.

Table 2.1: Solar elemental abundances, from Grevesse & Noels (1993). Abundances for ζ Oph are given for comparison, with the depletions, D_X (from Duley & Williams 1984). The notation $a(-b)$ denotes $a \times 10^{-b}$.

Element	Solar Abundance	Abundance in ζ Oph	Depletion, $-D_X$
H	1.00	0.37	0.43
He	0.10	–	–
O	7.4(-4)	5.0(-4)	0.17
C	4.0(-4)	1.6(-4)	0.40
N	9.3(-5)	7.2(-5)	0.11
S	1.6(-5)	8.2(-6)	0.29
Si	3.5(-5)	8.2(-7)	1.63
Na	2.1(-6)	2.1(-7)	1.00
Mg	3.8(-5)	1.0(-6)	1.58
Li	1.6(-9)	5.2(-11)	1.49
Ar	4.4(-6)	8.4(-7)	0.72
Ti	5.5(-8)	2.2(-10)	2.40
Ni	1.9(-6)	9.5(-9)	2.30
Cr	4.8(-7)	–	–
P	2.8(-7)	2.1(-8)	1.12
Cl	1.1(-7)	9.9(-8)	0.05
K	1.3(-7)	1.0(-8)	1.11
Ca	2.3(-6)	4.5(-10)	3.71
Fe	3.2(-5)	2.7(-17)	2.07
Al	2.5(-6)	1.3(-9)	3.28
Zn	2.5(-8)	1.4(-8)	0.25
Mn	2.6(-7)	1.5(-8)	1.24
Cu	2.8(-8)	6.3(-10)	1.65
Kr	1.7(-9)	–	–

2.3 Chemical networks

In the following sections we describe the important reactions in the hydrogen, carbon, oxygen, nitrogen and sulphur networks.

2.3.1 Hydrogen and deuterium chemistry

Hydrogen is the most abundant element in the Universe and plays a very important role in the chemistry of star forming regions. Molecular hydrogen is formed on the surfaces of grains as described in section 2.1.2, and is mainly destroyed by photodissociation with radiation of wavelengths near 1000 Å. The destructive mechanism is a two step process. Firstly radiation is absorbed and the molecule is excited to electronic states B and C from the ground electronic state X. The molecule will then emit radiation and in about 10 % of these transitions the molecule falls into the vibrational continuum of state X; i.e. the two atoms fly apart. The excitation occurs within very narrow wavelength bands and the radiation at wavelengths outside these bands do not destroy the molecule. When hydrogen molecules at the edge of a cloud are destroyed this reduces the intensity of the radiation in the narrow bands. Eventually the intensity is reduced to such an extent that the formation of H_2 is more rapid than the destruction. In this situation molecular hydrogen is self-shielding against destructive radiation and further into the cloud it becomes the main hydrogen carrier. H_2 can also be destroyed via chemical reactions which is of particular importance in dark clouds.

The cosmic ray ionization of H_2 produces $H_2{}^+$ in 97 % of the encounters (H^+ is created the remaining 3 % of the time). This then leads to the creation of the important molecular ion $H_3{}^+$,

$$H_2^+ + H_2 \rightarrow H_3^+ + H. \tag{2.2}$$

At the low temperatures of dark, dense interstellar clouds, carbon and oxygen do not react with H_2. Instead, reactions with $H_3{}^+$ initiate these chemistries. $H_3{}^+$ has only recently been detected in the interstellar medium (McCall et al. 1998; Geballe & Oka 1996).

Although H_2 cannot readily be produced by gas phase reactions, HD arises from gas phase reactions once H_2 has formed (see Fig. 2.4). However, HD is destroyed more rapidly by photodissociation than H_2 as due to its lower abundance it does not become self-shielding against the photodissociating radiation. We discuss the D chemistry further in section 2.4.

2.3.2 Carbon chemistry

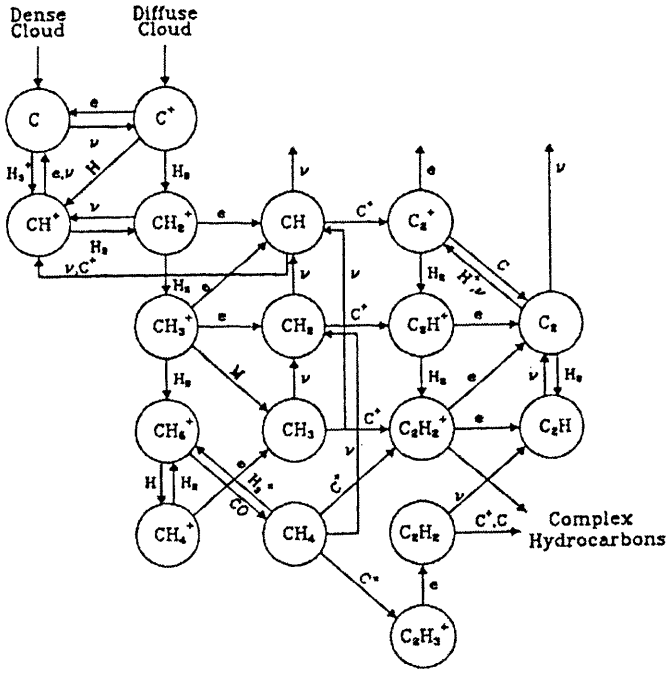

Figure 2.1: Carbon chemistry network, from van Dishoeck 1998.

Figure 2.1 depicts the initial steps of the carbon chemistry in both diffuse and dense clouds (van Dishoeck 1998). In diffuse clouds the majority of the carbon is in the form of C^+ because it has an ionization potential that is below 13.6 eV (at 11.3 eV). In dark clouds the abundance of C^+ is low due to shielding from the ultraviolet radiation of the background interstellar radiation field. Instead the main carbon carriers are C and CO.

The carbon chemistry in diffuse clouds in initiated by

$$C^+ + H_2 \rightarrow CH_2^+ + h\nu \tag{2.3}$$

which is a slow ($k \sim 10^{-15}$ cm^3 s^{-1}) process (Gerlich & Horning 1992; Smith 1989). CH_3^+ is then produced when CH_2^+ reacts with H_2. Dissociative recombination of CH_3^+ produces neutrals such as CH and CH_2. These and other hydrocarbons can be rapidly produced in diffuse clouds as C^+ is so abundant, although photodissociation limits their build up.

As the visual extinction increases the hydrocarbons react with neutral atomic oxygen which produces species such as H_2CO and CO. Carbon monoxide is a very stable molecule. CO photodissociation can only occur for photons with wavelengths shortward of 1118 Å and, like H_2, only through discrete lines which become increasingly optically thick into the cloud. CO can also be shielded by dust and the conincident lines of H and H_2 (van Dishoeck & Black 1988). Thus, as hydrocarbons are removed by reactions with oxygen bearing molecules, initiating the formation of CO, CO becomes the dominant carrier of carbon and the formation of hydrocarbons ceases. This has led to the hydrocarbons being referred to as "early-time" species; those which have abundance peaks early in a cloud's evolution whilst C^+ is the most abundant form of carbon.

In dark regions CO is destroyed by photons emitted as a consequence of cosmic ray induced ionizations and in reactions with He^+ produced by the cosmic ray induced ionizations of He. To initiate the carbon chemistry in dense clouds, C reacts with H_3^+ (cf. Fig. 2.1), to form CH^+. Complex hardrocarbons are also formed in dense clouds via several routes (Herbst 1995). The pathway which is considered to be dominant (as depicted in Fig. 2.1) involves carbon insertion reactions (e.g. $C^+ + CH_4 \rightarrow C_2H_2^+$).

2.3.3 Oxygen chemistry

Oxygen, unlike carbon, is mostly neutral in diffuse clouds as the ionization potential of O is equal to that of hydrogen. Like the carbon chemistry, the oxygen chemistry is started via reactions with H_3^+ to form OH^+, as shown in Fig. 2.2 (from van Dishoeck 1990). The oxygen chemistry can also be initiated with the charge transfer reaction between O and H^+ but the temperature must be at least about 100 K since this reaction is endothermic. Once OH^+ has been formed, OH and H_2O are created by

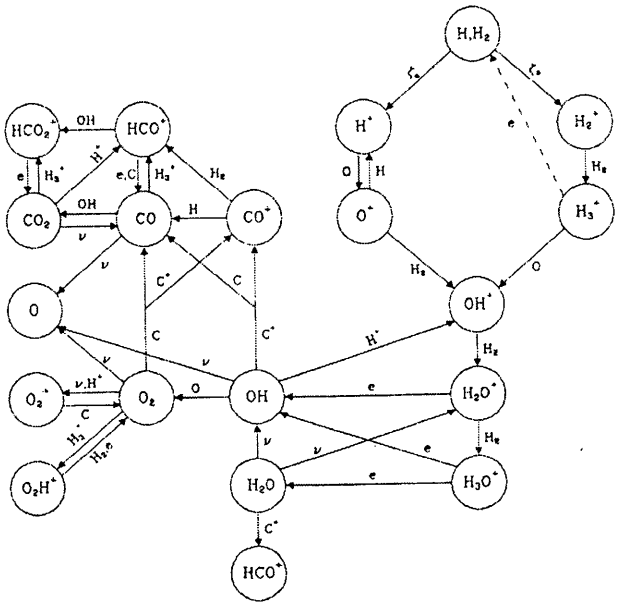

Figure 2.2: Oxygen chemistry network, from van Dishoeck 1990.

hydrogen abstractions and dissociative recombinations.

The main destruction mechanisms of neutral O-bearing molecules are reactions with C^+ in addition to photodissociation. In dense clouds where the photodissociaton rates are reduced, increasingly complex oxygen-bearing species can be produced.

2.3.4 Nitrogen chemistry

N has an ionization potential greater than 13.6 eV (at 14.6 eV). Unlike C and O, N does not react rapidly with H_3^+, as the proton transfer reaction is endothermic, though a reaction transferring H_2^+ has been proposed (Scott et al. 1997; see Chapter 4). The charge transfer reaction between N and H^+ is also too endothermic for it to be of importance.

The nitrogen chemistry is initiated by reactions of N with OH and CH to form NO and CN. N_2 is produced by the reaction of N with NO. He^+ removes N_2 creating superthermal N^+ which reacts endothermically with H_2 to form NH^+. Subsequent hydrogen abstractions give rise to NH, NH_2 and NH_3. The production of HC_3N, the simplest of the cyanopolyynes, is considered in detail in section 4.1. The N^+ is created via cosmic ray ionizations.

2.3.5 Sulphur chemistry

In diffuse clouds most of the sulphur will be ionized due to its low ionization potential (10.4 eV). Sulphur hydrides are not thought to be abundant in cold diffuse and dense clouds. This is due to the fact that the reaction of S^+ with H_2 is endothermic and the radiative association reaction is slow. S can react with H_3^+ to form SH^+, but the reaction of SH^+ with H_2 is also endothermic.

However, other S-bearing molecules are rapidly produced via ion-molecule and neutral-neutral reactions. Reactions of S^+ and S with CH and C_2 form CS. Reactions with OH produce SO. SO and OH react to create SO_2.

2.4 The ionization structure

Here we discuss the chemical effects that are important in establishing the ionization structure in a cloud. As we described in Chapter 1, the level of ionization is important in controlling the collapse of clumps and cores. In section 2.3.2 we detailed that C^+ is the most abundant form of C in diffuse regions. As oxygen and hydrogen are neutral in such conditions (cf. sections 2.3.1 and 2.3.3) then C^+ is the major ionization source (up to moderate depths) as it is the next most abundant species. The C^+ is formed as C is ionized by photons of the interstellar radiation field. The fractional ionization is therefore of the order of 10^{-4}.

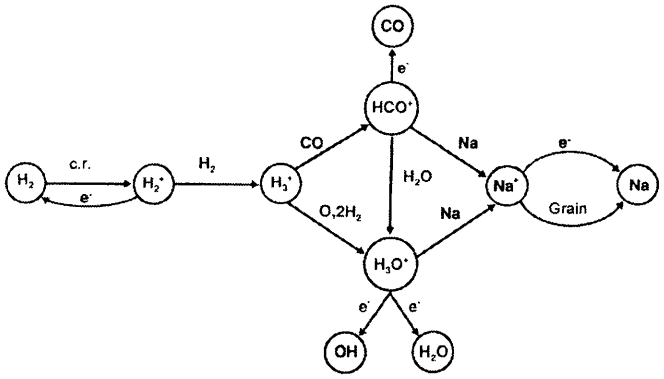

Figure 2.3: Chemistry controlling the ionization structure in a dark cloud, where sodium is the representative heavy metal, from Hartquist & Williams 1995.

At increasing visual extinctions more of the carbon will be neutral (see section 2.3.2). When A_V>5 mag, the major source of ionization is provided by cosmic rays (cf. section 1.1). In section 2.3.1 we saw how the cosmic ray ionization of H_2 leads to the formation of H_3^+. In dense cores the most abundant molecular ion is often HCO^+, formed when H_3^+ reacts with CO. The removal rates of HCO^+ are important in establishing the ionization level in dense cores. HCO^+ can dissociatively recombine with an electron to form CO or react with water to form H_3O^+. Alternatively, it can undergo charge transfer reactions with neutral metallic ions, such as Na or Mg (as H_3O^+ does too). This last pathway is extremely important as Na^+ and Mg^+ recombine slowly with electrons, at a rate that is $\sim 10^5$ times slower than that for HCO^+; these species are also relatively unreactive at low temperatures. Hence, these species are long lived and help to maintain high ionization levels in the cloud. The dominant removal mechanism of metallic ions are grain collisions, where the charge is transferred to the grain. The fractional ionization in dense cores is around 10^{-8}; it increases as $\sqrt{\zeta}$ (the cosmic ray ionization rate) and decreases with the number density as $n^{-1/2}$. In dense cores the most abundant ions are the metallic atomic ions, with HCO^+ being the next most important, with an abundance that is 10–100 times lower. Figure 2.3 depicts the chemistry that controls the ionization level in a dark cloud (Hartquist & Williams 1995).

The fractional ionization is important in controlling the evolution of clumps and cores, and depends on the cosmic ray ionization rate. The rate of cosmic ray ionization is an important yet unknown parameter for interstellar chemistry. In Fig. 2.4 we depict the formation and removal mechanisms for HD (Hartquist & Williams 1995). The cosmic ray ionization rate can be inferred for a diffuse cloud using the measured HD abundance once the cloud density and temperature structure, the cosmic deuterium abundance and the photodissociation rate of HD are known. Typically, the derived value is around 10^{-17} s^{-1}(Hartquist & Williams 1995).

In dark clouds the D chemistry can again be used in attempts to establish the ionization level. In Fig. 2.5 we display the chemistry that determines the DCO^+ to HCO^+ abundance (Hartquist & Williams 1995). Observations of the DCO^+ to

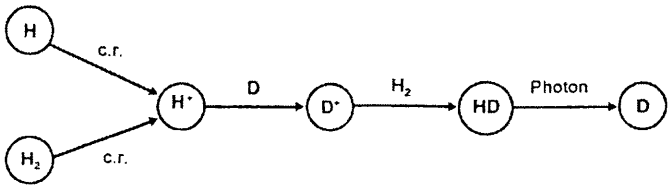

Figure 2.4: Diagram of HD formation, from Hartquist & Williams 1995.

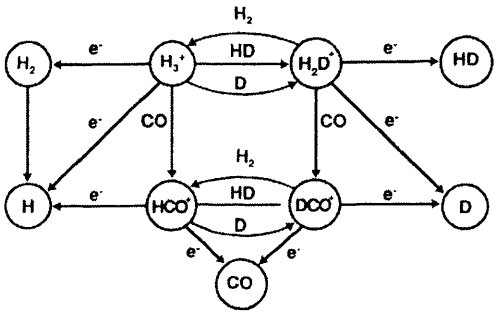

Figure 2.5: Diagram of DCO^+ and HCO^+ chemistry, from Hartquist & Williams 1995.

HCO^+ ratio can therefore be used to determine the fractional ionization within a dark cloud. This provides an upper limit to the cosmic ray ionization rate within the cloud, of the order if 10^{-17} s^{-1} per H_2 molecule (e.g. Caselli et al. 1998; Williams et al. 1998).

2.5 Physics of collapsing clouds

In this section we examine and recap on the physical processes that are important for inclusion in a model.

2.5.1 Freeze-out and desorption

The freeze-out onto dust grains of a species X containing an element more massive than helium occurs at a rate, following Rawlings et al. (1992), of

$$\Gamma_X = 1.1 \times 10^{-17} s^{-1} DA \left(\frac{m_X}{\text{a.m.u}}\right)^{-1/2} \left(\frac{T}{1\text{K}}\right)^{1/2} \left(\frac{n_H}{1\text{cm}^{-3}}\right) \quad (2.4)$$

where T is the temperature, m_X is the mass of one particle of the species, and

$$\begin{aligned} A = & \quad 1 \quad \text{(for neutral species)} \\ = & \quad 1 + \tfrac{167}{T} \quad \text{(for positive ions.).} \end{aligned} \tag{2.5}$$

We have mentioned previously that the grains in the low temperature dense clouds are negatively charged. (As electrons are lighter than the positive ions, they can move faster, typically ~100 times more rapidly, and therefore they collide more frequently with grains.) The grain size can be inferred from observations of the dust properties, and estimates for the grain radius lie in the range of 0.1 μm. The constant factor in equation 2.4 incorporates the grain radius, and uses the value that we adopt throughout this work of 0.1 μm. The parameter D is used to describe variations in the sticking efficiency and the grain size distribution. Results of laboratory measurements and quantum mechanical calculations suggest that the sticking efficiencies for species interacting with realistic grain materials lie in the range 0.1–1.0 (Leitch-Devlin & Williams 1985; for description of dust grain composition please refer to the discussion in section 6.4 of Chapter 6).

Return to the gas phase via desorption can also occur. We employed desorption in some of the models presented in the following chapters. We make no assumptions about the exact nature of the desorption process; when desorption is incorporated into a model only its effects are accounted for; namely the return of grain mantle species to the gas phase. The possible desorption mechanisms include, i) heating of the dust by cosmic rays such that weakly bound species may evaporate; ii) heavy ion impact to eject ice fragments which then evaporate; iii) indirect photodesorption to create hot spots which evaporate weakly bound species; and iv) chemical energy from exothermic reactions (although the chemical energy may result from cosmic rays) warms the ice and so species may be evaporated (cf. Williams & Taylor 1996).

From the comparison of observations with chemical models for NH_3 and CS, the inference is that freeze-out does occur, but is relatively inefficient (Willacy, Williams & Minh 1993; Taylor, Morata & Williams 1996). Therefore, we sometimes consider D to be an 'effective sticking coefficient'. In these cases we lower the value taken for D to simulate that competition between freeze-out and desorption processes. Eventually material will remain on the grain surface, but the freeze-out timescale is

enhanced. By this approach we can explore the competing effects of accretion and desorption on the chemistry.

2.5.2 Collapse

In some models $n_{\rm H}$ was taken to be fixed as was A_V. In other models $n_{\rm H}$ was assumed to increase from an initial level, $n_{\rm H_0}$, to account for collapse via free fall. In these cases, $n_{\rm H}$ was taken to vary, following Rawlings et al. (1992) (and references therein), as

$$\frac{{\rm d}n_{\rm H}}{{\rm dt}} = {\rm B}\left(\frac{n_{\rm H}^4}{n_{\rm H_0}}\right)^{1/3}\left\{24\pi G m_{\rm H} n_{\rm H}\left[\left(\frac{n_{\rm H}}{n_{\rm H_0}}\right)^{1/3} - 1\right]\right\}^{1/2}, \qquad (2.6)$$

where t is time, G is the gravitational constant, $m_{\rm H}$=1 a.m.u., and B is a constant (for gravitational free fall B=1). We can consider B to be a retardation factor. If magnetic effects and rotational support were to be accounted for then B would have a value <1.0 that is density dependent. After $n_{\rm H}$ reached some chosen value, $n_{\rm H_f}$, it was kept constant. In models with varying $n_{\rm H}$ the value of A_V was also taken to vary with time.

2.6 The model

In this section we provide a recipe for constructing a model by which the time-dependent abundances of a chosen set of species can be followed. For all of the chemical and dynamical models that are presented in the following Chapters (3, 4, 6 and 7) we used the UMIST rate file (Millar, Farquhar & Willacy 1997) as the source of reaction rate coefficients and rates. The UMIST database contains rate coefficients and rates for 3864 reactions between 395 species composed of 12 elements. The important reactions for both interstellar and circumstellar chemistries are included. The types of reactions that are incorporated are neutral-neutral, ion-neutral, radiative electron attachment, dissociative recombination, ionizations due to cosmic rays, photoreactions driven by the interstellar ultraviolet radiation field and cosmic ray induced photoreactions. The file gives values for the variables α,

β and γ for each reaction. These are then used to calculate k, the reaction rate coefficient.

For two-body reactions,

$$k = \alpha \left(\frac{T}{300}\right)^{\beta} e^{-\gamma/T} \mathrm{cm}^3\mathrm{s}^{-1} \tag{2.7}$$

where T is the gas kinetic temperature. For interstellar photoreactions

$$k = \alpha e^{-\gamma A_V} \mathrm{s}^{-1} \tag{2.8}$$

where α represents the rate in the unshielded UV radiation field and γ is used to account for the extinction of the UV radiation by dust particles. The Draine (1978) UV radiation field was used to determine α.

For direct cosmic ray ionizations

$$k = \alpha \mathrm{s}^{-1} \tag{2.9}$$

and for cosmic ray induced photoreactions

$$k = \frac{\alpha\gamma}{(1-\omega)} \mathrm{s}^{-1} \tag{2.10}$$

where ω is the grain albedo in the far UV (typically 0.6 at 150 nm) and γ is the probability per cosmic ray ionization that the appropriate photoreaction occurs (we use ω=0.5 and γ=1 in all models). For both these types of reactions the rates are given for a 'standard' value for the interstellar cosmic ray ionization rate of 1.3×10^{-17} s^{-1}. Any of the above parameters can be rescaled appropriately in the model.

As the physical characteristics of a star forming region evolve and change, so too do the relevant chemical processes (as we described in section 2.3). Different atomic and molecular species are important in different regions and at different epochs. In order to allow for this complexity in the models, we must specify a species set that is sufficiently comprehensive. This set does not contain all those that are available in the UMIST database. There are several reasons why the use of a limited species set is preferred. Firstly the computational overheads are reduced. The second reason is that we still do not understand the chemistries of many of the species contained in the UMIST database, and their addition to a model increases the uncertainties

Table 2.2: Table of parameters used in the model.

n	Density (cm^{-3})	
A_V	Visual Extinction (mag.)	
T	Temperature (K)	
B	Collapse retardation factor	
ζ	Cosmic Ray Ionization Rate	1.3×10^{-17} s^{-1}
a	Grain radius	10^{-5} cm
R	rate H_2 formed on grains	9.5×10^{-18} cm^3s^{-1}

inherent within it. We were able to limit our choice of species that are important for a particular object by considering which species have been observed. We then included additional species which are not observed but are important for the formation of the observed species.

As the rate file does not include any grain surface chemistry, when we wished to include it within a model then we had to add the relevant reactions to the UMIST rate file. We also made some modifications to incorporate any recent experimental or theoretical results for reaction rates. In addition, we checked to see if cosmic ray induced photoreactions are included in the rate file for the species we selected. This is a result of only cosmic ray induced photoreactions for which Gredel et al. (1989) gave values being incorporated in the UMIST rate file. For those species for which these types of reactions are not already present in the rate file, we used a value of 200 for the ratio of the photodissociation to ionization rate.

When the rate file has been finalized, a Fortran program DELOAD is used to write Fortran source code for the time-dependent non-linear differential equations, based on the chosen rate file and species set. The time dependent rate equations for the abundances of the species chosen are then integrated using a standard package (we used a GEAR integrator). To perform this last step, we had to specify many parameters, such as the density, temperature, cosmic ray ionization rate and visual extinction as functions of time. We calculated the chemistry in a single fluid within a cloud; in many cases, the physical properties were taken to vary. Models in which the physical properties remain constant are often referred to as being "pseudo-time-dependent", whereas "time-dependent models" are those in which the physical

properties vary. There are many parameters other than those listed above that must be specified (e.g. the grain size for calculation of freeze-out rates), and in Table 2.2 we present a compendium of these with their adopted values. For the models that we present in the following chapters these are the adopted values unless stated otherwise.

Chapter 3

Ionization structure and a critical visual extinction for turbulent supported clumps

In Chapter 1 we described the types of objects arising in different evolutionary stages in star forming regions. In section 1.2 we considered the structures of GMC complexes, and focused on one object, the Rosette Molecular Cloud. We described how translucent clumps in GMCs are initially supported by magnetic fields and turbulence. In this chapter we examine the initial support and the collapse of translucent clumps. Such collapse results in the formation of dense cores.

3.1 Introduction

In their work on the clumpy structure of the Rosette Molecular Cloud (RMC), Williams, Blitz & Stark (1995) identified seven star forming clumps, none of which has an estimated ^{13}CO column density, $N(^{13}\mathrm{CO})$, of less than 10^{16} cm^{-2}. From Fig. 3.1 (Fig. 21 from Williams, Blitz & Stark 1995) it appears that eight or nine other clumps have $N(^{13}\mathrm{CO})>10^{16}$ cm^{-2} but contain no stars. The estimated values of $N(^{13}\mathrm{CO})$ for the star forming clumps, with one exception, vary by only a factor of about 2, and the estimated masses vary by a factor of about 7 (cf. section 1.2). While one could argue that the Williams et al. (1995) data point to the existence

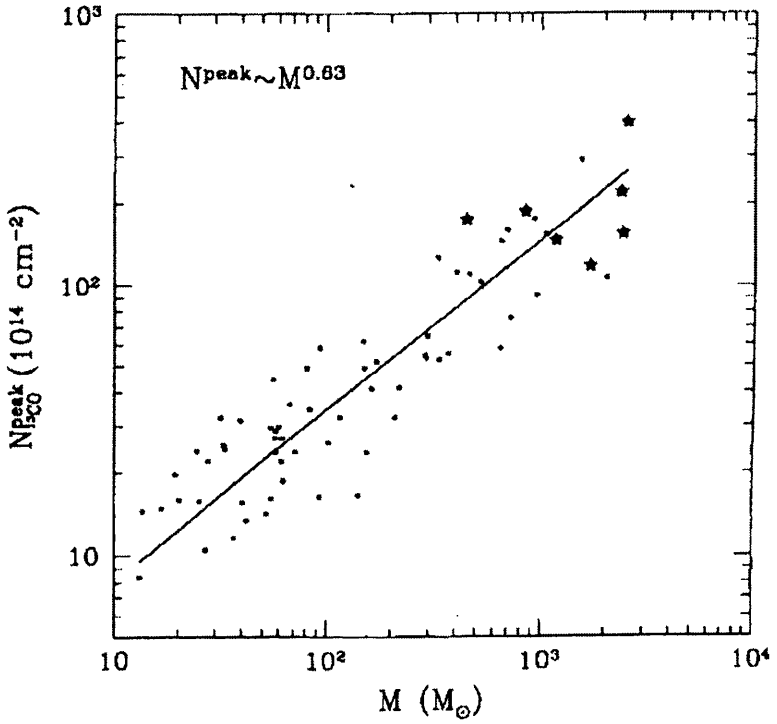

Figure 3.1: Relation of peak (central) ^{13}CO column density to clump mass, for clumps in the RMC. The straight line indicates a least-squares fit to the power law exponent relating the two (displayed in the top left hand corner). Asterisks represent cores with an IRAS source. From Williams, Blitz & Stark (1995).

of a minimum *mass* required for star formation to occur in the RMC, we suggest that they indicate, at least as strongly, the existence of a minimum *column density*, $N(^{13}\mathrm{CO}) \simeq 10^{16}$ cm^{-2}, for stars to be born.

Hartquist et al. (1993) suggested that there should be a maximum value of the visual extinction, A_V, of a clump supported against gravitational collapse along its large-scale magnetic field by internal Alfvén waves thought to comprise clump turbulence (Arons & Max 1975; Caselli & Myers 1995; Mouschovias & Psaltis 1995; section 1.2). Their idea was that above this critical visual extinction the damping rate of waves by ion-neutral friction is too rapid for the waves to be maintained at sufficient amplitudes to support a clump. The damping rate of an Alfvén wave in a weakly ionized medium due to ion-neutral friction (Kulsrud & Pearce 1969) is

$$\Gamma_D \approx \omega^2/2\nu_{ni} \quad \text{for } \omega \ll \nu_{in} \tag{3.1}$$

$$\Gamma_D > \quad \omega \quad \text{for } \nu_{ni} < \omega < \nu_{in} \tag{3.2}$$

$$\Gamma_D \approx \quad \nu_{in}/2 \quad \text{for } \omega \gg \nu_{in}, \tag{3.3}$$

where ω is the angular frequency of the wave, ν_{in} is the inverse stopping time of an ion by the neutrals, and ν_{ni} is the inverse stopping time of a neutral by the ions. For ions of mass m_i colliding with H_2 (Osterbrock 1961)

$$\nu_{ni} \approx 1.8 \times 10^{-9} \text{ s}^{-1} \left(\frac{m_i}{m_i + m_{H_2}}\right)^{1/2} \left(\frac{n_i}{\text{cm}^{-3}}\right) \tag{3.4}$$

and

$$\nu_{in} = \nu_{ni} \left(\frac{m_{H_2}}{m_i}\right) \left(\frac{n(H_2)}{n_i}\right) \tag{3.5}$$

where m_{H_2} is the mass of an H_2 molecule and n_i is the number density of ions. The value of n_i decreases with visual extinction. As discussed in section 2.4, the fractional ionization in the outer regions of a molecular cloud is generally at least 10^{-4} because the gas phase carbon remains primarily in C^+ due to the efficiency of photodissociation and photoionization processes, whereas the fractional ionization is several orders of magnitude lower than this in dark regions, in which the ionization is due almost entirely to cosmic rays. From equations 3.1 and 3.4 one sees clearly that the damping rate of waves in which the ion-neutral motions are well-coupled declines with extinction because it increases as the inverse of the number density of ions, n_i, (and proportionally to the square of the frequency). Recent numerical simulations of wave behaviour in self-gravitating clumps show that nonlinear magnetohydrodynamic waves can, in fact, support such clumps against collapse (Gammie & Ostriker 1996). In view of its relevance to wave damping in clumps, it is now particularly timely to return to the issue of the behaviour of the fractional ionization, x_i ($x_i \equiv n_i/n_H$, where n_H is the number density of hydrogen nuclei), as a function of the visual extinction, A_V.

The view taken by Hartquist et al. (1993) and by us in this work, is, thus, that much of the molecular material in giant molecular clouds is translucent to radiation and that photoionization affects its fractional ionization, which in turn plays a role in determining the rate at which material collapses. This view is one that has much in common with that adopted by McKee (1989) who argued that star formation regulates itself because the births of stars lead to the production of radiation which

raises the fractional ionization in translucent material and, consequently, lowers the rate of ambipolar diffusion. There are differences between McKee's and our points of view. We stress the role of turbulent support of clumps like those identified by Williams et al. (1995) (see also Bertoldi & McKee 1992); these are much more tenuous objects than the magnetically subcritical dense cores in which turbulent support is likely to be much less important than the support provided by the large-scale magnetic field and in which the collapse timescale is established by ambipolar diffusion (see section 1.1). Consequently, McKee's (1989) considerations are likely to be of more relevance to more evolved objects formed through the collapse of the sorts of clumps Williams et al. (1995) found in their CO studies. In this chapter we present results for the fractional ionization for a wide variety of conditions; so many of our ionization calculations are of direct relevance for the application of McKee's (1989) model to self-regulation of later stages of the formation of low-mass stars.

Another reason for returning to this issue is that in the last few years a revision of ideas about the fractional ionization in some molecular cloud environments has occurred. Pineau des Forêts et al. (1992) and Le Bourlot et al. (1993a) discovered, for a range of assumed H_3^+ dissociative recombination rate coefficients, a class of dark cloud gas phase chemical equilibrium solutions in which the H_3^+ abundance is much lower and x_i much higher than in the solutions of the previously known class. Shalabiea & Greenberg (1995) have studied the effects on the existence of solutions belonging to the two classes of the assumed gas phase elemental fractional abundances of sulphur, x_S, and low ionization potential metals, x_M, such as sodium and magnesium, and of the assumed nature of grain surface chemistry modifications to the dark cloud gas phase chemistry. Though Le Bourlot et al. (1993b) and Flower et al. (1994) gave the fractional abundance of C^+, $x(C^+)$, relative to hydrogen nuclei as a function of A_V for one cloud model with an assumed radiation field like that of the typical interstellar background field, there has been no exploration of the simultaneous dependence of the fractional ionization x_i on A_V, n_H, x_S, x_{Si} and x_M. The results of Le Bourlot et al. (1993b) and of Flower et al. (1994) indicate a transition at translucent depths for a model cloud in which n_H=10^3 cm^{-3} from a solution of the high ionization class to one of the low ionization class.

In section 3.2 we report the results of such an exploration and identify a variety of situations under which the gradient $-\mathrm{d}(\log x_i)/\mathrm{d}A_V$ is large. In section 3.3 we give results for the chemical evolution of a parcel of gas collapsing from $n_{\mathrm{H}}=10^3$ cm^{-3} with an initial A_V within the range in which $-\mathrm{d}(\log x_i)/\mathrm{d}A_V$ is large. In our description of the collapse dynamics we include a plane parallel collapse phase, representing collapse along the field lines, followed by a phase during which the collapse takes place both across and along the large scale magnetic field and is regulated by ambipolar diffusion, the rate of which depends on the fractional ionization which is taken from our calculations.

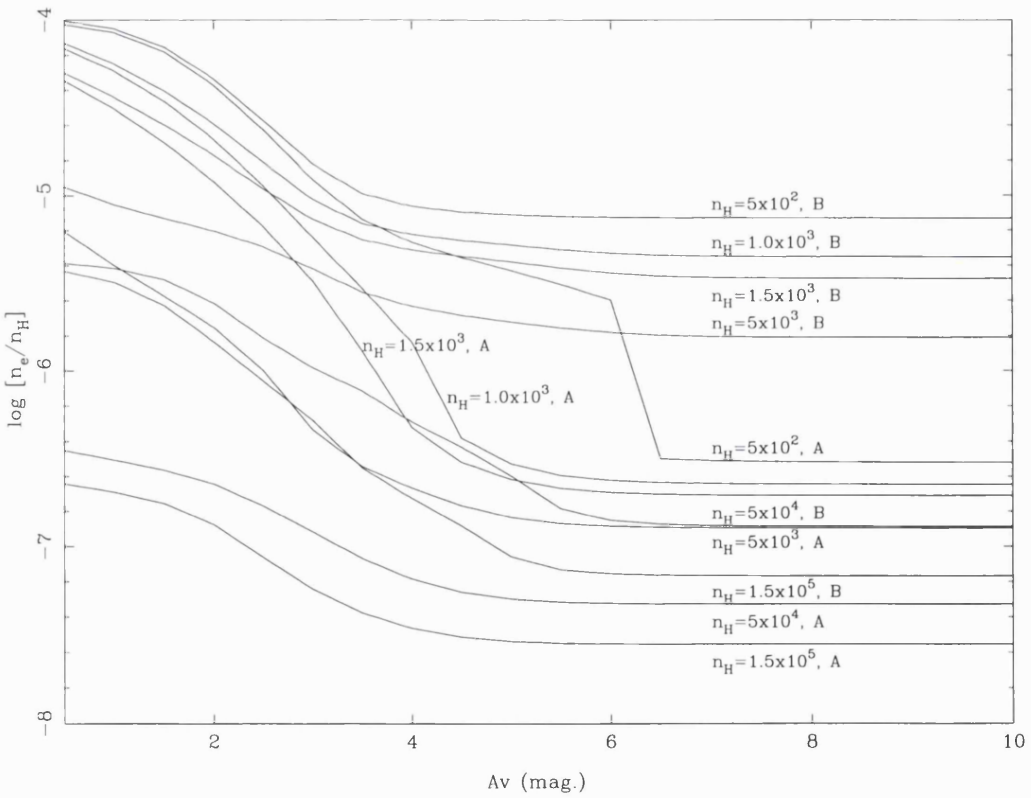

Figure 3.2: Steady state fractional ionization as a function of A_V, n_{H}, x_{S}, x_{Si}, x_{M}.

3.2 Fractional ionization as a function of A_V, n_H, x_S, x_{Si} and x_M.

Figure 3.2 contains the results of steady state equilibrium chemical models for x_i as a function of A_V, the visual extinction to the near edge of a semi-infinite plane-parallel cloud. Equilibrium results were obtained through the integration of rate equations from a time when all elements more massive than hydrogen were primarily in neutral and ionic atomic form, but most of the hydrogen was in H_2. The standard interstellar radiation background field was assumed to be incident on the near side of the cloud (a semi-infinite plane parallel clump), and it is assumed that a cosmic ray induced radiation field is present throughout the cloud (Prasad & Tarafdar 1983; see section 2.6). In addition to an extensive network of gas phase reactions for which rate coefficients were taken primarily from the UMIST compilation (Millar et al. 1997; see section 2.6), we included modifications to the gas phase chemistry due to the presence of grains. We assumed that all material striking grains undergoes simple chemical processing and is immediately returned to the gas phase, but that many of the species are processed in such a way that much of the material is returned in the form of saturated species like H_2, NH_3, H_2S and CH_4 (please refer to Table 3.1 for examples of these processes). The detection of NH in interstellar clouds (Meyer & Roth 1991; Crawford & Williams 1997) supports this view, at least for clouds with values of $A_V \sim 1$ (see Williams 1993).

Table 3.1: Examples of the gas grain reactions used in the model. The reactant and product species are given.

Reactant	Product
C	CH_4
O	H_2O
N	NH_3
S	H_2S
CH	CH_4
OH	H_2O
NH	NH_3
HS	H_2S

Table 3.2: Fractional elemental abundances relative to $n_{\rm H}$.

	A "dark"	B "diffuse"
He	7×10^{-2}	7×10^{-2}
C	1×10^{-4}	1×10^{-4}
N	2×10^{-5}	2×10^{-5}
O	2×10^{-4}	2×10^{-4}
S	2×10^{-8}	3×10^{-6}
Si	7×10^{-9}	1×10^{-6}
M	2×10^{-7}	1×10^{-6}

The rate at which particles of neutral species X were assumed to strike grain surfaces is

$$3.5 \times 10^{-18} \mathrm{s}^{-1} (m_{\rm X}/\mathrm{amu})^{-1/2} (n_{\rm H}/\mathrm{cm}^3), \tag{3.6}$$

where we used equation 2.4 and took the temperature to be 10 K. The charged particles were assumed to strike grains (mostly negatively charged) at a rate that is 18 times larger (following Rawlings et al. 1992; see section 2.5.1). All ions striking grains were assumed to return to the gas phase as neutral atoms and molecules. The cosmic ray ionization rate was taken to be 1.3×10^{-17} s^{-1} (cf. section 2.6). Molecular hydrogen is self-shielding, and CO was assumed to be sufficiently self-shielded and shielded by H_2 that only photons produced as a consequence of cosmic ray induced ionization are important for its photodissociation.

The results in Fig. 3.2 are for the two sets of assumed gas phase elemental abundances given in Table 3.2 (see Shalabiea & Greenberg 1995). Set A is similar to that required in many cases to reproduce chemical abundances measured for dark cores while Set B, which has higher fractional abundances of low ionization potential elements, is selected because diffuse clouds have much higher gas phase fractional abundances of those species than dark cores. The issue of the mechanisms that control the depletion of the elements with low ionization potentials is unclear at present (hence the parametrised approach adopted here), but is one of major importance for the chemistry of star formation, as the results in this chapter indicate.

Inspection of Fig. 3.2 shows that for $n_{\rm H}=5 \times 10^2$ cm^{-3} (typical of the RMC

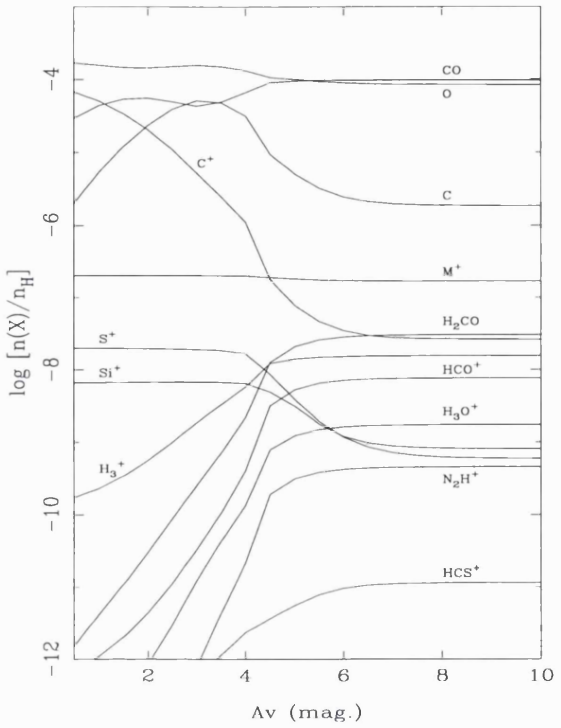

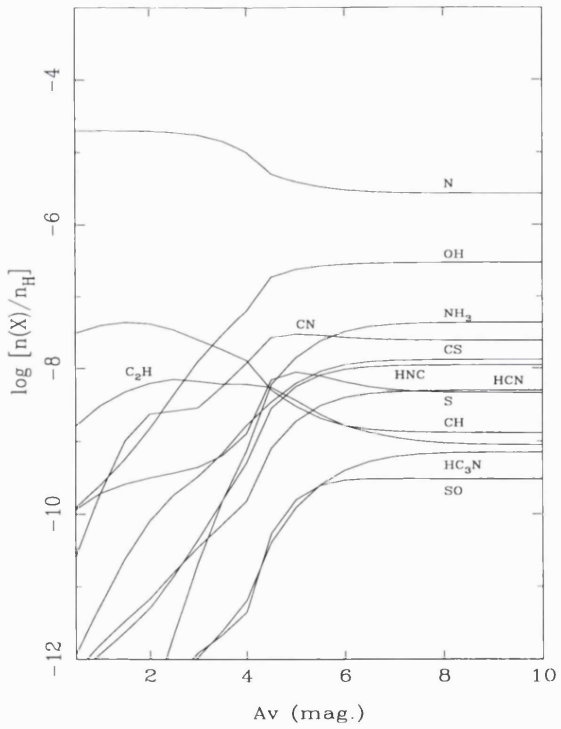

Figure 3.3: Steady state fractional abundances of species as functions of A_V for $n_{\rm H}$=10^3 cm^{-3} and case A depletions (see text for description).

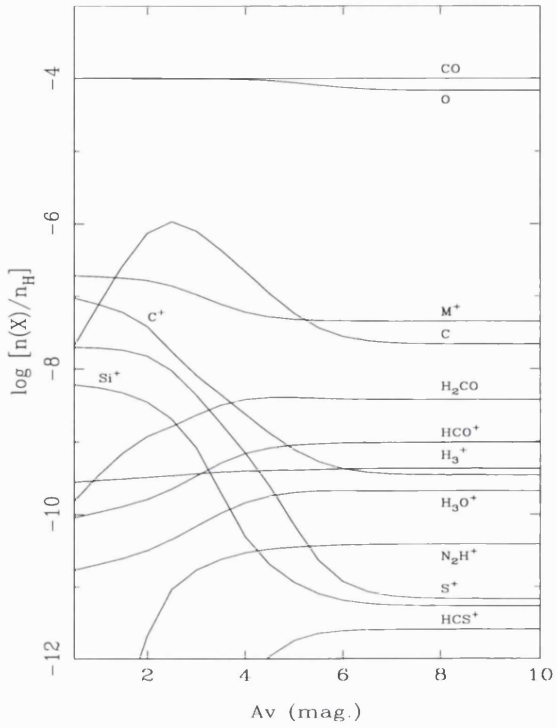

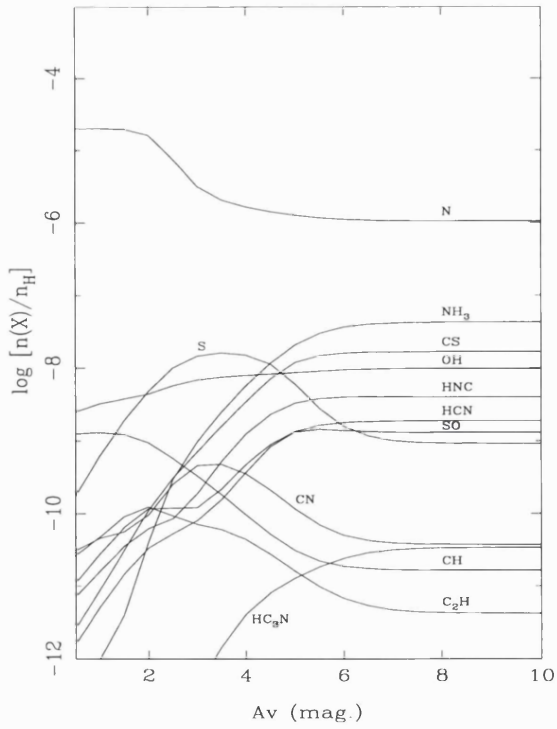

Figure 3.4: Steady state fractional abundances of species as functions of A_V for $n_{\rm H}$=5$\times$ 10^4 cm^{-3} and case A depletions (see text for description).

clumps) the gradient $-\mathrm{d}(\log x_i)/\mathrm{d}A_V$ reaches a maximum in the range $A_V \approx 2$–3 for Set B depletions and a local maximum for the same range of A_V for Set A depletions. For Set A depletions and n_H=500 cm^{-3} a much higher value of $-\mathrm{d}(\log x_i)/\mathrm{d}A_V$ exists for a very small range of high values of A_V where a chemical phase transition occurs, but the high value of $-\mathrm{d}(\log x_i)/\mathrm{d}A_V$ in the range of $A_V \approx 2$–3 for Set A as well as Set B depletions, is no doubt important for the ion-neutral damping of turbulence supporting RMC-like clumps. We can calculate the visual extinction that corresponds to the critical measured value of the ^{13}CO column density for RMC clumps (which is 1×10^{16} cm^{-2}). Taking (1×10^{16} cm^{-2}/2) to be half the critical measured value of the ^{13}CO column density from the edge of an RMC clump to its centre, $n(^{13}\mathrm{CO})/n_\mathrm{H}=1\times10^{-6}$ (Williams et al. 1995), and the standard conversion of the hydrogen nuclei column density to A_V (Savage & Mathis 1979), where

$$A_V = 5 \times 10^{-22} \text{ mag (H nuclei cm}^{-2})^{-1},$$

we find that the critical visual extinction from the centre of an RMC clump to its edge is 2.5, in agreement with the regime of maximum $-\mathrm{d}(\log x_i)/\mathrm{d}A_V$ for n_H=500 cm^{-3} identified in our calculations.

This agreement between the minimum A_V for the existence of stars and the A_V range of extreme logarithmic derivative of the fractional ionization is in harmony with the suggestion (Hartquist et al. 1993) that the minimum A_V for the existence of stars is associated with a maximum A_V at which turbulent support of clumps is effective in preventing collapse along magnetic field lines.

Results for x_i are also given in Fig. 3.2 for a range of values of n_H. As stated above, the ion-neutral damping rate of a wave of sufficiently low frequency is proportional to the square of the wave frequency divided by n_i. A comparison of the Set A graphs for $n_\mathrm{H}=5\times10^2$ cm^{-3} and $n_\mathrm{H}=5\times10^4$ cm^{-3} shows that at A_V=3, the values of n_i for the two model clumps are roughly equal. Therefore the ion-neutral wave damping rate for a given frequency has roughly the same functional dependence on A_V, implying that even for dense cores the A_V dependence of x_i must be taken into account in any consideration of wave propagation.

Unfortunately, the depletions in $n_\mathrm{H} \approx 10^3$ cm^{-3} clumps like those in the RMC are

unknown; while the set B depletions are closer to those measured in absorption line studies of diffuse interstellar clouds, the set A depletions are typical of those required for dense core chemical models to reproduce measured fractional abundances of species. A key outstanding set of questions in the chemistry and dynamics of star formation is that which concerns the nature of depletion and desorption processes of elemental S, Si, Fe, Na and Mg in translucent and dark clouds; it is remarkable that those elements are so much more depleted in many regions than O, C and N but still have high enough gas phase abundances in those regions for their presence in the gas phase to have significant chemical consequences (see Chapters 6 and 7). We therefore present further results from the chemical calculation yielding x_i, as information about the depth dependence of many other chemical abundances is also provided. Figures 3.3 and 3.4 give results for the fractional abundances of a number of species for a $n_{\rm H}$=1$\times$10^3 cm^{-3}, Set A clump and a $n_{\rm H}$=5$\times$10^4 cm^{-3}, Set A dense core. The model results indicate that other than CO emissions only CH and OH emissions are likely to be dctectable towards RMC clumps with $n_{\rm H}$=1000 cm^{-3}, and also that the CH, OH and CO fractional abundances are not sensitive to $x_{\rm S}$, $x_{\rm Si}$ and $x_{\rm M}$, making the inference of the values of those depletions in such objects a very difficult goal. Unfortunately, values of CH and OH abundances are difficult to infer observationally. A comparison of Fig. 3.4 with Fig. 3.3 shows that M^+ is the dominant ion throughout a dense core, while C^+ is the dominant ion over a large range of A_V in $n_{\rm H}$=1000 cm^{-3} gas. Unlike RMC-type clumps with A_V=3, a dense core with A_V=3 and $n_{\rm H}$=5$\times$10^4 cm^{-3} is likely to produce observable emissions in a number of molecular species other than CH, OH and CO, including HCO^+, N_2H^+, H_2CO, CN, NH_3, CS and possibly HNC and HCN.

Though our results are more extensive than those of previous authors, they are in harmony with those of Le Bourlot et al. (1993b), Flower et al. (1994), and Shalabiea & Greenberg (1995) in regions where comparisons can be made.

3.3 Collapse from $A_V = 3$

We propose that $A_V \approx 2.5$ to 3.0 represents a critical range for the stability of RMC-type clumps. Above this critical range, the level of ionization and hence the level of turbulent support both fall. We do not know what mechanism is most effective in increasing the extinction of a clump so that it is in or above this critical range, but various possibilities exist. These include compression by clump-clump collisions and increases in the interclump pressure caused by stellar winds or a supernova (e.g. Hartquist & Dyson 1997). In any case, in our study of the time dependent dynamics and chemical evolution of the centre of a collapsing clump, initial chemical conditions like those obtaining at A_V=3 in the $n_{\rm H}$=1000 cm^{-3} Set A model of the previous section may be reasonably realistic. Thus, we have adopted such initial conditions for two models of collapsing clumps, and in this section we describe the chemical evolution of a parcel of gas during the collapse phase, in a more realistic but simple version of cloud collapse. At this time our contention that a value between 2.5 and 3 for A_V is a critical one may be viewed as being based on a plausibility argument requiring a more rigorous demonstration through numerical MHD studies of the responses of turbulent clumps to perturbations (see Chapter 8). In any case, the RMC clumps are translucent and dense cores form in the collapse of such objects. Thus, the results of this section are relevant to clump collapse and core formation and evolution. The results presented are for initial conditions that differ from those used previously in investigations of chemistry during collapse but should be considered to be more representative of the chemical state in a typical RMC clump.

In each model, collapse was initially taken to be one-dimensional so that A_V remained at a constant value of 3. Such a collapse at constant A_V is an approximation to the type of collapse found to occur initially along the magnetic field in numerical simulations of the evolution of a cloud in which the magnetic pressure initially is by far the highest pressure (Fiedler & Mouschovias 1993; see section 1.1). The density was taken to be that which results from the collapse from rest of a plane-parallel cloud with a column density of hydrogen nuclei of 10^{22} cm^{-2} and an initial value of $n_{\rm H}$ of 10^3 cm^{-3}, until $n_{\rm H}$ reaches a critical value, $n_{\rm Hc}$. For the results in Fig. 3.5, $n_{\rm Hc}$=2×10^4 cm^{-3} (model 1); for model 2 (see Fig. 3.6), we set $n_{\rm Hc}$=6×10^4 cm^{-3}. Af-

ter $n_{\rm H}$=$n_{\rm Hc}$, collapse was taken to occur at a rate slower than the spherical free-fall timescale, given by equation 2.6, by a factor of

$$6.95\left(\frac{n_i}{10^{-3}{\rm cm}^{-3}}\right)\left(\frac{n_{\rm H}}{n_{\rm Hc}}\right)^{-1/2}, \tag{3.7}$$

in harmony with the object being magnetically subcritical (i.e., supported by the magnetic field) and subsequent collapse taking place at a rate controlled by ambipolar diffusion (Mouschovias 1987). For $n_{\rm H}$>$n_{\rm Hc}$ we set

$$A_V = 0.5 + 2.5\left(\frac{n_{\rm H}}{n_{\rm Hc}}\right)^{2/3} \tag{3.8}$$

in the models, where an interclump medium was assumed to be responsible for the constant contribution to the A_V. For the purposes of our calculation we assumed that the collapse halts at a density of 3×10^6 cm^{-3}, after which the cloud was treated as static. The models incorporate the grain-modified gas phase chemistry described in the previous section. Note that this implies that freeze-out is off-set by desorption. Results are given for both models in Table 3.3, where t_1 and t_2 are the times since collapse began in the cases $n_{\rm Hc}$=2×10^4 cm^{-3} (model 1) and the $n_{\rm Hc}$=6×10^4 cm^{-3} (model 2), respectively. Here, x_1(X) and x_2(X) denote the fractional abundance of species X relative to $n_{\rm H}$ in the two models ($x_1({\rm X})\equiv n_1({\rm X})/n_{\rm H}$), where i represents ions. These exploratory calculations of chemical evolution are the first in which the initial collapse is plane parallel along the field lines, setting up conditions for multidimensional collapse moderated realistically by ambipolar diffusion.

Note that the desorption of unsaturated species is here assumed to eject *all* molecules arriving at grain surfaces (see Williams & Taylor 1996), so that the abundances in Figs. 3.5 and 3.6 are not constrained by freeze-out. Consequently, the late-time peaks in hydrocarbons and related species (see Chapter 4) are not evident. In fact, the results in Figs. 3.5 and 3.6 are similar in character to those of Howe et al. (1996) who showed that reasonable fits to the chemistry in cores A–D of TMC-1 could be obtained if a low effective freeze-out rate is assumed.

In Table 3.3, when the collapse has attained a density of $n_{\rm H}$=2×10^4 cm^{-3}, the calculated fractional abundances for all species are the same in both models. At this point the two models have yet to diverge. After this point, the fractional ionization in model 1, in which the plane-parallel collapse at constant A_V occurs until $n_{\rm Hc}$=2×10^4

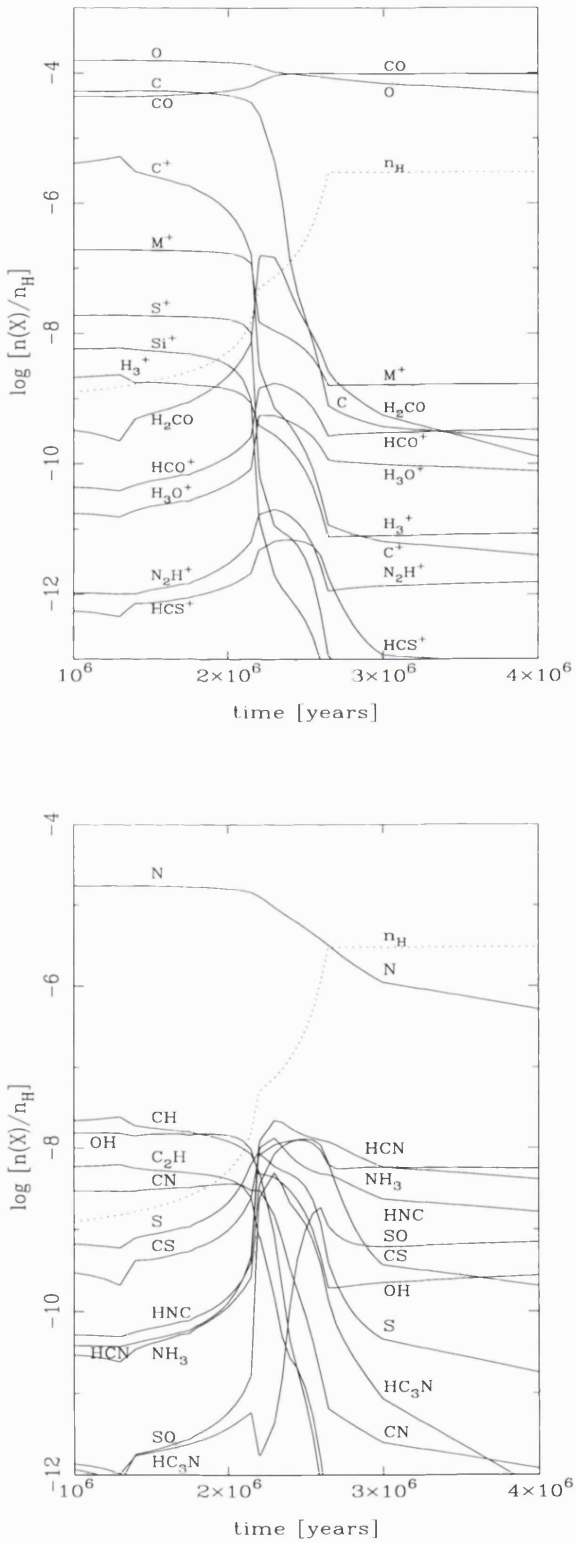

Figure 3.5: Fractional abundances as functions of time since the onset of collapse for model 1 ($n_{\rm Hc}$=2×10^4 cm^{-3}). The dashed curves give ($n_{\rm H}$/10^{12} cm^{-3}).

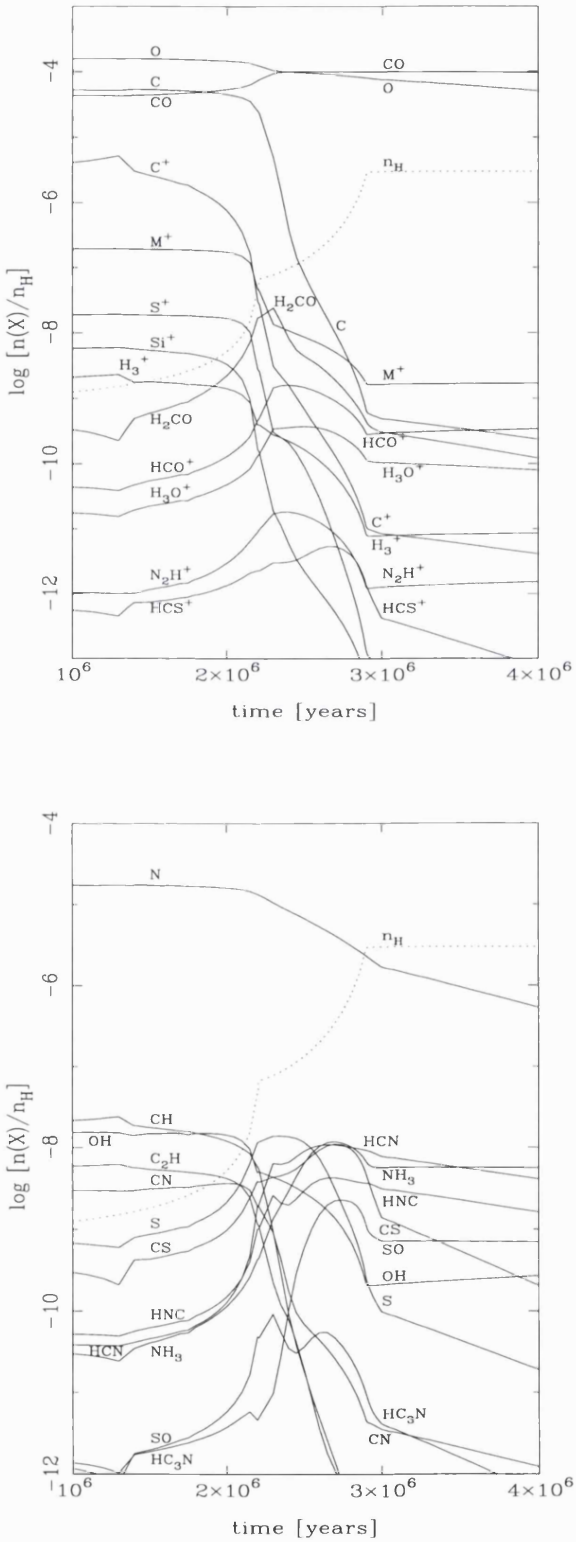

Figure 3.6: Fractional abundances as functions of time since the onset of collapse for model 2 ($n_{\rm Hc}$=6×10^4 cm^{-3}). The dashed curves give ($n_{\rm H}/10^{12}$ cm^{-3}).

Table 3.3: Fractional abundances as functions of $n_{\rm H}$ for two collapse models.

$n_{\rm H}$ (cm^{-3})	2×10^4	7×10^4	2×10^5	5×10^5
t_1 (10^6 yr)	2.15	2.30	2.45	2.55
t_2 (10^6 yr)	2.15	2.21	2.60	2.75
x_1(CO)	6.399(-05)	9.277(-05)	9.830(-05)	9.875(-05)
x_2(CO)	6.399(-05)	7.661(-05)	9.963(-05)	9.948(-05)
x_1(CH)	8.577(-09)	8.711(-10)	1.919(-11)	3.025(-12)
x_2(CH)	8.577(-09)	5.538(-09)	4.828(-12)	7.387(-13)
x_1(OH)	9.808(-09)	4.442(-09)	2.322(-09)	9.937(-10)
x_2(OH)	9.808(-09)	5.144(-09)	2.105(-09)	1.049(-09)
x_1(CN)	3.077(-09)	1.504(-09)	1.816(-10)	4.394(-11)
x_2(CN)	3.077(-09)	1.928(-09)	4.441(-11)	1.923(-11)
x_1(CS)	2.456(-09)	1.101(-08)	1.271(-08)	1.261(-08)
x_2(CS)	2.456(-09)	3.813(-09)	9.366(-09)	1.088(-08)
x_1(SO)	5.854(-12)	4.404(-12)	4.399(-10)	1.587(-09)
x_2(SO)	5.854(-12)	4.987(-12)	1.538(-09)	2.303(-09)
x_1(C_2H)	2.510(-09)	1.523(-10)	2.020(-11)	5.211(-12)
x_2(C_2H)	2.510(-09)	1.118(-09)	3.554(-12)	6.780(-13)
x_1(HCN)	4.762(-10)	2.218(-08)	1.585(-08)	1.332(-08)
x_2(HCN)	4.762(-10)	2.020(-09)	1.067(-08)	1.057(-08)
x_1(HNC)	4.001(-10)	1.335(-08)	6.744(-09)	5.262(-09)
x_2(HNC)	4.001(-10)	1.039(-09)	4.060(-09)	4.159(-09)
x_1(H_2CO)	7.316(-09)	1.519(-07)	2.498(-08)	9.245(-09)
x_2(H_2CO)	7.316(-09)	1.743(-08)	3.120(-09)	1.437(-09)
x_1(NH_3)	2.646(-10)	8.574(-09)	1.253(-08)	1.148(-08)
x_2(NH_3)	2.646(-10)	4.505(-10)	1.042(-08)	1.145(-08)
x_1(HC_3N)	1.668(-11)	5.036(-09)	1.631(-09)	7.510(-10)
x_2(HC_3N)	1.668(-11)	4.723(-11)	5.500(-11)	3.724(-11)
x_1(M^+)	1.212(-07)	4.376(-08)	6.948(-09)	4.368(-09)
x_2(M^+)	1.212(-07)	1.366(-08)	9.742(-09)	7.768(-09)
x_1(C^+)	1.681(-07)	7.368(-10)	2.645(-10)	8.348(-11)
x_2(C^+)	1.681(-07)	2.786(-08)	3.048(-10)	8.494(-11)
x_1(S^+)	1.035(-08)	1.144(-11)	5.705(-12)	1.764(-12)
x_2(S^+)	1.035(-08)	2.649(-09)	2.931(-11)	3.127(-12)
x_1(HCO^+)	2.604(-10)	1.753(-09)	1.241(-09)	7.370(-10)
x_2(HCO^+)	2.604(-10)	5.028(-10)	1.222(-09)	7.683(-10)
x_1(i)	3.095(-07)	1.480(-08)	9.122(-09)	5.345(-09)
x_2(i)	3.095(-07)	7.790(-08)	8.915(-09)	5.330(-09)

cm^{-3}, is lower than in model 2 where $n_{Hc}=6\times10^4$ cm^{-3}. This is a consequence of the visual extinction being lower in model 2, leading to the background interstellar photons continuing to be important for longer than in model 1. This leads to a suppression by photodissociation of the peaks at early times of some species in model 2, which do exhibit early-time peaks in model 1. In addition, greater amounts of C, C^+ and O^+ occur in model 2 than in model 1 at $n_H=7\times10^4$ cm^{-3}. However, one may account for the timescale difference between the two models; model 2 reaches the density of $n_H=7\times10^4$ cm^{-3} earlier than model 1 and then reaches the following displayed density of $n_H=2\times10^5$ cm^{-3} at a later time than model 1.

The late-time abundances of early-time species is reduced in model 2 as a result of the lower visual extinction at $n_H=2\times10^5$ cm^{-3} and the longer time that model 2 takes to reach that density. However, NH_3, SO and CS are seen to be increasing further in abundance in model 2, whilst in model 1 their abundances have already peaked.

In Chapter 4 we argue that the abundances of HC_3N and C_2H will rise at late times in dense cores as depletion occurs; Caselli et al. (1998) have even used the measured fractional abundances of HC_3N in numerous cores to infer the depletions, relative to solar abundances, of C, N and O on the assumption that they did not vary from element to element. Ultimately, to establish reliably that depletion is usually the cause of high abundances of such putative early-time molecules, considerable data about the behaviour of species with abundances that are sensitive to the relative depletions of trace elements must be gathered (see Chapters 6 and 7). Our current results show that for cores in which high fractional abundances of HC_3N and C_2H exist but are not due to high depletions, the ratio of the abundances of those two species will be significant for the inference of how A_V varied with n_H during collapse.

In some regions, the emission from young low-mass stars may have a significant effect on the ionization structures of dense cores (McKee 1989), even though those stars are not strong sources of far ultraviolet (FUV) radiation. For some gas phase abundances of elements such as magnesium and sodium, photons from nearby low-mass stars may maintain a much higher fraction of those metals in ionized states than would be expected on the basis of the sorts of calculations that we have performed.

Non-FUV radiation may be responsible for the fractional ionizations that have been inferred for some dense core material from observational data to be sufficiently large that the ambipolar diffusion timescales are at least 10^7 yr (Myers & Khersonsky 1995). It should be remembered that the results in Fig. 3.4 are for gas that is collapsing directly from an initially much lower density object in a relatively starless region; the results are of most relevance to the chemistry in the cores in which the first stars to form locally are born.

3.4 Conclusions

The sharp decline in fractional ionization at $A_V \simeq 2$–3 is here associated with the distinction between starless and star-containing cores in the RMC, through changes in turbulent support. This concept has led us to perform a preliminary study of the chemical evolution of a collapsing cloud, in which the cloud can first collapse only along the magnetic field lines. As the collapse proceeds, the fractional ionization declines until a multidimensional collapse moderated by ambipolar diffusion ensues. The nature of the collapse dynamics – in particular the density at which multidimensional collapse becomes significant – affects the chemical abundances. We predict that observations can distinguish between the models used and may be used to infer the details of collapse.

Chapter 4

Cyanopolyynes as indicators of late-time chemistry and depletion in star forming regions

In section 1.4 we described a cluster of dense cores in the Taurus – Auriga complex (Fig. 1.2) called TMC-1. A chemical gradient is observed along this object and in this chapter we discuss a variety of different explanations for this gradient. We examine in detail the assumption that some observed molecules can be used to differentiate between different evolutionary stages of star formation and consider the implications of the results to the interpretation of the observed chemistry in TMC-1.

4.1 Introduction

An assumption frequently (but not always) made in the construction of models of the chemistry in dense molecular regions is that all elements more massive than hydrogen (which is normally assumed to be primarily in H_2) are initially in atomic form. The fractional abundances of some molecular species reach pronounced maxima in many such models at times that are a few tenths as long as those required for chemical equilibrium to be reached (e.g. Millar 1990). Species with such maxima are often referred to as "early-time" molecules, while those that have fractional

abundances that increase as equilibrium is approached are sometimes called "late-time" molecules. The timescale for equilibrium to be approached for gas phase fractional abundances of elements more massive than helium being about 10^{-4} with respect to hydrogen nuclei and a cosmic ray induced ionization rate of H_2 of about 10^{-17} s^{-1} is around 10^6 years.

In section 1.4 we described TMC-1, a dense core cluster that contains 5 cores (called A to E) and a young star at the Northern end of the cluster, that lies near core B (see Fig. 1.6) and how a chemical gradient exists across TMC-1. Emission from the cyanopolyynes (HC_3N, HC_5N) is observed to peak at core D (Fig. 1.7) whilst the ammonia emission peaks at core B (Fig. 1.6). Hirahara et al. (1992) and Howe, Taylor & Williams (1996) have argued that core D, in which the cyanopolyynes abundances peak, is dynamically and chemically less evolved than core B, further to the North in TMC-1, in which the ammonia abundance peaks because HC_3N is found in chemical models to be an early-time molecule whereas NH_3 is found to be a late-time molecule. In Fig. 4.1 we display the principal formation routes of HC_3N and C_2H. Clearly, reasonably large abundances of C^+ and CH_3 (or CH_4) must be obtained simultaneously for these formation routes to be effective. A substantial fraction of a chemical timescale must have passed for CH_3 and CH_4 to become abundant, but after the passage of many chemical timescales in undepleted dense gas C^+, CH_3 and CH_4 become rarer as the CO abundance increases (cf. section 2.3.2). The gas phase NH_3 abundance does not decrease significantly with time as long as depletion onto dust grains is either inoperative or counterbalanced by desorption. Thus, Hirahara et al. (1992) have suggested that a North to South propagation of collapse in TMC-1 could account for the young star's Northerly position and core B being more evolved than Core D.

While fully accepting that the Hirahara et al. (1992) interpretation of the chemical variations in TMC-1 is viable (as explored by Howe et al. 1996) Hartquist, Williams & Caselli (1996) offered several alternative conjectures. The ultimate aim is the development of means of discriminating amongst the possible explanations. Here, our more modest goal is the quantitative verification of the validity of part of a speculation advanced by Hartquist et al. (1996), that cyanopolyynes in general and

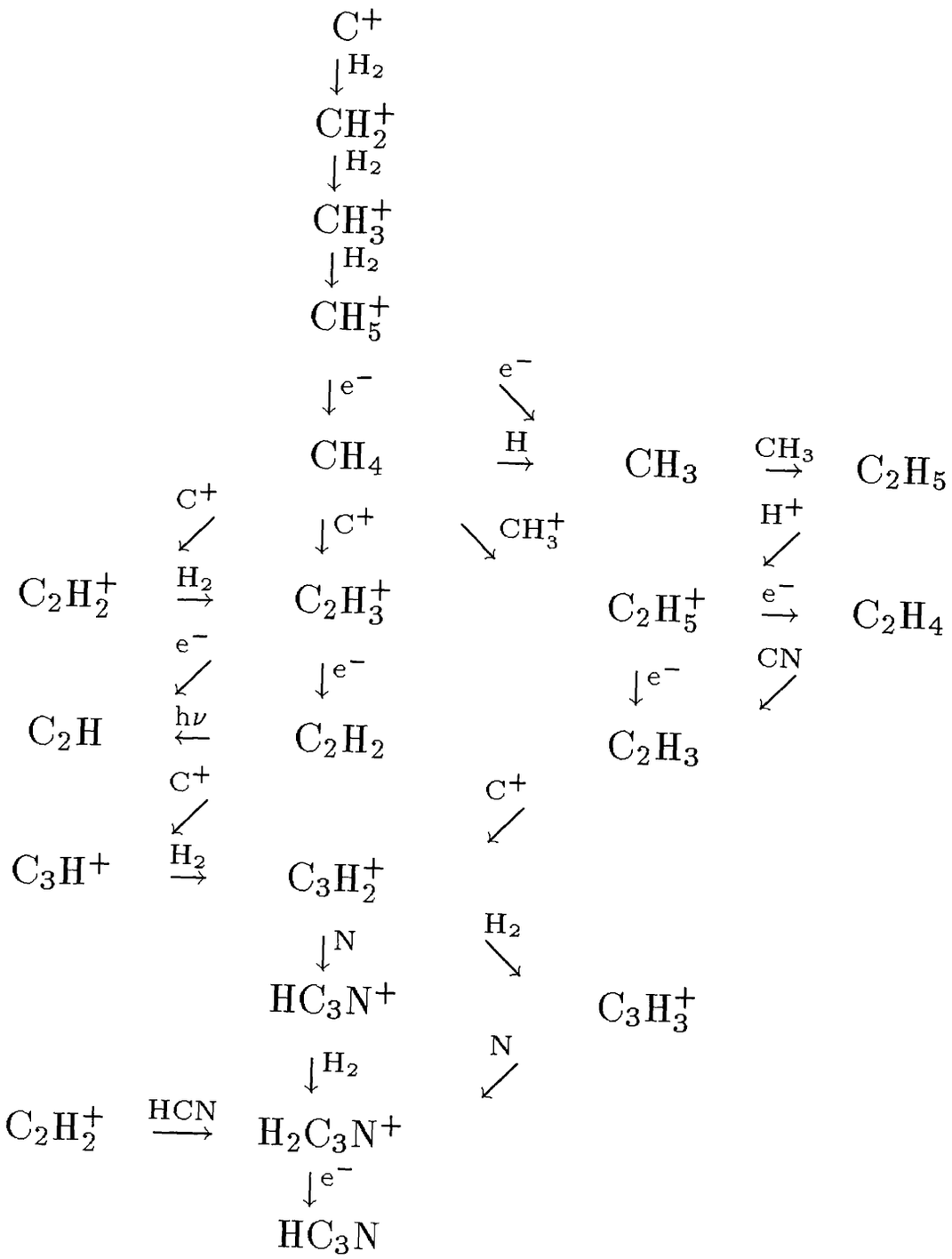

Figure 4.1: Routes to HC_3N and C_2H formation.

HC_3N in particular have later secondary maxima in their fractional abundances, for a variety of conditions, after depletion has become significant. No reliable models for the production of cyanopolyynes more complicated than HC_3N currently exist, and we restrict ourselves to the consideration of HC_3N rather than all of the detected cyanopolyynes. To date, the largest cyanopolyyne to be detected in TMC-1 is $HC_{11}N$ (Bell & Matthews 1985).

However, before we embark on this investigation, we briefly summarise the other proposed explanations by Hartquist et al. (1996) for the observed chemical gradient along TMC-1. In one picture, the higher depletion in core D is attributed to desorption from grain surfaces being more efficient in core B than in core D, a possible consequence of the proximity of core B to the protostar. This proposed explanation is based on the assumption that the chemistry has reached an equilibrium in each core and also relies on the result that the HC_3N abundance increases with increasing depletion. There is a large cloud-to-cloud variation of the minimum visual extinction at which H_2O-ice features (due to vibrational transitions) at a wavelength of 3.1 μm are observable in absorption against embedded young stars. Williams, Hartquist & Whittet (1992) have argued that this implies that desorption must be driven by radiation that is attenuated significantly in material through which the magnitude of the visual extinction is a few to ten. Infrared radiation at a wavelength of 3.1 μm experiences such attenuation. Hartquist et al. (1996) pointed out that the infrared radiation field arising from the nearby star's interaction with diffuse material around it may limit depletion in core B but have little effect on depletion in core D.

Alternatively, the origin of the higher HC_3N abundance in core D is due to formation in the boundary layer between the dense core and the stellar wind. Williams & Hartquist (1991) and Hartquist et al. (1996) have suggested that mixing of stellar wind ions into dense core material in the interface between the stellar wind material and the dense core material in TMC-1 creates conditions favourable for HC_3N production. Though they explored mixing within a somewhat different physical context, the model results of Chièze, Pineau des Forêts & Herbst (1991) are consistent with this suggestion. The peak in the HC_3N is at core D rather than core B because the thickness of a boundary layer and, hence, the degree of mixing (if mixing occurs

at all) increases along the boundary layer.

A noticeable characteristic of the HC_3N emission from TMC-1 is its sharp gradient downwind from the cores (Fig. 1.7). This sharp boundary may be at the location of a wind termination shock positioned just upstream of a contact discontinuity between the stellar wind (mass-loaded with the material that it has ablated and with which it has mixed from the cores) and an ambient intercore or circumcore medium into which the wind-blown bubble is propagating.

We close this section with some comments on the possible dynamics that established the current physical state of TMC-1. These comments are of particular relevance to the "early-time" and boundary-layer models of the production of HC_3N in core D but they bear on other chemical models as well.

The decrease of core density with distance from the star, as found by Hirahara et al. (1992), is compatible with the pressure in each core being equal to the local ram pressure of the stellar wind. Cores in a variety of stages of structural and chemical evolution may have been present before the stellar wind turned on and then been compressed by shocks driven into them by the stellar wind. A shock speed of only 1 km s^{-1} gives rise to a density increase of a factor of about 10, if it propagates into gas at 10 K in which the magnetic pressure is negligible, and it takes approximately 10^5 yr to implode a core having a radius of 0.1 pc. This implosion timescale is shorter than the gas phase chemical timescale, which implies that the chemical composition of a pre-implosion state would survive as depletion becomes significant. For standard assumptions, depletion takes place on a timescale comparable to 10^5 yr at densities around those given by Hirahara et al. (1992) for core D (see Table 1.3). Thus, a less dense pre-implosion core with a chemical age (in the early-time chemical picture) of several times 10^5 yr could have been the site of the production of the HC_3N to be observable in core D for the next 10^5 yr (Hartquist et al. 1996).

Another possibility is that the entire TMC-1 ridge was formed by the stellar wind interacting with an initially more extended clump that fragmented into separate cores due to instabilities arising during the interaction. In this dynamical picture the birth of a star within a single core near a more extended clump triggers the

formation of other cores (e.g Hanawa, Yamamoto & Hirahara 1994).

In the next section we describe the model assumptions. Section 4.3 contains results, while section 4.4 is a discussion of the results and their relevance to studies of TMC-1 and other regions of star formation. In section 4.5 we discuss some new observations of TMC-1 and some initial attempts to reproduce the observed abundances.

4.2 Model assumptions

The time dependent rate equations for the abundances of 196 gas phase species were integrated in each model calculation. The rate coefficients for gas phase reactions were taken from the UMIST rate file (Millar et al. 1997; section 2.6), and we included dissociation by photons produced as a consequence of cosmic ray ionization (as described in section 2.6) and due to photons of the interstellar background radiation field. The cosmic ray induced ionization rate, ζ, was taken to be 1.3×10^{-17} s^{-1}. (We explored the effect of the altering the value taken for ζ on the calculated fractional abundances, by halving and doubling the value of ζ quoted above in turn; very little effect was found on the values obtained for the fractional abundances.) The visual extinction to the nearest point on the edge of a semi-infinite plane-parallel cloud, A_V, was specified (and in some models varied with time as described in the next section) so that the contributions of photons of external origin to the dissociation rates could be evaluated. The contributions of photons of external origin to the dissociation rate of CO was calculated with software developed by Wagenblast (1992). This method accounts for the line self-shielding of CO, as described in section 2.3.2.

We used equation 2.4 for the freeze-out rate of each species X containing an element more massive than helium onto dust. We took the temperature to be equal to 10 K for all runs and we varied the parameter D in equation 2.4, which is used to account for variations in the sticking efficiency and the grain size distribution. Return to the gas phase via desorption processes was assumed not to occur unless we state otherwise.

In some models $n_{\rm H}$ was taken to be fixed as was A_V. In other models $n_{\rm H}$ was

assumed to vary as described by equation 2.6, for spherical free-fall. The parameter B in equation 2.6 was set equal to a value of 1 or less. After $n_{\rm H}$ reached 4×10^5 cm^{-3} it was kept constant. In models with varying $n_{\rm H}$ the value of A_V was also taken to vary with time as described below.

Hydrogen was assumed to initially be almost entirely in H_2. All other elements were taken to be in atomic form initially, except for carbon which was ionized. The initial gas phase elemental fractional abundances relative to hydrogen by number were set to 1.7×10^{-4}, 7.3×10^{-5}, 2.1×10^{-5}, 2×10^{-8} for O, C, N, and S respectively. The fractional elemental abundance of sulphur is often taken to be so small so that model results for the CS fractional abundance are not unrealistically high. The sulphur depletion problem is the topic of investigation in Chapter 6.

4.3 Results

Figure 4.2 shows the time evolution of the fractional abundances of a number of species for a core at a constant density with $n_{\rm H}=2\times10^4$ cm^{-3} and $A_V=10$; $D=0.1$. In this model, which we designate as model 1, a late-time maximum as well as an early-time maximum, occurs in the HC_3N fractional abundance. A pronounced late-time C_2H maximum and noticeable late-time rise in the CH fractional abundance are also evident.

Figure 4.3 shows analogous results for model 5 which is for dense material that increases in density from $n_{\rm H}=1\times10^3$ to 2×10^5 cm^{-3} according to equation 2.6 and for which

$$A_V = 0.7 + 1.5\left(\frac{n_{\rm H}}{n_{\rm H_0}}\right)^{2/3}, \tag{4.1}$$

where $n_{\rm H_0}$ is the initial number density. An intercore medium is assumed to contribute 0.7 magnitudes to the visual extinction while the increase of the visual extinction arising in the core itself is assumed to scale as it would for spherically symmetric collapse. For model 5, $B=1$ and $D=0.1$. Late-time rises are evident here, for the same species as in Fig. 4.2.

Table 4.1 gives the parameters characterizing the various models for which we obtained results. $n_{\rm H_f}$ is the final value of $n_{\rm H}$. If $n_{\rm H}$ is constant for a model then the

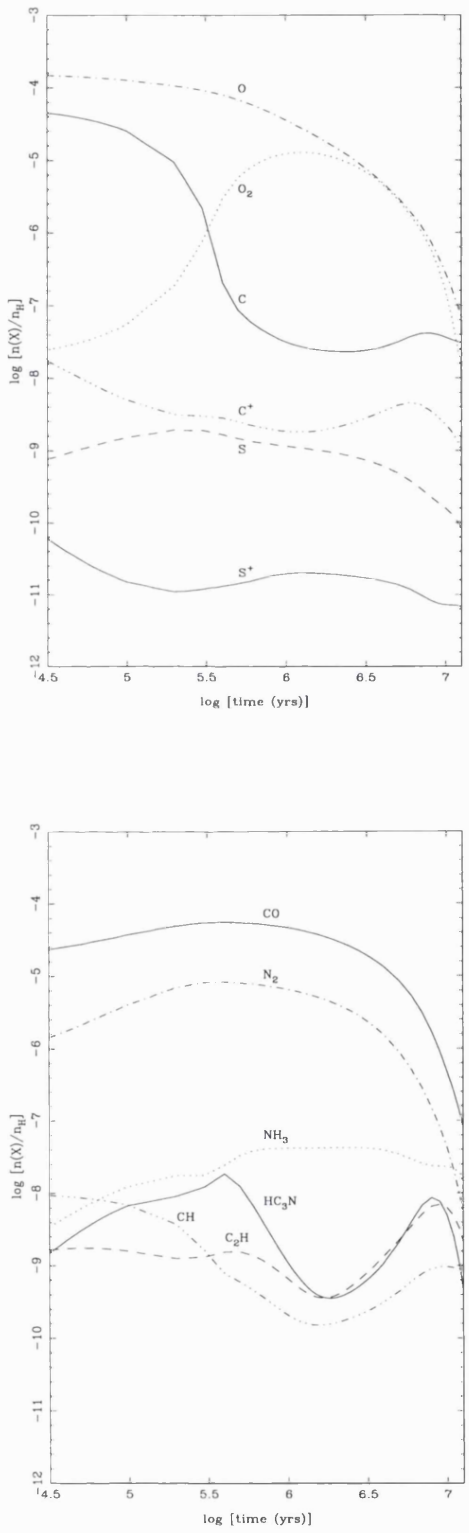

Figure 4.2: Fractional abundances in model 1; $n_{\rm H}$=10^4 cm^{-3}, A_V=10, D=0.1, CO and N_2 are not desorbed from the grain.

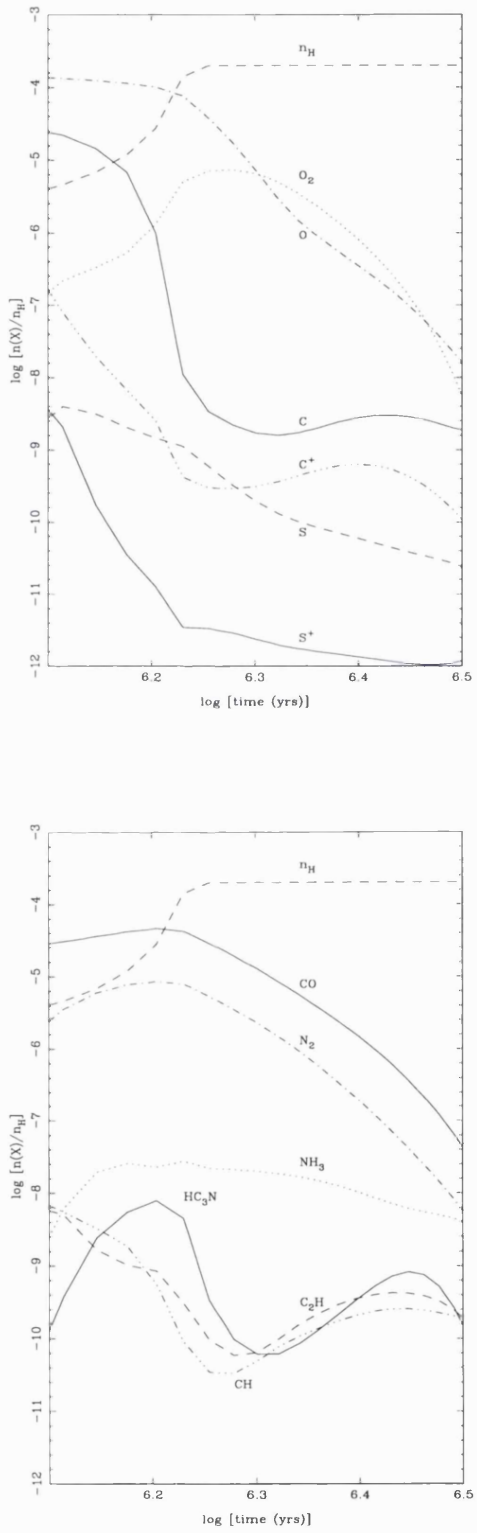

Figure 4.3: Fractional abundances in model 5; $n_{\rm H}$=10^3–2×10^5 cm^{-3}, D=0.1, B=1, A_V follows equation 4.1, CO and N_2 are not desorbed from the grain. The dashed line represents $n_{\rm H}/10^9$ cm^{-3}.

constant value of A_V is given; if n_H is not constant then (4.1) is used to indicate that equation 4.1 was assumed to govern the evolution of A_V and (4.2) is used to indicate that A_V was assumed to evolve as

$$A_V = 0.5 \left(\frac{n_H}{n_{H_0}} \right)^{2/3} . \tag{4.2}$$

The values of D and B for each model are given. CO and N_2 ices are generally more readily desorbed than many other ices including those of H_2O, NH_3 and CH_4 (cf. Hasegawa, Herbst & Leung 1992). Hence, in some models CO and N_2 molecules that strike grains were assumed to be immediately returned unaltered to the gas phase. A column is included in Table 4.1 to indicate for which models this assumption was made.

Due to the screening of CO, by itself and by H_2, from photons of external origin that induce CO dissociation, CO is often the only very abundant molecule in clouds that are not dark. Dense cores may in some cases form in such clouds on a timescale shorter than the chemical timescale. Thus, for two models almost all carbon was assumed to be initially in CO. In both of these models all nuclei more massive than the hydrogen nucleus and not contained in CO were assumed to be initially in atoms and not molecules. A column in Table 4.1 gives $[x(CO)/x_c]_i$, the initial value of the fraction of carbon that is contained in CO.

Table 4.1: Parameters for late-time chemistry models.

Model	n_{H_0}	n_{H_f}	A_V	D	B	$(CO\&N_2)_{freeze-out}$	$(X(CO)/X_C)_i$
1	2.0×10^4	2.0×10^4	10.	0.1	–	yes	0.00
2	2.0×10^4	2.0×10^4	10.	0.1	–	no	0.00
3	2.0×10^4	2.0×10^4	5.	0.1	–	yes	0.00
4	2.0×10^4	2.0×10^4	10.	0.01	–	yes	0.00
5	1.0×10^3	2.0×10^5	(4.1)	0.1	1	yes	0.00
6	1.0×10^3	2.0×10^5	(4.1)	0.1	1	no	0.00
7	1.0×10^3	2.0×10^5	(4.1)	0.1	1	yes	0.99
8	1.0×10^3	2.0×10^5	(4.1)	0.1	1	no	0.99
9	1.0×10^3	2.0×10^5	(4.2)	0.1	1	yes	0.00
10	1.0×10^3	2.0×10^5	(4.2)	0.1	1	no	0.00

Table 4.2: Times of and fractional abundances at HC_3N maxima. t_1 and t_2 refer to the times of the early and late-time HC_3N maxima, respectively. The notation $a(-b)$ refers to $a\times10^{-b}$.

Model	t_1, t_2 (yr)	(CO)	(N_2)	(NH_3)	(HC_3N)	(C_2H)
1	4.0(5)	5.557(−5)	8.307(−6)	2.439(−8)	1.858(−8)	1.540(−9)
	8.0(6)	1.715(−6)	1.514(−7)	2.371(−8)	8.647(−9)	6.559(−9)
2	4.0(5)	6.265(−5)	9.249(−6)	2.275(−8)	1.891(−8)	1.526(−9)
	2.4(7)	4.565(−6)	4.510(−6)	4.317(−8)	4.026(−8)	8.180(−9)
3	4.0(5)	5.760(−5)	8.306(−6)	1.809(−8)	6.232(−9)	2.584(−9)
	8.0(6)	1.876(−6)	1.915(−7)	1.593(−8)	4.462(−9)	2.732(−8)
4	4.0(5)	6.591(−5)	9.790(−6)	2.204(−8)	1.827(−8)	1.208(−9)
	8.0(7)	1.564(−6)	1.300(−7)	2.542(−8)	8.142(−9)	2.891(−9)
5	1.6(6)	4.593(−5)	8.560(−6)	2.284(−8)	7.933(−9)	8.578(−10)
	2.8(6)	3.693(−7)	4.136(−8)	6.110(−9)	8.223(−10)	4.172(−10)
6	1.6(6)	5.729(−5)	9.427(−6)	1.787(−8)	1.095(−8)	1.204(−9)
	8.0(6)	6.348(−6)	5.042(−6)	1.693(−8)	1.387(−8)	9.395(−10)
7	1.5(6)	6.530(−5)	8.516(−6)	3.000(−8)	1.986(−9)	2.636(−10)
	2.9(6)	3.153(−7)	2.338(−8)	4.845(−9)	5.205(−10)	3.591(−10)
8	1.5(6)	6.992(−5)	8.795(−6)	2.777(−8)	2.111(−9)	2.757(−10)
	9.0(6)	5.350(−6)	4.472(−6)	1.695(−8)	1.389(−8)	9.728(−10)
9	1.7(6)	1.955(−5)	6.850(−6)	4.847(−8)	1.674(−10)	9.453(−12)
	2.9(6)	1.092(−7)	2.150(−8)	6.411(−9)	8.264(−11)	8.994(−11)
10	1.7(6)	2.328(−5)	7.711(−6)	4.633(−8)	1.816(−10)	1.011(−11)
	5.0(6)	5.297(−6)	5.735(−6)	2.103(−8)	1.311(−8)	9.519(−10)

Table 4.2 gives results for the times at which HC_3N fractional abundance maxima occur in each model and the fractional abundances of several species at each time for each model. An early-time maximum and a late-time maximum was found in each model.

4.4 Discussion

The model results show that a late-time HC_3N fractional abundance maximum occurs in a dense, dark core in which depletion has taken place. This behaviour

was forecast by Hartquist et al. (1996) from earlier considerations of Hartquist & Williams (1989) that led them to realize that the CH fractional abundance rises as depletion occurs as long as

$$He^+ + CO \rightarrow C^+ + O + He \tag{4.3}$$

is the dominant mechanism for removing He^+. He^+ is produced at a constant rate by cosmic ray induced ionization; hence, as long as reaction 4.3 is its primary removal mechanism the production rate of C^+ remains unaffected by depletion. However as depletion occurs, C^+ is more likely to react with H_2 than with oxygen bearing species leading to an increase in the rates of production of CH and other carbon bearing species that contain no oxygen. In addition the rates of removal of carbon-bearing species containing no oxygen decrease as depletion reduces the fractional abundances of oxygen-bearing species that remove them (see Fig. 2.1).

Comparison of the results for models 1 and 5 shows that the initial HC_3N maximum is slightly less pronounced and later in model 5. This is due in part to the importance of photodissociation in model 5 until A_V reaches a sufficiently high value. That photodissociation induced by photons of external origin is important at low A_V is confirmed by the contrast between HC_3N results for models 1 and 3. Comparison between results for models 1 and 5 also show that the late-time HC_3N maximum is less pronounced in higher density regions.

Results for the pairs of models 1 and 2, 5 and 6, 7 and 8, and 9 and 10 indicate that if CO and N_2 are returned immediately to the gas phase after striking grains, rather than retained as ices on the grains, the late-time HC_3N maximum is much greater. We constructed some models in which N_2 remained on grains but CO did not; in each the late-time HC_3N maximum was not significantly enhanced relative to that in an analogous model in which all species more massive than helium remained on grains.

The contrasts between models 5 and 7 and between models 6 and 8 show that if carbon is initially primarily in CO the early-time HC_3N peak is substantially reduced. The behaviour of C_2H is similar to that of HC_3N, as is that of C_2S and C_3S (see Fig. 4.4).

High late-time HC_3N maxima are achieved only when the freeze-out timescale

is long compared to the chemical timescale. In a model of a collapsing core it must also be long compared to the collapse timescale.

The point made by Hartquist et al. (1996) that the presence of HC_3N in a dense core does not necessarily indicate chemical or dynamical youth is supported by the work reported here. This point is of importance for the study of low-mass star forming cores in general (e.g. Williams, Hartquist & Caselli 1996; references therein) and possibly for TMC-1 in particular (Hartquist et al. 1996). However, CI emission is observed to rise towards the cyanopolyyne emission peak in TMC-1, (Schilke et al. 1995), and the inferred value of the C^0 and CO column density ratios is larger than that of roughly 0.03 that we have found to obtain in the models during the duration of the late-time HC_3N maximum. Schilke et al. (1995) suggested that the CI emission arises in gas at least an order of magnitude less dense than that in which the cyanopolyyne emission originates, in which case the presence of the CI emission probably gives information about an intercore medium rather than the core. Alternatively, the CI emission may be associated with the denser core gas and may have been formed as a consequence of mixing in boundary layers of stellar wind ions and gas in a previous generation of cores and survived until now because that mixture of material collapsed on a timescale short compared to the chemical timescale (Williams et al. 1996; references therein). Considerably more mapping of the CI emission needs to be performed in the direction of the TMC-1 cyanopolyyne peak in order to establish where it forms and its relationship to the cyanopolyynes there.

Another argument in favour of this model may be that the total column density of gas increases with time. Although we have assumed that $n_{\rm H}$ is constant when it reaches the value $n_{{\rm H}_f}$, if times later than this are associated with the phase in which magnetic support is lost from the core, then hydrodynamic models suggest the density will continue to slowly increase. Hence, although the fractional abundance may not change, the actual column of each species may increase significantly at late times.

We conclude this section by suggesting that HC_3N is an excellent species to observe in attempts to detect core collapse if the absence of evidence of such collapse

in NH_3 features is due to depletion (Menten et al. 1984; Rawlings et al. 1992; Nejad, Hartquist & Williams 1994; see section 1.6).

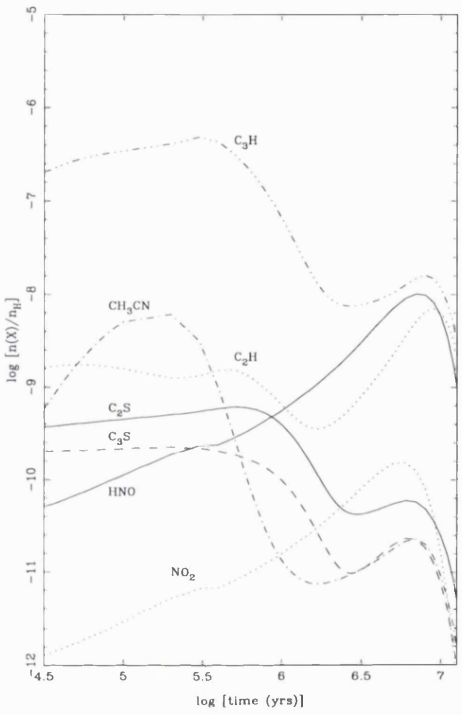

Figure 4.4: Fractional abundances for potential observational pointers from the model.

However, it is difficult to identify other species as unambiguous signals of early-time or late-time HC_3N. Several sulphur-bearing species may turn out to be useful discriminants, but at present we regard the chemistry of sulphur-bearing species as unreliable (cf. Chapter 6). Nitrogen bearing species are also possible indicators: in the models CH_3CN is prominent at early times, whereas various nitrogen hydrides, HNO, and NO_2 are late-time indicators. The molecules C_2H and C_3H potentially provide useful indicators; C_2H peaks at early-time while C_3H peaks at late-time, and the ratio of these species changes by several orders of magnitude from early- to late-time. Figure 4.4 displays the evolution of fractional abundances of these potential observational pointers (results are for model 1). Perhaps the best possible current discriminant is C^0 which also suffers a dramatic decline from an early-time peak (see Figures 4.2 and 4.3). As remarked above, more mapping in CI emission is required.

The existence of a plethora of explanations for chemical variations in TMC-1 requires that more species be mapped because their abundance variations will no doubt differ between models. Also, considerably more theoretical exploration of the models must be undertaken.

4.5 New observations of TMC-1

In Table 4.3 we present some of the very recent values for molecular abundances in core D of TMC-1, determined by Ohishi & Kaifu (1998) through a multi-line study. For comparison we also give abundances determined in previous studies (where available). One can clearly see that the abundance of the hydrocarbons and sulphur-bearing species are enhanced relative to the previously inferred values. In this section we briefly present the results of our initial attempts to improve the correlation between the theoretically calculated abundances for these species and the new observed values.

Table 4.3: Observed fractional abundances in core D of TMC-1. Those in the first column (Abun 1) are from Ohishi & Kaifu (1998), values in the second column (Abun 2) are from Hirahara et al. (1992). The notation $a(-b)$ denotes $a\times10^{-b}$.

Species	Abun 1	Abun 2
C_4H	6(-7)	2(-7)
HC_3N	8(-8)	8.5(-9)
H_2CO	7.5(-8)	–
NH_3	3(-8)	2(-8)
C_3H	2(-8)	–
CCS	9(-9)	5(-9)
CS	8(-9)	1(-8)

As we have described in the previous sections, late-time chemistry and depletion can be used to explain the high abundances of cyanopolyynes and hydrocarbons in core D of TMC-1. Some of the models which we discussed in section 4.4 utilized the limited desorption of species from grain surfaces. Our contention is that a more detailed model of both accretion onto and desorption from grain surfaces should be explored to achieve better agreement between the observed and calcu-

lated abundances (e.g Hasegawa & Herbst 1993). However, in this work, due to time limitations, we used a simple approximation of desorption. We chose only one species, which can be considered to be representative, to be desorbed from the icy grain mantle. Our hope is that this limited first attempt will demonstrate whether this is a viable path to pursue.

Hall & Williams (1995) studied the effects of the injection of small hydrocarbon molecules into the gas phase chemistry of diffuse clouds. The species were assumed to be injected by the erosion of carbonaceous grains at the cloud boundaries. Here, we investigate the effect of the injection of small hydrocarbons on the chemistry in dark cores. In our model we assume that the hydrocarbons are ejected from the grain surface as a result of desorption from the grain mantle, by one of the many possible desorption processes (cf. sections 1.1, 2.5.1).

As argued by Hall & Williams (1995), C_4H_2 is a good candidate species to be injected as its chemistry is relatively well understood. We assumed that the injection was continuous; any C_4H_2 that is accreted onto a grain surface is immediately removed, by some desorption process, and injected back into the gas phase. We did not incorporate the production of C_4H_2 by grain surface chemistry. We employed the same model as described in section 4.2, with modifications to account for the injection. We found that the effect on the calculated abundances was minor, and that only slight increases in the abundances were found. This limited effect was deduced to be partly due to the fact that the chosen injected species, C_4H_2, is never very abundant in the models. We therefore changed the injected species to be C_4H, which also has a reasonably well known chemistry, yet is found (in the models presented in the previous sections) to be more abundant in molecular clouds than C_4H_2 (for model 1 at 10^6 years $x(C_4H)=6\times10^{-8}$ whereas $x(C_4H_2)=9\times10^{-11}$). However, the effects on the chemistry were again not very significant. We are forced to conclude that the high abundances, especially for HC_3N determined by Ohishi & Kaifu (1998) in TMC-1 are not presently understood.

Although this initial study has not proven to be very successful in enhancing the abundances of hydrocarbons further at late-times, we believe that there are several alternative approaches that are worth exploring. Firstly, we suggest that if an in-

stantaneous injection were to be utilized, then the effects on the gas phase chemistry may be more significant, and may further boost the production of hydrocarbons in late-time chemistry. The use of a different species to be injected may also prove to be beneficial. The selection should be treated carefully, with preference given to species that have chemistries that we understand well and that have significant abundances. Another approach may be to consider the effects of ions on the late-time chemistry. This idea follows from the discussion in section 4.1 that the mixing of dense core material with stellar wind ions in a boundary layer may favour the production of HC_3N. We plan to explore these proposals through further modelling.

4.6 New rate for the reaction of N with H_3^+

We now briefly describe a study of the effects on the model chemistry of the inclusion of a new reaction. As we mentioned in section 2.3.4, on the nitrogen chemsitry of interstellar clouds, a new reaction has been proposed to transfer H_2^+ to N. The reaction in question is

$$N + H_3^+ \rightarrow NH_2^+ + H. \tag{4.4}$$

The earlier theoretical study of Herbst, DeFrees & McLean (1987) suggested that this reaction would proceed at a negligible rate; hence it was not included into the UMIST rate file (Millar et al. 1997). However, Scott et al. (1997) have measured this reaction to be rapid at room temperature, with a rate coefficient of k=4.5×10^{-10} cm^3 s^{-1}. Consequently, we performed some calculations to test the effect of the inclusion of this reaction onto the chemistry used in the models presented in the previous sections (also see similar studies by Scott, Freeman & McEwan 1997; Terzieva & Herbst 1998). We included the reaction in our models with a value for the rate coefficient as quoted above. The production of ammonia should be affected by the inclusion of this reaction; the product species NH_2^+ will react with H_2 to form NH_4^+, which then dissociatively recombines with an electron to form NH_3.

We found that the calculated abundances were affected by the inclusion of this reaction. The calculated fractional abundances of NH_2^+, NH_3 and N_2 were all seen to rise by up to two orders of magnitude. However, this occurred at early times

and only for low densities conditions (in models identical to model 9 presented in section 4.2, the increase occurred during the initial collapse). These species are not observed in translucent environments, but are detected in higher density regions (refer to Chapter 5). However, the new, increased abundances achieved are still not detectable. When this reaction is incorporated into a model identical to the dense core model 1 presented in 4.2, the increase is not significant; for NH_2^+, NH_3 and N_2 the rise in the fractional abundance is of the order of 10% or less. The effect is more prominent at early-times and for low density regions as these conditions lead to N being the main nitrogen-bearing species; at higher densities most of the nitrogen is locked into N_2, as we describe in the next chapter. N_2 is formed through rapid neutral-neutral reactions in dense cores, as described in section 2.3.4.

Chapter 5

On the detection of interstellar homonuclear diatomic molecules

In the majority of the work presented in this thesis we have employed theoretical models of the physics and chemistry in star forming regions in attempts to explain existing observational data and to infer the physical parameters and evolutionary state of those regions. In some cases, we have been able to suggest from the model results that the observation of other species would be particularly useful to explore the different types of clouds. In this chapter we diverge from this approach; here we explore whether homonuclear diatomic molecules may be detectable in interstellar clouds. The models that we have used (Chapters 3, 4, 6 and 7) predict that homonuclear diatomic molecules may be abundant in dense, low temperature interstellar clouds (see the description below). However, a homonuclear diatomic molecule does not possess a permanent dipole moment and therefore does not have a pure rotational spectrum. Consequently, low temperature homonuclear diatomics are considered undetectable (though, of course, at high temperature they emit vibrational spectra; H_2 1–0 is the prime example of this). It is possible to infer abundances for these species via related species (see below). However, in this chapter we consider a novel approach that may provide a *direct* measure of the abundance of these species at low temperature; we explore whether homonuclear diatomic molecules may in fact be observable. Such observations would provide an accurate measure of the abundances of these species in cool interstellar clouds, in addition to providing direct limits on

the theoretical models that we utilize.

5.1 Introduction

Table 5.1: Fractional abundance of O_2 and N_2 in different diffuse and dense regions. See text for description of the models. Results are given for a time of 10^6 years.

Region	O_2	N_2
Diffuse*	9.6 (-12)	1.9 (-10)
Dense†	1.2 (-5)	6.5 (-6)

*n_H=10^3cm^{-3}, A_V=1; †=n_H=2×10^4cm^{-3}, A_V=10.

In general, the abundances of homonuclear diatomic molecules in interstellar molecular clouds are poorly known. It is expected from theoretical studies that in dense clouds considerable fractions of the nitrogen and oxygen are in the form of N_2 and O_2. Table 5.1 gives predicted abundances of both N_2 and O_2 in different types of clouds. These results are from the models presented in Chapters 3 (one of the models used to create Fig. 3.2, with n_H=10^3 cm^{-3}, A_V=1, set B) and 4 (model 1). (Figures 4.2 and 4.3 also show the evolution of the N_2 and O_2 abundances.) We can see from Table 5.1 that N_2 and O_2 are important carriers of N and O in dense cores. In fact, N_2 is the main nitrogen-bearing species in dense cores, with the next abundant carriers being NO and N, with fractional abundances of 5.5×10^{-7} and 2.3×10^{-7} respectively (from Chapter 4, model 1). Direct detection of these species via the dipole-forbidden rotational emission is not possible. However, in principle the detection of isotope-substituted molecules (e.g. HD, $^{16}O^{18}O$, or $^{13}N^{14}N$) is possible. Radio and infrared searches for such species have been attempted but so far have not been very successful (although there is a tentative detection of $^{16}O^{18}O$ in L134N by Pagani et al. 1993). Protonated versions of these molecules, N_2H^+ and O_2H^+, have been detected. Measurements of the abundances for these species can be used to infer the abundance of N_2 and O_2 (see Herbst et al. 1977; Womack et al. 1992; Fuente et al. 1993; Benson, Caselli & Myers 1998), as we now illustrate. The primary

formation route of N_2H^+ is

$$N_2 + H_3^+ \rightarrow N_2H^+ + H_2. \tag{5.1}$$

The main destruction routes are

$$N_2H^+ + CO \rightarrow HCO^+ + N_2 \tag{5.2}$$

$$N_2H^+ + e \rightarrow N_2 + H. \tag{5.3}$$

Hence, an expression for the abundances of N_2 can be derived, which depends on the rates of the above three reactions, and the fractional abundance of CO, H_3^+, N_2H^+ and electrons (refer to Benson, Caselli & Myers 1998 for a detailed discussion). A similar relation can be found for O_2 and O_2H^+. Observations of N_2H^+ and O_2H^+ support the view that N_2 and O_2 are abundant in dense clouds (e.g. Benson, Caselli & Myers 1998). This method, though, is limited by the accuracy of the measurements made for several different species and the reliability of the rates for several reactions. Consequently, there is uncertainty in the inferred abundances of N_2 and O_2. Therefore, it would be of great benefit to obtain a direct measure of the N_2 and O_2 fraction in dense cores. We now describe how these species may be observable.

Molecular hydrogen is widely detected in regions of high excitation through its vibrational emission. In principle, other homonuclear diatomics should also emit in a similar fashion, though such emission has not, to date, been detected. However, these excited regions may not be characteristic of the denser regions in molecular clouds, and it would therefore be useful to measure directly the abundances of homonuclear molecules in quiescent dense clouds, and to improve our knowledge of the nitrogen and oxygen budgets in these environments. In this chapter we propose that dense quiescent clouds may be sources of vibrational emissions normally associated with regions of high excitation such as post-shock or photon-dominated regions. The energy for this process is proposed to arise from non-thermal energy sources available even in dark clouds.

In quiescent dense, dark clouds sources of non-thermal energy are rather few. Chemical reactions constitute one possible source (Duley & Williams 1992); in the

case of N_2 such a process might work as follows

$$N_2 + H_3^+ \rightarrow N_2H^+ + H_2 \tag{5.4}$$

$$N_2H^+ + e \rightarrow N_2^* + H \tag{5.5}$$

$$N_2^* \rightarrow N_2 + h\nu. \tag{5.6}$$

Here, N_2^* represents a rovibrationally excited N_2 molecule; internal excitation normally arises in reactions that are sufficiently exothermic. The emission of the photon, $h\nu$ (equation 5.6), occurs via a quadrupole transition, if the gas density is low enough (as it is in the interstellar medium) for collisional de-excitation to be negligible.

Estimates for similar processes involving CO and for emission from H_2 newly formed on dust have been made by Duley & Williams (1992, 1993). Another possible energy source is the cosmic ray induced radiation field (Prasad & Tarafdar 1984):

$$H_2 + \text{c.r.} \rightarrow H_2^+ + e^* \tag{5.7}$$

$$H_2 + e^* \rightarrow H_2^* + e^{*\prime} \tag{5.8}$$

$$H_2^* \rightarrow H_2 + h\nu, \tag{5.9}$$

where H_2^* represents a rovibrationally excited H_2, e^* denotes a fast electron and $E(e^{*\prime})<E(e^*)$. The radiation field arising from equation (5.9) is present even when the ambient interstellar radiation field is totally excluded. This induced radiation field may excite other molecules present. However, it seems likely that direct excitation of homonuclear diatomics by superthermal electrons will be more effective:

$$e^* + X_2 \rightarrow X_2^* + e^{*\prime} \tag{5.10}$$

$$X_2^* \rightarrow X_2 + h\nu' \tag{5.11}$$

where $h\nu'$ is a photon emitted by the internally excited molecule X_2^*.

To explore the effectiveness of this process, in this chapter we estimate the intensity of emission from N_2 molecules in a dense interstellar cloud, ignoring all chemical and radiative excitation. The excitation of rotational and vibrational levels within N_2 is assumed to be caused by the superthermal electrons generated within the cloud by the flux of cosmic rays (cf. equation 5.11). In section 5.2 we estimate the superthermal electron flux, and describe the cascade process following excitation.

In section 5.3 we calculate the intensity of emission in several of the strongest lines and discuss the detectability of this emission.

5.2 Vibrational emission from N_2

The mean energies of electrons generated by the cosmic ray ionization of H_2 in interstellar clouds are around 32–36 eV, (Dalgarno & McCray 1972), but much of the energy is radiated away quickly through excitation of resonance transitions in H and H_2. Electron energies therefore fall rapidly to below 10.2 eV, the excitation energy of H(2p). Energy loss below this value continues mainly through elastic collisions with H_2 and He. The non-thermal electron energy spectrum for energies less than 10.2 eV is therefore assumed in this paper to be determined by these processes. Inelastic or elastic collisions with N_2 leading to energy loss are very minor channels, and do not significantly affect the superthermal electron spectrum.

The rotational emission from cold ($\sim$10 K) interstellar N_2 in its ground vibrational and J=0,1 rotational levels following excitation through collision with a non-thermal electron are:

$$e^* + N_2(0;0,1) \rightarrow e^{*\prime} + N_2(v,J) \tag{5.12}$$

$$N_2(v,J) \rightarrow N_2(v'',J'') + h\nu, \tag{5.13}$$

and the subsequent cascade from state (v,J) will produce a large number of infrared lines. We need to determine which of the many possible transitions will be the strongest and hence the most likely to be observable. We have therefore calculated the *cascade table* of rovibrational transitions for N_2. In relaxing from an excited rovibrational level, the N_2 molecule may cascade through many different levels governed by the selection rules for transitions. The selection rules governing rovibrational transitions are as follows:

$$\triangle v = v - v'' \geq 0 \tag{5.14}$$

$$\triangle J = J - J'' = -2, 0, 2 \; (0 \rightarrow 0 \text{ forbidden}). \tag{5.15}$$

Therefore, pure rotational transitions and pure vibrational transitions are allowed,

although J=0 to J''=0 transitions are forbidden. Consequently, there are many different combinations of allowed cascade routes.

We initially calculate cascade efficiency factors, a set of branching ratios from one initial excited rovibrational level to all the allowable lower levels. From these cascade efficiency factors we construct the cascade table, generated by the summation of the transition probabilities for all allowable routes between two levels giving a total cascade coefficient. In order to calculate the cascade table the vibrational cross-sections and the transition probabilities for decay between vibrational-rotational levels for N_2 in the ground electronic state are needed.

Table 5.2: Vibrational excitation cross-sections for N_2. Absolute values are in cm^2. From Allan (1985). The notation a(-b) denotes $a\times10^{-b}$.

Transition	Energy(eV)	Relative	Absolute
$0 \rightarrow 1$	1.95	1	5.6(−16)
$0 \rightarrow 2$	2.00	0.66	3.7(−16)
$0 \rightarrow 3$	2.15	0.55	3.1(−16)
$0 \rightarrow 4$	2.22	0.37	2.1(−16)
$0 \rightarrow 5$	2.39	0.23	1.3(−16)
$0 \rightarrow 6$	2.48	0.13	7.1(−17)
$0 \rightarrow 7$	2.64	6.8(−2)	3.8(−17)
$0 \rightarrow 8$	2.82	2.8(−2)	1.6(−17)
$0 \rightarrow 9$	2.95	1.1(−2)	6.1(−18)
$0 \rightarrow 10$	3.09	3.9(−3)	2.2(−18)
$0 \rightarrow 11$	3.30	1.1(−3)	6.3(−19)
$0 \rightarrow 12$	3.87	2.5(−4)	1.4(−19)
$0 \rightarrow 13$	4.02	8.0(−5)	4.5(−20)
$0 \rightarrow 14$	4.16	2.2(−5)	1.3(−20)
$0 \rightarrow 15$	4.32	6.5(−5)	3.6(−21)
$0 \rightarrow 16$	4.49	1.6(−6)	9.1(−22)
$0 \rightarrow 17$	4.66	4.3(−7)	2.4(−22)

Table 5.3: Table of vibrational matrix elements for N_2 in the ground state. From Cartwright & Dunning (1974). The notation a(-b) denotes $a \times 10^{-b}$.

	0	1	2	3	4	5
0	-1.241(+00)	4.137(−02)	-2.653(−03)	3.232(−04)	-1.418(−04)	6.902(−05)
1		-1.232(+00)	5.865(−02)	-4.780(−03)	6.652(−04)	-2.159(−04)
2			-1.222(+00)	7.197(−02)	-6.856(−03)	1.026(−03)
3				-1.213(+00)	8.319(−02)	-8.947(−03)
4					-1.203(+00)	9.308(−02)
5						-1.193(+00)
	6	7	8	9	10	11
0	3.788(−06)	-3.703(−05)	2.402(−05)	5.378(−06)	-2.029(−05)	1.295(−05)
1	8.493(−05)	-2.566(−06)	-3.262(−05)	2.585(−05)	-2.793(−06)	-1.234(−05)
2	-3.107(−04)	1.247(−04)	-1.723(−05)	-3.787(−05)	4.118(−05)	-1.503(−05)
3	1.440(−03)	-4.199(−04)	1.570(−04)	-2.326(−05)	-4.172(−05)	4.803(−05)
4	-1.105(−02)	1.878(−03)	-5.322(−04)	1.942(−04)	-3.820(−05)	-3.975(−05)
5	1.020(−01)	-1.315(−02)	2.350(−03)	-6.628(−04)	2.382(−04)	-5.145(−05)
6	-1.183(+00)	1.102(−01)	-1.528(−02)	2.853(−03)	-8.011(−04)	2.812(−04)
7		-1.174(+00)	1.178(−01)	-1.742(−02)	3.381(−03)	-9.494(−04)
8			-1.164(+00)	1.249(−01)	-1.957(−02)	3.941(−03)
9				-1.154(+00)	1.315(−01)	-2.175(−02)
10					-1.144(+00)	1.379(−01)
11						-1.133(+00)
	12	13	14	15	16	17
0	3.740(−06)	-1.346(−05)	1.016(−05)	5.012(−07)	-8.845(−06)	9.245(−06)
1	1.164(−05)	-1.812(−06)	-6.443(−06)	7.469(−06)	-2.672(−06)	-2.923(−06)
2	-1.082(−05)	1.888(−05)	-1.007(−05)	-3.691(−06)	1.119(−05)	-8.988(−06)
3	-2.139(−05)	-6.978(−06)	1.841(−05)	-1.230(−05)	-6.644(−07)	9.322(−06)
4	5.637(−05)	-3.407(−05)	2.418(−06)	1.696(−05)	-1.788(−05)	6.828(−06)
5	-4.192(−05)	6.660(−05)	-4.519(−05)	9.024(−06)	1.634(−05)	-2.145(−05)
6	-6.432(−05)	-4.035(−05)	7.198(−05)	-5.489(−05)	1.852(−05)	1.100(−05)
7	3.317(−04)	-8.229(−05)	-3.721(−05)	7.836(−05)	-6.715(−05)	3.061(−05)
8	-1.112(−03)	3.870(−04)	-1.003(−04)	-3.602(−05)	8.505(−05)	-7.725(−05)
9	4.532(−03)	-1.284(−03)	4.440(−04)	-1.203(−04)	-3.156(−05)	8.902(−05)
10	-2.394(−02)	5.149(−03)	-1.468(−03)	5.077(−04)	-1.445(−04)	-2.529(−05)
11	1.439(−01)	-2.615(−02)	5.799(−03)	-1.668(−03)	5.766(−03)	-1.706(−04)
12	-1.123(+00)	1.496(−01)	-2.838(−02)	6.480(−03)	-1.881(−03)	6.476(−04)
13		-1.113(+00)	1.550(−01)	-3.064(−02)	7.188(−03)	-2.112(−03)
14			-1.102(+00)	1.602(−01)	-3.292(−02)	7.923(−03)
15				-1.092(+00)	1.652(−01)	-3.524(−02)
16					-1.082(+00)	1.700(−01)
17						-1.071(+00)

The cross sections for reaction (5.12) are required as functions of energy. In fact, these cross sections appear only to have been measured at a single energy, 2 eV (Allan 1985). We have, therefore, assumed that the molecule has a distribution of internal excited states as determined by Allan for the excitation of N_2 by 2 eV electrons, and follow the cascade from those states. The values for the vibrational excitation cross-sections are given in Table 5.2.

Explicit measurements of the Einstein A-values for rovibrational transitions of N_2 in the ground electronic state are not available as discussed by Itiwaka et al. (1994). This is due to the longevity of the rovibrational levels of N_2 making accurate experimental measurements of them impractical. Molecular nitrogen is a homonuclear diatomic molecule and therefore has no electric dipole moment; however, its quadrupole moment is non zero. The transition probabilities for quadrupole transitions are smaller than those for dipole transitions by a factor of typically 10^{-8}, which has led to quadrupole transitions being labelled as forbidden. Calculations of the quadrupole matrix elements for N_2 (Cartwright & Dunning 1974) are available for transitions between the vibrational levels v=0,17 and for the rotational levels J=2 to J''=0, which are given in Table 5.3. Through the use of standard equations (e.g. James & Coolidge 1938), the matrix elements are used to determine the Einstein A-values.

5.2.1 Calculating Einstein A-values

The matrix elements of the quadrupole moment are denoted by $R_{v,J,v'',J''}$ (in a.u.), where v, J refer to the upper rovibrational level and v'', J'' the lower. The equation to convert these into A-values is:

$$A_{v,J,v'',J''} = \frac{32\pi^6}{5hc^5} \frac{\nu^5_{v,J,v'',J''}}{(2J+1)^2} R^2_{v,J,v'',J''} f(J,J'') \tag{5.16}$$

where $\nu_{v,J,v'',J''}$ represents the frequency of the transition and $f(J,J'')$ are the branching ratios, where

$$\begin{aligned} f(J,J'') &= \frac{(J+1)(J+2)}{(2J+3)} \qquad \triangle J = 2 \\ &= \frac{2J(J+1)(2J+1)}{3(2J-1)(2J+3)} \quad \triangle J = 0 \end{aligned}$$

$$= \frac{J(J-1)}{(2J-1)} \qquad \triangle J = -2.$$

Equation 5.16 can be simplified to the form:

$$A_{\upsilon,J,\upsilon'',J''} = b\,\nu^5_{\upsilon,J,\upsilon'',J''}\,R^2_{\upsilon,J,\upsilon'',J''}\,f(J,J'') \tag{5.17}$$

where b=1.6796127$\times 10^{-22}$, and the branching ratios $f(J,J'')$ are now

$$\begin{aligned} f(J,J'') &= \frac{(J+1)(J+2)}{(2J+1)^2(2J+3)} && \triangle J = 2 \\ &= \frac{2J(J+1)}{3(2J-1)(2J+3)(2J+1)} && \triangle J = 0 \\ &= \frac{J(J-1)}{(2J-1)(2J+1)^2} && \triangle J = -2. \end{aligned}$$

A computer program was written to convert the quadrupole matrix elements of Cartwright & Dunning (1974) into Einstein A-values using equation 5.17. Cartwright & Dunning (1974) found that the matrix elements were largely independent of J and as a result only presented values for the J=2 to J''=0 case. We therefore take the values of the matrix elements for J=2 to J''=0 cases for all the J dependent cases, for J=0,10.

Table 5.4: Spectroscopic data for N_2 (in cm^{-1}), from Herzberg (1950).

ω_e	$\omega_e x_e$	$\omega_e y_e$	B_e	α_e
2359.61	14.456	+0.00751	2.010	0.0187

The frequencies of the transitions, $\nu_{\upsilon,J,\upsilon'',J''}$, are also needed for the calculation of the A-coefficients. The frequencies of the transitions were obtained from spectroscopic data taken from Herzberg (1950), given in Table 5.4, and the equation,

$$\begin{aligned} E_{\rm tot} &= E_{\rm vib} + E_{\rm rot} \\ &= {\rm hc}\omega_e\left(\upsilon+\frac{1}{2}\right) - {\rm hc}\omega_e x_e\left(\upsilon+\frac{1}{2}\right)^2 + {\rm hc}\omega_e y_e\left(\upsilon+\frac{1}{2}\right)^3 \\ &\quad + {\rm hc}BJ(J+1) - {\rm hc}DJ^2(J+1)^2 \end{aligned} \tag{5.18}$$

where

$$D = \frac{4B_e^3}{\omega_e^3} \tag{5.19}$$

and

$$B = B_e - \alpha_e(v + 1/2). \tag{5.20}$$

From the data described above a complete list of Einstein A-values was produced for rovibrational transitions in the ground electronic state of N_2, for v=0,17 and J=0,10.

In order to test the accuracy of the program, attempts were made to reproduce the A-values found for H_2 by Black & Dalgarno (1976). The transition frequencies were calculated using the same technique developed for N_2 and the spectroscopic data for H_2 was taken from Herzberg (1950). Black & Dalgarno (1976) did not give the exact values of the quadrupole matrix elements which were used in their calculations. In fact, their form of the equation for converting matrix elements into A-values is different to the one that we use, because they performed the integration over quadrupole moments implicitly to find the matrix elements. They used quadrupole moments for H_2 from Dalgarno et al. (1969), in which matrix elements are available. Unfortunately, only for transitions to v''=0. Hence, a rigorous testing was not feasible. Given the restrictions involved in this comparison, the results were acceptable.

5.2.2 Cascade

The calculated Einstein A-values are required to construct the cascade table which we then used to determine which transitions may be observable in dark clouds. We assumed that initially all the N_2 is in the ground vibrational level v''=0 and the ground rotational levels J''=0, 1. An excited electron that has been produced by cosmic ray ionization of H_2 was then assumed to collide and excite the N_2 molecule. The excitation could be into any of the rovibrational levels. Once excited, the molecule eventually relaxes to the ground state. We assumed a rate of one excitation per second, and normalised the excitation using the experimental cross-sections for rovibrational excitation of N_2 at 2 eV (Allan 1985; Table 5.2).

Table 5.5: Table of transition wavelength, Einstein A value, and number of photons r (normalized to the excitation rate of 1 s^{-1}) emitted in each transition of N_2. The notation $a(-b)$ denotes $a \times 10^{-b}$.

Transition	λ	A	r
$v''J'' \rightarrow vJ$	μm	s^{-1}	2eV
$10 \rightarrow 02$	4.3127	1.2845(−08)	2.6692(−01)
$11 \rightarrow 01$	4.2906	1.7573(−09)	2.9668(−01)
$11 \rightarrow 03$	4.3277	2.5247(−09)	4.2624(−01)
$12 \rightarrow 00$	4.2687	5.4082(−10)	2.6684(−01)
$12 \rightarrow 02$	4.2907	7.5301(−10)	3.7153(−01)
$12 \rightarrow 04$	4.3429	1.2759(−09)	6.2953(−01)
$13 \rightarrow 01$	4.2544	5.0509(−10)	2.7068(−01)
$13 \rightarrow 03$	4.2909	5.0188(−10)	2.6896(−01)
$13 \rightarrow 05$	4.3583	8.2908(−10)	4.4431(−01)
$14 \rightarrow 02$	4.2402	4.4384(−10)	2.2377(−01)
$14 \rightarrow 04$	4.2912	3.8009(−10)	1.9163(−01)
$14 \rightarrow 06$	4.3738	6.0468(−10)	3.0486(−01)
$15 \rightarrow 03$	4.2262	3.9157(−10)	1.9380(−01)
$15 \rightarrow 05$	4.2915	3.0688(−10)	1.5188(−01)
$15 \rightarrow 07$	4.3895	4.7099(−10)	2.3310(−01)
$16 \rightarrow 04$	4.2124	3.4977(−10)	4.6412(−02)
$16 \rightarrow 06$	4.2920	2.5765(−10)	3.4188(−02)
$16 \rightarrow 08$	4.4054	3.8268(−10)	5.0779(−02)
$17 \rightarrow 05$	4.1987	3.1632(−10)	3.8227(−02)
$17 \rightarrow 07$	4.2924	2.2216(−10)	2.6848(−02)
$17 \rightarrow 09$	4.4215	3.2019(−10)	3.8695(−02)

Table 5.5: cont'd

Transition	λ	A	r
$v''J'' \rightarrow vJ$	μm	s^{-1}	2eV
$20 \rightarrow 02$	2.1642	1.6599(−09)	7.2166(−03)
$20 \rightarrow 12$	4.3668	2.4256(−08)	1.0546(−01)
$21 \rightarrow 01$	2.1586	2.2419(−10)	8.3252(−03)
$21 \rightarrow 03$	2.1680	3.2909(−10)	1.2220(−02)
$21 \rightarrow 11$	4.3443	3.3187(−09)	1.2324(−01)
$21 \rightarrow 13$	4.3821	4.7674(−09)	1.7703(−01)
$22 \rightarrow 00$	2.1531	6.8123(−11)	7.5700(−03)
$22 \rightarrow 02$	2.1587	9.6067(−11)	1.0675(−02)
$22 \rightarrow 04$	2.1719	1.6776(−10)	1.8642(−02)
$22 \rightarrow 10$	4.3222	1.0214(−09)	1.1351(−01)
$22 \rightarrow 12$	4.3445	1.4221(−09)	1.5803(−01)
$22 \rightarrow 14$	4.3975	2.4091(−09)	2.6771(−01)
$23 \rightarrow 01$	2.1495	6.3087(−11)	7.2395(−03)
$23 \rightarrow 03$	2.1588	6.4029(−11)	7.3476(−03)
$23 \rightarrow 05$	2.1757	1.0996(−10)	1.2618(−02)
$23 \rightarrow 11$	4.3076	9.5400(−10)	1.0947(−01)
$23 \rightarrow 13$	4.3447	9.4782(−10)	1.0877(−01)
$23 \rightarrow 15$	4.4131	1.5654(−09)	1.7963(−01)
$24 \rightarrow 02$	2.1460	5.4973(−11)	5.5209(−03)
$24 \rightarrow 04$	2.1590	4.8491(−11)	4.8699(−03)
$24 \rightarrow 06$	2.1797	8.0904(−11)	8.1251(−03)
$24 \rightarrow 12$	4.2932	8.3835(−10)	8.4195(−02)
$24 \rightarrow 14$	4.3450	7.1781(−10)	7.2089(−02)
$24 \rightarrow 16$	4.4289	1.1416(−09)	1.1465(−01)

Table 5.5: cont'd

Transition	λ	A	r
$v''J'' \rightarrow vJ$	μm	s^{-1}	2eV
$25 \rightarrow 03$	2.1425	4.8095(−11)	4.8733(−03)
$25 \rightarrow 05$	2.1591	3.9150(−11)	3.9670(−03)
$25 \rightarrow 07$	2.1837	6.3574(−11)	6.4417(−03)
$25 \rightarrow 13$	4.2790	7.3966(−10)	7.4948(−02)
$25 \rightarrow 15$	4.3453	5.7953(−10)	5.8722(−02)
$25 \rightarrow 17$	4.4449	8.8914(−10)	9.0094(−02)
$26 \rightarrow 04$	2.1390	4.2604(−11)	7.3159(−04)
$26 \rightarrow 06$	2.1593	3.2870(−11)	5.6444(−04)
$26 \rightarrow 08$	2.1877	5.2114(−11)	8.9489(−04)
$26 \rightarrow 14$	4.2649	6.6072(−10)	1.1346(−02)
$26 \rightarrow 16$	4.3458	4.8657(−10)	8.3552(−03)
$26 \rightarrow 18$	4.4610	7.2240(−10)	1.2405(−02)
$27 \rightarrow 05$	2.1356	3.8213(−11)	6.1760(−04)
$27 \rightarrow 07$	2.1596	2.8343(−11)	4.5808(−04)
$27 \rightarrow 09$	2.1918	4.3994(−11)	7.1104(−04)
$27 \rightarrow 15$	4.2510	5.9757(−10)	9.6581(−03)
$27 \rightarrow 17$	4.3463	4.1955(−10)	6.7808(−03)
$27 \rightarrow 19$	4.4774	6.0440(−10)	9.7684(−03)

We were particularly interested in predicting the intensity of the interstellar transitions v=2 $\rightarrow$ v''=0 and v=2 $\rightarrow$ v''=1. We also considered the v=1 $\rightarrow$ v''=0 transitions, the radiation of which are absorbed in the atmosphere, yet may be detectable with space borne observatories. In order to calculate the intensities of transitions from the levels v=2,1 to lower levels, the populations of all the rotational levels of the v=2,1 levels need to be determined. The population, $n(v, J)$ of any level is determined simply by the rate of cascade into that level (Q_{casc}) from higher initial levels v_0, J_0 and the rate of direct excitation (Q_{direct}) from the ground state:

$$n(v, J) = \frac{Q(v, J)}{A_{v,J}} \tag{5.21}$$

$$Q(v, J) = Q_{\text{casc}} + Q_{\text{direct}} \tag{5.22}$$

Therefore one must evaluate, using the selection rules for quadrupole transitions stated earlier (equations 5.14, 5.15), all the different cascade paths passing through a given v,J state from all the initial v_0,J_0 states.

In order to reduce the computational overheads of this lengthy calculation the contribution from pure rotational transitions was discarded. This is a very good approximation as these transitions have very small A-values because of the extremely long lifetimes of the states. We also limited the number of higher levels which contribute to the cascade, assuming excitation of the states v_0=0,6 and J_0=0,10 only. The cross-section curves of Allan (1985) show that this is a reasonable approximation as cross-sections for v>6 are an order of magnitude smaller than those for the lower lying vibrational levels (cf. Table 5.2).

In the calculation of the cascade coefficient from an initial to a final level, the branching ratios of each transition in the cascade between the two levels must be added to the sum. The contribution of cascades from any allowable combination of the 77 levels, v=0,6 and J=0,10, was included in the calculation. A code to calculate the cascades was produced. This code was extensively tested through the use of dummy input, and an internal test was always made to ensure the sum of branching ratios from any given level was unity.

To calculate the equilibrium populations of the v=2, J and v=1, J levels the program was used to sum the probabilities of arrival in these levels from all the higher

levels, (v_0=3, 6 J_0=0, 10) for v=2 and (v_0=2, 6 J_0=0, 10) for v=1. The Table 5.5 indicates r, the numbers of photons per second emerging in the strongest transitions out of the levels v''=2,1 (for an assumed excitation rate of 1 per second), and a distribution into initial internal excited states before cascade as determined by Allan (1985). In this calculation we have ignored the collisional quenching of the excited levels, that may occur at the highest densities of $n(H_2)=10^5$ cm^{-3}.

5.3 An estimate of the detectability of the emission

We now calculate whether such quadrupole transition lines may be observable. The photon generation rate per unit volume (cm^{-3} s^{-1}) from N_2, v''=2,1 in specific lines is

$$R_p = r \sum_{v''>2,1} \int_E n(e^*, E)\, v(e^*, E)\, \sigma(v'', E)\, n(N_2)\, dE \tag{5.23}$$

where $n(e^*, E)dE$ is the number density of excited electrons with energy in the range E, E+dE, and $v(e^*, E)$ is the corresponding speed; $\sigma(v, E)$ is the cross section for vibrational excitation at energy E, and $n(N_2)$ is the number density of N_2. We assumed that $n(e^*)$ is determined by the cosmic ray ionization rate, ζ, as

$$n(e^*) \sim \zeta n \tau$$

where n is the number density and τ is the mean lifetime of e*, given by

$$\tau^{-1} \sim n \sigma_{el} v(e^*). \tag{5.24}$$

Estimating R_p, using the cross sections of Allan (1985) at 2 eV and equation (5.24), we find, approximately, that

$$R_p \simeq \zeta n(N_2) r \tag{5.25}$$

which, for example, with $\zeta=3\times10^{-17}$ s^{-1}, $n(N_2)$=1 cm^{-3} and r=0.01–0.1 (cf. Table 5.5), gives R_p in the range 10^{-18} – 10^{-17} photons cm^{-3} s^{-1}.

For a cloud of dimension L at a distance d with the cloud just filling the telescope beam, we find that the intensity is given by

$$I \sim 10^{-16}\,\mathrm{Wm^{-2}\mu m^{-1}} \left(\frac{\zeta}{3\times10^{-17}\ \mathrm{s^{-1}}}\right)\left(\frac{n(\mathrm{N_2})}{1\ \mathrm{cm^{-3}}}\right) \times \left(\frac{L}{10^{16}\ \mathrm{m}}\right)^3 \left(\frac{3\times10^{18}\ \mathrm{m}}{d}\right)^2 \left(\frac{10^{-5}\ \mu\mathrm{m}}{\Delta\lambda}\right)$$

where $\Delta\lambda$ is the wavelength resolution. In the case of Core D of TMC-1 at a distance of 140 pc and with a radius of about 0.1 pc, then with $n(\mathrm{N_2})$=10 $\mathrm{cm^{-3}}$ the predicted intensity is about 1.4×10^{-17} $\mathrm{Wm^{-2}\mu m^{-1}}$. If the current detection limit is about 10^{-16} $\mathrm{Wm^{-2}\mu m^{-1}}$ then slightly more favourable parameter choices could make this object detectable in these lines. Other objects may be more favourably placed. In any case, with the likely improvements in sensitivity there is a real hope of detecting this emission from $\mathrm{N_2}$. For other diatomics, the situation may be more favourable; e.g. $\mathrm{O_2}$ is expected to be significantly more abundant than $\mathrm{N_2}$ in interstellar clouds (cf. Table 5.1). Recently, Maréchal, Viala & Benayoun (1997) have performed detailed calculations of the chemistry of $\mathrm{O_2}$ in interstellar clouds, and concluded that several transitions may be detectable by future satellite and balloon borne submillimetre receivers (ODIN, SWAS, PRONAOS-SMH and PIROG 8). Indeed, our work strengthens the predictions of Maréchal et al. , as our process provides more emission than the thermal excitation processes they incorporated into their model.

5.4 Conclusions

The non-thermal tail of the electron distribution in dark clouds generated by cosmic ray ionization will excite rovibrational levels of molecules, in particular, homonuclear diatomics. Emission from these levels is normally regarded as characteristic of regions of high excitation, but should also occur at the levels indicated in section 5.3 in cold quiescent regions. We have made a crude estimate of the intensities of some of the stronger lines from $\mathrm{N_2}$ excited by superthermal electrons, and found these lines to be below the current limit of detectability for a canonical source, core D of TMC-1. Improvements in sensitivity in the near future should bring these lines into the detectable regime. Other excitation mechanisms will, however, also contribute to the emission. Of these, direct formation of $\mathrm{N_2}$ on dust or other diatomics

may be important in denser regions ($n \sim 10^5$ cm^{-3}) where hydrogenation reactions are suppressed in favour of the formation of heavier diatomics (Pickles & Williams 1977). In addition, excitation of the N_2 triplet system by superthermal electrons with energies in the range 6.5–10.2 eV will also decay into the ground vibrational system. The triplet state also overlaps with the Lyman band fluorescence of H_2 and so may couple with the cosmic ray induced radiation field. The predicted intensity of lines is, therefore, likely to be an underestimate.

We therefore believe that a search for 2–1 lines of N_2 and O_2 in nearby cold, dark, dense molecular clouds is recommended. This novel observational approach, if successful, would provide the first direct measure of the N_2 and O_2 fraction in dense clouds. An immediate benefit would be a more accurate limit on the N_2 and O_2 abundances in theoretical models. Furthermore, such measurements could be used to constrain the N, C and O abundances in dense clouds, if other parameters (e.g. $n_{\rm H}$, T, interstellar radiation field) are well defined (Maréchal, Viala & Benayoun 1997). We have an observing proposal in preparation to search for the 2–1 lines of N_2 and O_2 in the well studied object TMC-1, in which N_2H^+ has been detected.

Chapter 6

The sulphur depletion problem

In several of the preceding chapters we have referred to and described the "sulphur depletion problem". In this chapter we investigate this problem and propose a mechanism to explain the unusual behaviour of sulphur.

6.1 Introduction

At visual extinctions of less than two to three magnitudes the dominant ion in a dense core may be C^+, S^+ or a metallic ion, such as Mg^+ or Na^+, depending on the depletions of elemental carbon, sulphur and metals (see Fig. 3.4). The fractional ionization is an important parameter in a dense core, for it determines the rate of ambipolar diffusion and controls the rate at which material from the envelope of a dense core accretes onto a star that forms within it (e.g. Ciolek & Mouschovias 1995; also see sections 1.1, 2.4 and 3.1). Hence, the ways in which carbon, sulphur and metals freeze-out of the gas phase onto grains have consequences for the dynamics of star formation. The depletion of sulphur is also important for observational studies of star formation, as CS is one of the species frequently observed in attempts to find spectral signatures of dense core collapse (e.g. Zhou et al. 1993; cf. sections 1.5 and 1.6).

In diffuse regions, the abundance of sulphur is near its cosmic abundance as shown in Fig. 6.1, from Federman et al. (1993). However, if models of dark cloud chemistry are reliable, sulphur must be depleted by two to three orders of magnitude

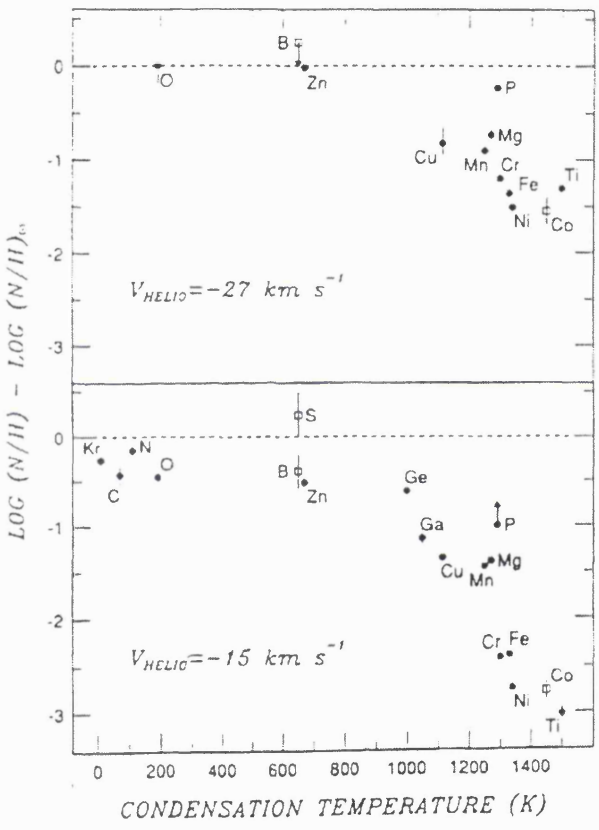

Figure 6.1: Metallic depletion indices for two diffuse cloud components towards ζ Oph as a function of condensation temperature, from Federman et al. 1993.

in dark regions – even where elemental carbon, oxygen and nitrogen are depleted by factors of only a few or less, for computed abundances of CS and other simple gas phase sulphur-bearing species to agree with the measured fractional abundances. This is the sulphur depletion problem: why is sulphur so much more depleted than carbon, oxygen and nitrogen in dense cores?

In this chapter, we propose that sulphur is much more highly depleted in dense interstellar regions than some of the other common elements because in a collapsing translucent clump a large fraction of the gas phase sulphur is in the form of S^+ (see Fig. 3.4 in Chapter 3). In such regions grains typically carry one negative charge (Gail & Sedlmayr 1975; Bel et al. 1989; also see section 2.5.1) and therefore S^+ may collide with grains on a timescale that is an order of magnitude smaller than those associated with the neutral species containing most of the carbon, oxygen and nitrogen in translucent regions. Collisions of ions with grains may well be characterised by higher sticking coefficients (i.e. the probabilities that collisions will result in depletion) than collisions of neutrals with grains, although some controversy exists about this point (e.g. Watson & Salpeter 1972). As collapse continues, the visual extinction increases and the fraction of gas phase sulphur incorporated in neutral species will increase. Thus, any enhancement in the elemental sulphur depletion rate due to S^+ containing a large fraction of the gas phase sulphur will decline as the collapse continues, resulting in enough residual gas phase sulphur for species containing it to be observable for long periods.

We present here the results of model calculations for the chemistry in a collapsing cloud in which S^+ is assumed to be removed from the gas phase at a rate much larger than the rates associated with the removal of neutral species and other ions. We identify removal rates for S^+ and other species which lead to computed abundances compatible with those measured for some simple sulphur-bearing species and other simple species. The material is assumed to have undergone a spherical collapse at the free-fall rate.

Table 6.1: Initial fractional elemental abundances used in the model. The notation a(-b) denotes $a\times10^{-b}$.

He	C	N	O	NA	S	Si
0.07	1 (-4)	2 (-5)	2 (-4)	1 (-6)	3 (-6)	1 (-6)

6.2 The model of sulphur chemistry

Initially, $n_{\rm H}$, the number density of hydrogen nuclei and the visual extinction to the edge of the cloud, A_V, were taken to be 1×10^3 cm^{-3} and 3, characteristic of many clumps in giant molecular clouds (Williams, Blitz & Stark 1995; also see Chapters 1 and 3). Collapse was taken to occur at a the free fall rate, the evolution of $n_{\rm H}$ was governed by equation 2.6, with the parameter B set equal to 1. Collapse was halted at $n_{\rm H}$=2×10^5 cm^{-3}, typical of dense cores. Our assumption is that the cloud is supported at this density by the large-scale magnetic field; a magnetically subcritical dense core is assumed to have formed. The visual extinction obeyed

$$A_V = 0.5 + 2.5\left(\frac{n_{\rm H}}{n_{\rm H_0}}\right)^{2/3}, \tag{6.1}$$

appropriate for spherical collapse of a clump embedded in an interclump medium that contributes 0.5 magnitudes to the visual extinction.

During the collapse, freeze-out of gas phase species j onto dust grains was assumed to occur at a rate given by equation 2.4, that is

$$\Gamma({\rm j}) = 1.1\times10^{-17}{\rm s}^{-1}D({\rm j})A\left(\frac{m({\rm j})}{\rm a.m.u}\right)^{-1/2}\left(\frac{T}{\rm 1K}\right)^{1/2}\left(\frac{n_{\rm H}}{\rm 1cm^{-3}}\right)$$

where equation 2.5 specifies the value of A for neutral species and positive ions, and D(j) describes variations in the sticking efficiency and grain size distribution; m(j) is the mass of a single particle of species j and T is the clump temperature taken to be 20 K. In fact we set D(j)=D^* for all species except S^+. We specify models by giving values of D^* and $D(S^+)$. As during most of the evolution almost all carbon, oxygen and nitrogen are in neutral species the values adopted for quantities such as $D(C^+)$, $D(O^+)$ and $D(N^+)$ have little effect on results, and we have taken only $D(S^+)$ to differ from D^*.

All hydrogen was assumed to be initially in the form of H_2, and all other elements except carbon, sulphur and sodium (which were assumed to be contained entirely in C^+, S^+ and Na^+) were assumed to be initially completely in neutral atomic form. The fractional elemental abundances used initially are given in Table 6.1 (note these are the same as Set B abundances for diffuse clouds specified in Chapter 3). The value for S is consistent with its depletion behaving with density like that of Zn (which has about the same condensation temperature as S) in diffuse clouds (see Fig. 6.1; also see Jenkins 1987).

The model included 217 gas phase species which are connected through 2773 reactions. We took the reactions from the UMIST rate file, which incorporates the sulphur chemistry of Millar & Herbst (1990) (Millar et al. 1997; see section 2.6). We also included dissociation of molecules by photons that arise from the cosmic ray ionization of H and H_2. We adopted a cosmic ray ionization rate of 1.3×10^{-17} s^{-1}. In addition we incorporated dissociation induced by photons of the interstellar background radiation field.

6.3 Results

Table 6.2 is a compilation of measured fractional abundances of sulphur-bearing species in a number of clouds. Comparisons between entries in it and numerical model results presented in the figures in this chapter allow us to identify values of D^* and $D(S^+)$ which are compatible with observations. Figure 6.2 presents results for a model with D^*=0.1 and $D(S^+)$=1 and Fig. 6.3 for a model with D^*=0.1 and $D(S^+)$=2. Each of these models displays a rapid decrease followed by significant plateau in the gas phase CS fractional abundance. The sensitivity of the CS plateau abundance value to $D(S^+)$ is obvious from inspection of the two figures. However, it is clear that the model results for CS are compatible with observations for a choice of $D(S^+)$ which in no way seems unrealistic. For D^*=0.1, significant abundances of species, including sulphur-bearing species, remain in the gas phase for times that are likely to exceed the dense core lifetimes, which are limited by ambipolar diffusion.

The parameters D^* and $D(S^+)$ depend on the sticking efficiency of species onto

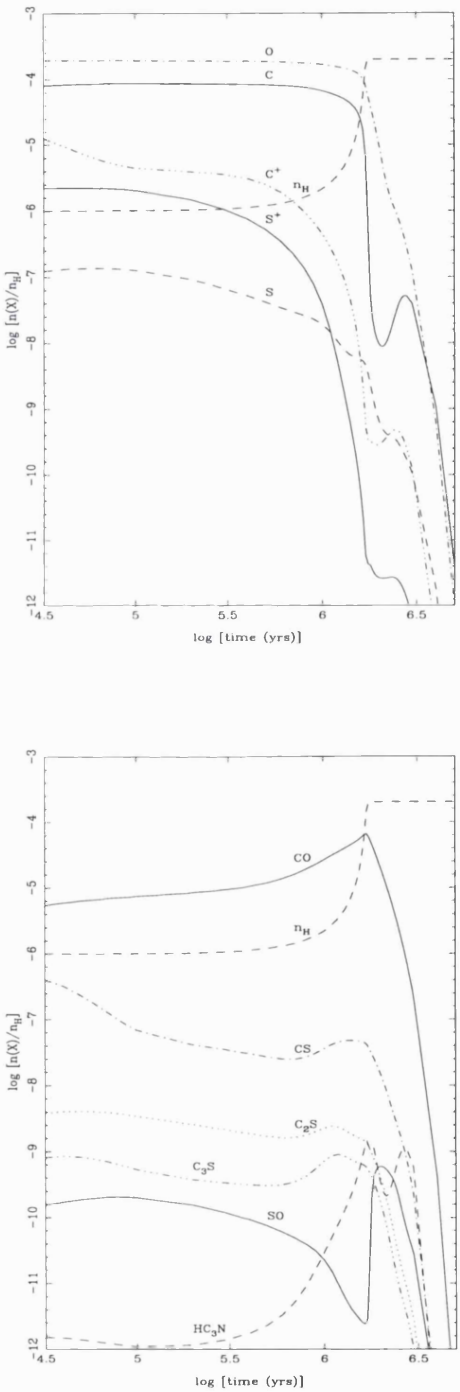

Figure 6.2: Fractional abundances for D^*=0.1, $D(S^+)$=1. The dashed curve gives $n_H/10^9$ cm^{-3}.

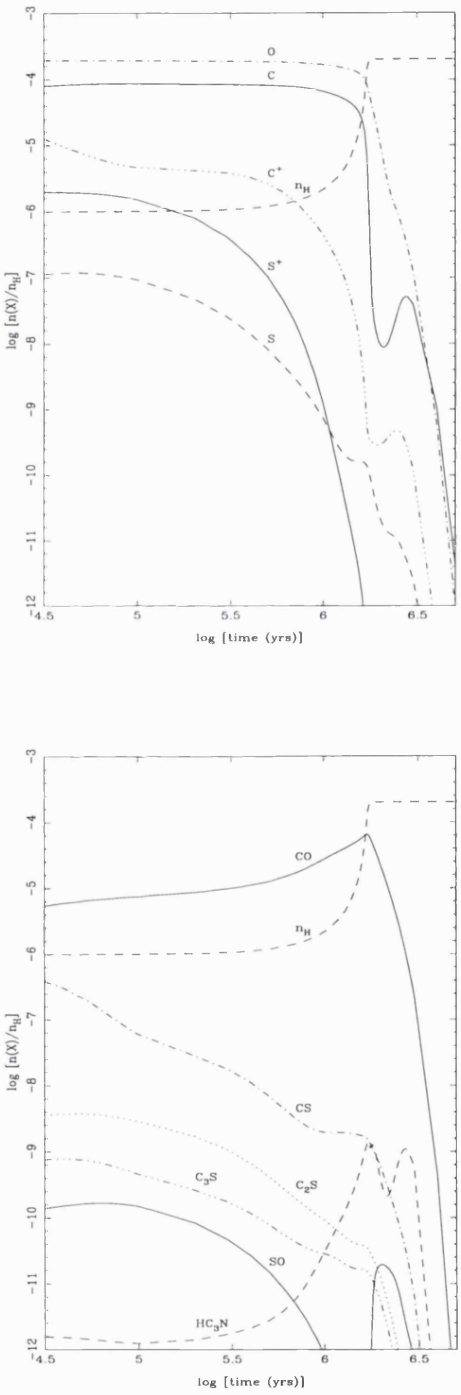

Figure 6.3: Fractional abundances for D^*=0.1, $D(S^+)$=2. The dashed curve gives $n_H/10^9$ cm^{-3}.

Table 6.2: Observations of sulphur-bearing molecules in dense clouds. The notation a(-b) denotes $a\times10^{-b}$.

Object	TMC-1 Core D[a]	TMC-1[b]	L134N[c]	B5[d]	IRAS 16293[e]
CS	8(-9)	1(-8)	7(-10)	1(-9)	1.1(-9)
CCS	9(-9)				
C_3S	1(-9)		<2(-10)[f]		
SO	4(-9)	5(-9)	2(-8)	<2(-9)	3.9(-9)
SO_2		<1(-9)[g]	2(-9)	<7(-10)	1.5(-9)
H_2S			8(-10)		1.5(-9)
H_2CS	8.5(-10)	3(-9)	6(-10)[f]	<6(-10)	1.7(-10)
HCS^+	5(-10)	6(-10)	1(-10)		2(-11)
OCS		2(-9)	7(-9)		7.1(-9)
NS[h]		8(-10)	6(-10)		

[a] Ohishi & Kaifu 1998; [b] Irvine et al. 1985; [c] van Dishoeck et al. 1992; [d] Kelly et al. 1996; [e] Blake et al. 1994 [f] Ohishi et al. 1992; [g] Irvine et al. 1987; [h] Values for NS from McGonagle et al. 1994.

grain surfaces; values for this efficiency lie in the range 0.1–1.0 (Leitch-Devlin & Williams 1985; cf. section 2.5.1). If the parameter D^* is set equal to 1, the freeze-out of species occurs rapidly such that the abundance of species in the gas phase at late times are negligible. The parameter D^* can be considered to be an effective sticking coefficient to account for the competition between freeze-out and desorption processes (cf. section 2.5.1). Therefore, the use of D^*=0.1 to improve the correlation between model results and observations can be considered to be accounting for desorption processes in a limited way.

We now compare the model results with the observations presented in Table 6.2. (Of course, this comparison is limited as the model results presented were not calculated for the conditions pertaining in the individual objects.) For B5 and IRAS 16293 the model results given in Fig. 6.2 at times of $\gtrsim10^6$ years can adequately match the observed values within an order of magnitude. For L134N the model results of Fig. 6.3 appear to provide a better correlation (again within an order of magnitude). However, we can see that neither of the model results given here can account for the observed abundances of sulphur-bearing species in TMC-1. Here we have another failure of our models in reproducing the observed abundances of

species in TMC-1 (cf. section 4.5). Perhaps in TMC-1 the sulphur-bearing species that have been lost from the gas phase by freeze-out are being returned efficiently by desorption processes, resulting in the high observed abundances. In section 4.5 we began an investigation into whether a model that incorporated the injection of mantled species into the gas phase may better produce the unusually high observed abundances of hydrocarbons and cyanopolyynes in TMC-1. From the comparisons made here, it is clear that we should include the desorption of S-bearing species in any such study. We are forced to again conclude that the observed high abundances of hydrocarbons, cyanopolyynes and S-bearing species in TMC-1 is not understood.

The fractional abundances of C_2S and C_3S are more sensitive to $D(S^+)$ than that of CS is. The SO to CS abundance ratio is a particularly sensitive function of time and can be used as a chemical clock.

6.4 Discussion

In section 2.3.5 we described the sulphur chemistry in translucent clumps and dense cores; the sulphur hydrides are not thought to be abundant as the reactions to form them are endothermic. However, the organo-sulphides and sulphur oxides can be formed rapidly by ion-molecule and neutral-neutral reactions. In Chapter 5 we described how homonuclear diatomic molecules are difficult to observe, although we have predicted that it may be possible to detect non-thermal vibrational emission from N_2 and O_2 in cold, dense cores. The cosmic abundance of sulphur is an order of magnitude less than that of nitrogen. Hence, as the intensity of non-thermal vibrational emission from a species is proportional to its fractional abundance (cf. equation 5.26), if the majority of sulphur were to be stored as S_2 in dark cores it would be difficult, but potentially feasible to detect by the process proposed in Chapter 5. However, the main formation routes of S_2 are slow; two involve reactions with S_2H^+ which has a low abundance (cf. section 2.3.5) and a third involves the neutral-neutral reaction of S with SO, which has a low reaction rate coefficient. As a result, the S_2 fractional abundance produced in models of translucent clumps and dense cores is very low, typically of the order of 10^{-14}. If the 'missing' S in dark

Table 6.3: Observations of sulphur-bearing molecules in ices and Hot Molecular Cores. The notation a(-b) denotes $a\times10^{-b}$.

Species	ices[i]	W3 IRS4[j]	W3 IRS5[j]	W3 H_2O[j]	Orion Hot Core[k]
CS		3 (-9)	8 (-10)	5(-9)	5 (-9)
SO		1 (-9)	2 (-8)	7(-9)	1 (-7)
SO_2	< 1 (-7)	1 (-9)	8 (-8)	5(-9)	9 (-8)
OCS	2 (-8)	4 (-10)	3 (-10)	1(-9)	9 (-9)
H_2S	< 1 (-7)	8 (-10)	8 (-10)	5(-9)	<5 (-6)[l*]
H_2CS		3 (-10)	5 (-11)	8(-10)	7 (-10)
HCS^+		<1 (-10)	2 (-12)	$\leq$ 8.9(-11)	

[i] Tielens & Whittet 1997; [j] Helmich & van Dishoeck 1997; [k] Sutton et al. 1995; [l] Minh et al. 1990; * Could be 10–100 times smaller

clouds were to be stored as S_2 it would have to attain a fractional abundance of around 10^{-7}. It is difficult to see how this could be achieved by the chemistry (which is believed to be appropriate); unless perhaps some grain surface reactions could produce large quantities of diatomic sulphur. In addition, S_2 is readily destroyed through rapid reactions with He^+ on a timescale of the order of 10^5 years (see Table 1.3). It therefore seems unlikely that the sulphur depletion problem is due to the chemical model results giving underestimates of the abundance of molecules that are difficult to observe.

Constraints on any model proposed to explain the sulphur depletion problem may be provided by observations of species in the solid phase (see Table 1.2) and in Hot Molecular Cores (HMCs). HMCs are associated with ultra-compact HII regions and massive star formation. These are dense ($n(H_2)\sim10^6$–10^8 cm^{-3}), hot (T$\sim$100–300 K), massive (several tens of $M_\odot$) and small (radius $\leq$0.1 pc) clumps of gas with large visual extinctions ($A_V\gtrsim$100 mag.). They are observed to contain large abundances of hydrogenated species, such as NH_3, H_2O, CH_4 and H_2S (Ohishi 1997; and references therein). These observed species are thought to have been formed in grain mantles which are produced during the cold core collapse phase. They are released into the gas phase when the grain mantles are evaporated, as the core temperature rises due to the associated young, massive hot stars. Table 6.3 provides a summary of observations of sulphur-bearing species in both ices and HMCs.

Hatchell et al. (1998) and Charnley (1997) have attempted to model the observed HMC sulphur chemistry. Initially, an injection of H_2S into the gas phase is specified (which is assumed to have been formed in the grain mantle), and the subsequent chemical evolution is followed. Hatchell et al. (1998) and Charnley (1997) found that an assumed H_2S injection of 10^{-6} (from the Minh et al. 1990 measurements of H_2S in Orion) overproduces most of the observed sulphur-bearing species, by at least an order of magnitude. However, the value of 10^{-6} for H_2S in Orion of Minh et al. (1990) is uncertain, because the H_2 column density is not well known. In addition, Minh et al. assumed that the H_2S transitions are collisionally thermalised, which may not be true. Hence, the measured value may be lower by a factor of 10–100 (Charnley 1997). Therefore, the results of Hatchell et al. (1998) and Charnley (1997) indicate a problem with the S chemistry in HMCs too; in particular with the initial abundance of S that is available for injection into the gas phase. We propose that this problem is related and linked to the S depletion problem in dense cores. We believe that the nature of the S depletion during the cold core collapse phase may be used to explain the S chemistry problem in HMCs.

In the model that is proposed in this chapter for the sulphur depletion problem in dense cores, sulphur is accreting onto grain surfaces rapidly, faster than neutral species are. Therefore the sulphur goes 'down' onto the grain surface before oxygen does; accreted oxygen will undergo H abstractions to form water ice (Williams & Taylor 1996). Consequently, it is conceivable that the S is somehow trapped on the grain surface as a layer below that of the icy mantle, and does not mix with the mantle. This picture could explain the detection of S-bearing species in ices and HMCs with abundances that are very similar to the observations of S-bearing species in dense cores (cf. Tables 6.3 and Table 6.2), as we now describe. The sulphur accreted during the early stages of collapse, before the water ice is formed, is locked beneath the icy mantle. Some S is still available in the mantle to form the observed solid phase species (Table 6.3), as our model predicts the accretion of sulphur bearing species at late times. (Bergin & Langer 1995 found that sulphur-bearing species exhibit large depletions at the later stages of evolution, independent of the grain mantle properties.) It is this sulphur that is observed in ices that can

be released into the gas phase, in some form, in HMCs. We therefore suggest that the model presented here supports the reduction of the initial abundance of sulphur-bearing species that is utilized in the treatment of the chemistry of HMCs; rather than using abundances near the 'cosmic' values, depleted values for S (as measured in dark cores) should be employed.

Caselli, Hasegawa & Herbst (1994) considered the production of condensed phase CO in dense cores, which has a fractional abundance in such regions of the order of $>10^{-5}$ (Whittet & Duley 1991); their model incorporated both gas phase and grain surface chemistry. Caselli, Hasegawa & Herbst invoked large depletions of sulphur in order for their model results to reproduce the observed abundances of condensed phase CO. The sulphur on the grain converts H into H_2 through reactions that involve HS and H_2S; thus reducing the amount of H available to hydrogenate CO and the models were therefore able to reproduce the observed values.

An interesting point noted by Hatchell et al. (1998) is the detection of high fractional abundance of S-bearing species (of the order $>10^{-7}$) towards shocked regions, such as the molecular outflow of L1157 (Bachiller et al. 1997). Hartquist, Oppenheimer & Dalgarno (1980) predicted that shock chemistry may produce large quantities of sulphur-bearing species. In the scheme that we propose, the trapped sulphur can be returned to the gas phase only when grain cores are destroyed by sputtering and/or grains collisions. Perhaps this is occuring in such shocked regions as the molecular outflow of L1157; the freed sulphur can then be involved in the shock chemistry.

An interesting question is the form of the sulphur in the dust, which will naturally depend on the nature of the grain surface, which is not well known (e.g. Williams & Taylor 1996). However, it is believed that the dust contains both silicates (which are amorphous) and carbons (crystalline and amorphous, which is partly hydrogenated); it is not clear if the grains are either silicate or carbonaceous, or whether some sort of core/mantle structure exists (see Williams & Taylor 1996; Dorschner & Henning 1995). Perhaps the S^+ is inserted into the HAC (Hydrogenated Amorphous Carbon) layer, to then be released as C_nS when the grains are eroded. (This picture could be helpful in attempting to model the observed high abundances in TMC-1.) An

alternative route is that the S^+ is inserted into silicons or oxides. However, Klemperer favours that the S is trapped on the grain as sulphuric acid, H_2SO_4 (private communication).

6.5 Conclusions

The freeze-out rate of S ions onto negatively charged grains in molecular clouds is expected to be enhanced over the rate for neutrals. We have computed the abundances of sulphur-bearing species in a single-point model of chemistry, using the two parameters, $D(S^+)$ and D^*, to explore the consequences of relative freeze-out rates of S^+ and other species. The results of these computations support the proposal that the differences between depletions in diffuse clouds and dense clouds are compatible with S^+ being incorporated into dust grains more efficiently than the neutral species.

Chapter 7

Selective depletions and the abundances of molecules used to study star formation

In section 1.5 we gave a detailed account of the observations that have been made of regions of infall and in section 1.6 we discussed theoretical studies of dense core collapse. In Chapter 6 we have explored the behaviour of the sulphur depletion, and seen that it does not follow that of carbon, nitrogen and oxygen. Indeed, there is no reason to expect that all the species will freeze-out at the same rate. Hence, it is worthwhile to investigate the dependences of the fractional abundances of a number of species on the selective depletions of elemental carbon, nitrogen, oxygen and sulphur, as well as metals.

7.1 Introduction

In the last several years numerous detections of line profiles showing putative signatures of the collapse of dense cores to give birth to low mass stars have been reported (e.g. Zhou et al. 1993; Zhou et al. 1994; Mardones et al. 1994; Myers et al. 1995; Velusamy, Kuiper & Langer 1995; Wang et al. 1995; Zhou, Evans & Wang 1996; Gregersen et al. 1997; Mardones et al. 1997), as described in detail in section 1.6. In order to gain insight into the dynamics of collapse, models of the radiative trans-

fer must be constructed to interpret the line profiles (e.g. Choi et al. 1995; Myers et al. 1996). Though in most cases the use of radiative transfer models to interpret the infall signatures has been based on the assumption that the fractional abundances of gas phase species are invariant in the collapsing gas, knowledge of the ways in which the gas phase chemistry varies in the infalling material is also vital.

Pickles & Williams (1981) examined the effects of various combinations of carbon and oxygen depletions on gas phase abundances of a limited number of very simple species. Menten et al. (1984) suggested that the freeze-out onto dust grains of elements more massive than helium has a considerable effect on the gas phase abundances of some species with emissions observed in attempts to detect spectral signatures of infall. Hartquist & Williams (1989) gave arguments that for some ranges of depletion, some species should actually have gas phase fractional abundances that increase with depletion. Rawlings et al. (1992) made a first attempt to identify species that are more likely to show signatures of infall in line profiles if depletion is responsible for the absence of such signatures in many observed NH_3 line profiles (see sections 1.5 and 1.6). In that calculation, the time-dependent and spatially dependent chemical evolution in the collapse of a singular isothermal sphere was followed in each of a large number of fluid elements. The complexity of the dynamical description prevented the investigation of the effects of selective depletion and it was assumed that the sticking coefficients for many species were equal.

In fact, we know that some elements become highly depleted from the gas phase well before others do. For instance, as we have discussed in Chapter 6, sulphur must be a couple of orders of magnitude more depleted in many dense core regions than it is in diffuse clouds in order for the gas phase abundance of CS to be as low as is observed, even though in those same regions the abundances of other species show that the elements carbon, nitrogen and oxygen are each not depleted by more than a factor of a few than in diffuse clouds. As described in Chapter 6, we suggest that this is a consequence of a much higher fraction of sulphur than of those other elements being ionized at moderate densities, in addition to the collision rates and sticking coefficients of ions with grains being higher than those of neutrals. Nevertheless, we do not know for certain why the sulphur depletion differs so much from those of some

other elements. More generally, we do not know how the depletions of the elements vary relative to one another in regions of star formation, making the interpretation of spectral signatures of collapse an area full of uncertainty.

Those uncertainties are unlikely to be removed in the near future by the use of a priori theoretical arguments. Rather, a semi-empirical approach is required to determine the relationship between the depletions of the different elements in star forming regions. In this chapter we perform an initial study of the effects of different elemental depletions on the gas phase chemistry, for a fixed density. This approach allows the exploration of the effect of the consequences of varied initial conditions. No assumptions on the exact nature of the dynamics of infall need to be made. Therefore, a benefit is the simplicity of the models used, as no complex calculations for detailed dynamical models need to be performed. In Section 7.2 we describe and present the results of gas phase equilibrium model calculations for a number of different sets of selective depletions of carbon, nitrogen, oxygen, sulphur and sodium. (We could have chosen magnesium or another such element instead of sodium as the representative metal.) Section 7.3 is a discussion of the results and of an approach that could underlie an observational program to investigate the selective depletions of elements in star forming regions.

7.2 The model and the results

Table 7.1: Standard elemental abundances used in the model.

He	C	N	O	NA	S	Si
0.07	1 (-4)	2 (-5)	2 (-4)	1 (-6)	3 (-6)	1 (-6)

The gas phase abundances of species were calculated for dark regions with $n_{\rm H}$=1$\times$10^5 cm^{-3}, where $n_{\rm j}$ is the number density of nuclei of element j. We define $x_{\rm j}$≡$n_{\rm j}/n_{\rm H}$ and x(k)≡n(k)$/n_{\rm H}$ where n(k) is the number density of species k. The cosmic ray induced ionization rate was assumed to be 1.3$\times$10^{-17} s^{-1} and the temperature to be 20 K. The chemistry was assumed to be a pure gas phase chemistry as described above, and the UMIST rate file (Millar et al. 1997; section 2.6)

was taken as the source of most data. The model included 238 gas phase species which are connected through 2732 reactions. In these models we do not incorporate the freeze-out of species onto the dust grain; instead the depletions are determined at the start of the calculation. As 'standard' elemental abundances with respect to hydrogen we took the values displayed in Table 7.1 (note these are the same values as used in Chapters 3 and 6). The value for $x_{\rm He}$ was the same in all models. To designate a particular model we give each element's symbol in upper case if the corresponding $x_{\rm j}$ is taken to be the 'standard' value, and to be in lower case if the corresponding $x_{\rm j}$ is 1/3 the 'standard' value. For three models we used a value of $x_{\rm O}$ that is 1/9 times the 'standard' value, which is indicated by $_9$. For instance, CNONAS is the one for which all elements are assumed to have their 'standard' abundances, while the model designated cNONAS is the one for which all elements except carbon are assumed to have 'standard' abundances, but carbon has an abundance 1/3 its standard value. cno$_9$nas signifies that the abundances of each of carbon, nitrogen, sodium and sulphur is 1/3 its 'standard' value and the abundance of oxygen is 1/9 its 'standard' value.

Table 7.2 gives the ratio of the value of x(k) in one model to its value in another model for a number of important species and for a number of pairs of models. (Table A.1 in Appendix A gives the values of x(k) for some important species once steady state has been reached in all 35 of the calculated models.)

7.3 Discussion

In Table 7.2, column 7 for CNoNAS/CNONAS shows the well known differences between chemistries in oxygen-rich and carbon-rich environments. As the oxygen abundance is reduced, less carbon is locked into CO and fewer oxygen-bearing species are available to destroy the build up of carbon-bearing species (cf. sections 2.3.2 and 2.3.3). Consequently, large increases are seen in the abundance of C-bearing species (see Watt 1985; Terzieva & Herbst 1998).

The columns to the left of column 7 are for carbon-rich environments and those to the right are for oxygen-rich environments. We shall focus first on the oxygen-rich

Table 7.2: Table of model comparisons for observable species. The notation $a(-b)$ refers to $a \times 10^{-b}$.

	1	2	3	4	5	6	7
	cno$_9$nas	cno$_9$nas	CNo$_9$NAS	CnoNAS	CNonaS	CNoNAs	CNoNAS
Species	Cno$_9$nas	Cnonas	CNoNAS	CNoNAS	CNoNAS	CNoNAS	CNONAS
CH	3.6(−01)	3.2(−01)	7.9(−01)	9.4(−01)	7.8(−01)	1.0(+00)	7.1(+03)
CN	3.4(−01)	7.5(−01)	2.1(+00)	8.4(−01)	8.5(−01)	1.0(+00)	2.9(+03)
CO	9.8(−01)	3.2(−01)	3.3(−01)	1.0(+00)	1.0(+00)	1.0(+00)	6.7(−01)
CS	1.0(+00)	9.5(−01)	9.5(−01)	1.0(+00)	1.0(+00)	3.3(−01)	1.1(+00)
NO	3.9(+01)	1.9(+01)	5.5(−01)	4.2(−01)	1.5(+00)	1.0(+00)	2.3(−02)
OH	2.0(+01)	7.6(+00)	4.4(−01)	9.1(−01)	1.3(+00)	1.0(+00)	2.3(−01)
SO	1.9(+02)	4.1(+01)	2.8(−01)	1.0(+00)	1.6(+00)	3.4(−01)	7.2(−05)
C_2H	6.7(−02)	1.4(−01)	1.7(+00)	8.4(−01)	6.0(−01)	1.0(+00)	2.6(+04)
C_2S	8.3(−01)	1.4(+00)	1.7(+00)	1.0(+00)	1.0(+00)	3.4(−01)	2.5(+02)
H_2O	7.7(+00)	2.1(+00)	2.7(−01)	1.1(+00)	1.0(+00)	1.0(+00)	5.3(−03)
H_3^+	1.7(+00)	2.7(+00)	1.5(+00)	1.1(+00)	1.0(+00)	1.0(+00)	1.6(+00)
HCN	3.8(−01)	9.8(−01)	2.2(+00)	4.1(−01)	8.7(−01)	1.0(+00)	2.5(+01)
HCO	9.9(−01)	8.9(−01)	7.2(−01)	1.0(+00)	7.6(−01)	1.0(+00)	1.3(+01)
HCO^+	3.1(+00)	9.4(−01)	3.6(−01)	1.0(+00)	1.5(+00)	1.0(+00)	8.6(−01)
HNC	2.2(−01)	8.1(−01)	3.0(+00)	3.8(−01)	8.0(−01)	1.0(+00)	1.2(+01)
HNO	3.2(+00)	4.6(+00)	1.2(+00)	3.7(−01)	1.1(+00)	1.0(+00)	4.5(+01)
N_2H^+	2.3(+00)	4.2(+00)	1.8(+00)	3.6(−01)	1.3(+00)	1.0(+00)	2.0(+00)
NH_2	4.5(−01)	2.1(+00)	3.9(+00)	3.5(−01)	1.1(+00)	1.0(+00)	2.2(+02)
OCS	1.2(+00)	4.1(−01)	3.2(−01)	9.8(−01)	8.4(−01)	3.3(−01)	1.6(+00)
SO_2	1.5(+03)	1.6(+02)	1.6(−01)	8.7(−01)	2.0(+00)	3.4(−01)	3.4(−06)
C_2H_2	1.7(+00)	2.3(+00)	1.4(+00)	1.0(+00)	1.2(+00)	1.0(+00)	1.7(+00)
C_3H	2.9(−01)	4.5(−01)	1.5(+00)	1.0(+00)	8.2(−01)	1.0(+00)	1.6(+03)
C_3N	4.7(−01)	5.2(−01)	9.4(−01)	4.0(−01)	8.2(−01)	1.0(+00)	6.0(+03)
H_2CO	4.4(−01)	5.8(−01)	1.1(+00)	9.6(−01)	8.3(−01)	1.0(+00)	7.4(+01)
H_2CS	1.8(−01)	7.1(−01)	3.7(+00)	9.0(−01)	9.4(−01)	3.3(−01)	9.2(+00)
H_3O^+	2.9(+01)	4.1(+00)	1.8(−01)	1.1(+00)	1.8(+00)	1.0(+00)	5.4(−03)
NH_3	3.5(+00)	2.9(+00)	7.8(−01)	4.2(−01)	1.2(+00)	1.0(+00)	1.6(−01)
C_3H_2	3.7(−01)	8.5(−01)	2.1(+00)	1.1(+00)	7.7(−01)	1.0(+00)	4.1(+03)
C_4H	1.6(−01)	4.0(−01)	2.5(+00)	1.0(+00)	9.8(−01)	1.0(+00)	4.2(+04)
CH_2CN	1.3(−01)	2.5(−01)	1.8(+00)	3.8(−01)	1.0(+00)	1.0(+00)	8.7(+02)
CH_4	5.6(−01)	2.9(−01)	6.0(−01)	9.4(−01)	1.2(+00)	1.0(+00)	4.8(+01)
HC_3N	2.6(−01)	8.9(−01)	2.9(+00)	6.0(−01)	9.0(−01)	1.0(+00)	1.3(+03)
CH_3OH	4.6(+00)	7.7(−01)	1.8(−01)	1.0(+00)	1.1(+00)	1.0(+00)	2.9(−01)

Table 7.2: cont'd

Species	8 cNONAS CNONAS	9 cNoNAS CNONAS	10 cNoNAS cNONAS	11 CnONAS CNONAS	12 CNOnaS CNONAS	13 CNONAs CNONAS
CH	1.9(−01)	6.2(+00)	3.2(+01)	1.0(+00)	9.3(−01)	1.0(+00)
CN	8.6(−02)	3.4(+00)	4.0(+01)	6.4(−01)	8.2(−01)	1.0(+00)
CO	3.3(−01)	3.3(−01)	1.0(+00)	1.0(+00)	1.0(+00)	1.0(+00)
CS	2.9(−01)	8.6(−01)	3.0(+00)	9.9(−01)	9.0(−01)	3.3(−01)
NO	2.3(+00)	3.7(+00)	1.6(+00)	1.0(+00)	1.0(+00)	1.0(+00)
OH	2.1(+00)	3.1(+00)	1.4(+00)	1.1(+00)	1.0(+00)	1.0(+00)
SO	3.4(+00)	1.8(+00)	5.3(−01)	1.1(+00)	1.4(+00)	3.4(−01)
C_2H	4.4(−02)	7.4(+00)	1.7(+02)	1.2(+00)	1.3(+00)	1.0(+00)
C_2S	9.5(−03)	3.8(+00)	4.1(+02)	1.4(+00)	1.1(+00)	3.4(−01)
H_2O	1.3(+00)	3.6(−01)	2.7(−01)	1.0(+00)	7.8(−01)	1.0(+00)
H_3^+	2.0(+00)	2.7(+00)	1.4(+00)	1.1(+00)	1.0(+00)	1.0(+00)
HCN	3.4(−01)	1.1(+00)	3.4(+00)	3.4(−01)	4.8(−01)	1.0(+00)
HCO	8.7(−01)	2.7(+00)	3.1(+00)	1.1(+00)	5.4(−01)	1.0(+00)
HCO^+	6.9(−01)	9.1(−01)	1.3(+00)	1.0(+00)	1.7(+00)	1.0(+00)
HNC	2.4(−01)	1.5(+00)	6.1(+00)	3.5(−01)	5.6(−01)	1.0(+00)
HNO	2.3(+00)	1.2(+01)	5.4(+00)	3.7(−01)	1.0(+00)	1.0(+00)
N_2H^+	3.2(+00)	4.5(+00)	1.4(+00)	3.5(−01)	1.2(+00)	1.0(+00)
NH_2	2.2(+00)	1.2(+01)	5.5(+00)	3.7(−01)	1.0(+00)	1.0(+00)
OCS	8.3(−02)	5.0(−01)	6.1(+00)	9.5(−01)	1.2(+00)	3.4(−01)
SO_2	4.5(+00)	1.2(+00)	2.7(−01)	1.0(+00)	1.4(+00)	3.3(−01)
C_2H_2	4.1(−02)	1.7(+00)	4.2(+01)	1.1(+00)	1.2(+00)	1.0(+00)
C_3H	6.5(−03)	1.7(+00)	2.7(+02)	2.2(+00)	1.1(+00)	1.0(+00)
C_3N	4.6(−03)	3.1(+00)	6.7(+02)	7.5(−01)	1.1(+00)	1.0(+00)
H_2CO	2.4(−01)	1.8(+00)	7.3(+00)	1.0(+00)	7.3(−01)	1.0(+00)
H_2CS	3.8(−02)	1.1(+00)	2.9(+01)	1.0(+00)	1.4(+00)	3.4(−01)
H_3O^+	1.6(+00)	5.8(−01)	3.6(−01)	1.0(+00)	1.8(+00)	1.0(+00)
NH_3	1.5(+00)	1.9(+00)	1.2(+00)	3.5(−01)	7.7(−01)	1.0(+00)
C_3H_2	1.2(−02)	1.1(+01)	8.9(+02)	2.4(+00)	7.4(−01)	1.0(+00)
C_4H	1.4(−03)	6.9(+00)	4.8(+03)	2.3(+00)	5.2(−01)	1.0(+00)
CH_2CN	6.3(−02)	7.5(−01)	1.2(+01)	3.4(−01)	7.7(−01)	1.0(+00)
CH_4	1.3(−01)	8.0(−01)	6.1(+00)	9.9(−01)	1.3(+00)	1.0(+00)
HC_3N	6.4(−03)	3.0(+00)	4.8(+02)	7.5(−01)	7.1(−01)	1.0(+00)
CH_3OH	1.9(−01)	3.6(−01)	1.9(+00)	9.9(−01)	9.6(−01)	1.0(+00)

environments as they are generally considered to be more characteristic of Galactic star forming regions.

Column 9 for cNoNaS/CNONaS shows the sensitivity of abundances to the simultaneous change of the depletions of carbon and oxygen by the same amount in an oxygen-rich environment. It was this sensitivity that was considered by Hartquist & Williams (1989) and by Hartquist, Williams & Caselli (1996) who suggested that the HC_3N fractional abundance would increase for some ranges of depletion when the carbon and oxygen depletions were lowered by the same amount, a result firmly established in Chapter 4 and employed by Caselli et al. (1998) in their estimations of depletions in dense cores. The fractional abundances of HC_3N, CN, C_3N, NO and HCO go up roughly inversely proportionally to the depletions of carbon in this case, while the fractional abundance of C_2H increases markedly more.

It is interesting that $x(H_2CO)$ increases somewhat with decreasing x_C for fixed x_C/x_O in an oxygen-rich dark core, while $x(CS)$ and $x(HCO^+)$ remain fairly constant; spectral signatures of infall have most commonly been detected in features of these species (as discussed in section 1.5). Results given in column 13 together with those of column 9 suggest that $x(CS)$ would drop proportionally to x_S, if x_S decreased as x_C and x_O did. Careful analysis of multi-line data of comparable and high enough angular resolution for both CS and HCO^+ towards the same source in principle can yield information about whether x_S decreases with increasing infall velocity and n_H; establishment of the way that x_S varies in infalling gas is important for the analysis of collapse dynamics when only CS data are available.

Column 8 shows that in an oxygen-rich dark core $x(HCO^+)$ does somewhat depend on x_C/x_O. However, the dependence is sufficiently weak that no matter whether the carbon is selectively depleted with respect to oxygen, information about the behaviour of x_S should be obtainable, from data as described immediately above, unless x_C drops very rapidly compared to x_O and x_S. Results in column 8 also indicate the extreme sensitivities of the fractional abundances of a number of species to x_C/x_O in oxygen-rich dark material. $x(HC_3N)$ is roughly proportional to $(x_C/x_O)^{4.6}$ while $x(C_2H)$ goes up approximately as $(x_C/x_O)^{2.8}$ if power law fits are assumed. $x(H_2CO)$ is a weaker function of (x_C/x_O), depending on that quantity to the power

of 1.3. That the nonlinear dependence of the fractional abundance of $x(H_2CO)$ is less pronounced than those of species containing two or more carbon atoms is to be expected, because ion-neutral reactions beyond those in the basic hydrogen abstraction sequence creating CH_3^+ are required for the formation of species containing two or more carbon atoms. These additional ion-molecule reactions lead to the creation of relatively long-lived ions that are the observed precursors of the neutral polyatomic carbon species, but which can be removed in reactions with atomic oxygen (Bettens & Brown 1992). The fractional abundances of a number of other species containing multiple carbon atoms are also very sensitive to (x_C/x_O). Results in column 10 indicate that the sensitivity of the fractional abundances of many of these species to (x_C/x_O) increases as x_O decreases.

Columns 11 and 13 show that many of the commonly observable nitrogen-bearing species have fractional abundances that are roughly proportional to x_N and many of the commonly observed sulphur-bearing species have fractional abundances that are roughly proportional to x_S. Exceptions are HC_3N and C_3N, the fractional abundances of which are each roughly proportional to $x_N^{1/2}$.

Column 12's entries give the responses of fractional abundances to the variations of the fractional abundance of metals in the gas phase, shown by Oppenheimer & Dalgarno (1974) and Elmegreen (1979) to affect the fractional ionization in dark clouds (cf. section 2.4). McKee (1989) has argued that photoionization of the metals affects the fractional ionization in many dense cores, which are formed from translucent clouds (cf. Chapter 3). The fractional abundances of HCN, HNC, C_4H and HCO are amongst the most sensitive to x_{Na} but depend on x_{Na} less strongly than linearly.

Column 2 indicates that, just as in oxygen-rich environments, in carbon-rich environments the fractional abundances of some species increase as x_C and x_O drop by the same amount. The species with fractional abundances varying most rapidly with x_C for fixed x_C/x_O in carbon-rich environments are OH and HNO. The abundance of N_2H^+ increases substantially as x_C drops with a constant value of x_C/x_O maintained whether the environment is oxygen-rich or carbon-rich.

Results in column 1 show marked increases in the fractional abundances of some

species containing no carbon and large decreases in the fractional abundances of some carbon-bearing species if x_C is reduced and x_O remains constant in a carbon-rich regions. As one would expect, roughly opposite but not so dramatic changes occur when x_O is reduced and x_C is held fixed in a carbon-rich environment as demonstrated in column 3.

Columns 4, 5 and 6 give results that show the dependences of fractional abundances to variations in x_N, x_{Na} and x_S, respectively, in carbon-rich dark material. Comparison of these values to those found for oxygen-rich dark material, columns 11, 12 and 13, reveal that the results for these species do not differ greatly from the carbon-rich to oxygen-rich cases.

7.4 Conclusions

We have investigated the dependences of the fractional abundances of a number of species on the selective depletions of elemental carbon, nitrogen, oxygen and sulphur, as well as metals. This has been achieved through the use of pseudo-time-dependent models. Calculations of equilibrium chemistry for pure gas phase models were made for a fixed density. This approach reduced the complexity of the models used and allowed conclusions to be inferred with no reference to the exact nature of collapse.

The species that are most commonly observed in searches for infall signatures are ^{13}CO, $C^{18}O$, CS, C_2S, HCN, C_3H_2, H_2CO and HCO^+ (cf. section 1.5). Of the species that produce the emission features, HCO^+ is the one having the abundance least dependent on the selective depletions of the elements. If all observational factors (e.g. angular resolution, accessibility of line, signal-to-noise) were the same for all species, HCO^+ would clearly be the molecule having emission features that should be observed in attempts to study collapse dynamics.

However, observations at lower frequencies than those associated with HCO^+ transitions may be desirable because of the wider availability of telescopes, especially interferometers, with which transitions can be detected for molecules having rotational constants smaller than that of HCO^+ (Table 7.3 gives rotational constants for some of the most commonly observed species in attempts to detect infall

Table 7.3: Table of rotational constants (in MHz) for species used to detect infall. From Encrenaz et al. (1992) and references therein.

CS	C_2S	HCN	C_3H_2	H_2CO	HCO^+
24495.6	6477.8	44316.0	10588.6	38836.05	44594.4

signatures). Then, because of their different dependences on selective depletions, several different species could be observed, allowing the inference of the evolution of the selective depletions in the collapsing material and the probing of the collapse dynamics. In principle, observations of C_3H, C_4H and H_2CO (which does not have a small rotation constant but does have observable transitions at 6 cm) should enable the derivation of the evolution of the selective depletions of carbon and oxygen, as well as provide information about collapse dynamics. If data were also obtained for HC_3N and C_2S, the evolution of the selective depletions of nitrogen and sulphur would also be derivable. Of carbon, nitrogen, oxygen and sulphur, sulphur is likely to be the element whose selective depletion is most likely to be like that of metals, which as stated above are important in controlling the ionization structure, which in turn, through its influence on the ambipolar diffusion rate, greatly affects the collapse dynamics.

The abundances of a number of the species, including C_2H, which have abundances that are very sensitive to the elemental depletions, also depend on the ionization rate (Krolik & Kallman 1983; Gerin et al. 1997). Therefore, any attempt to infer selective depletions from observations in the manner that we are suggesting should include the use of data for both the deuterated and protonated varieties of a species to gain information about the fractional ionization (e.g. Caselli et al. 1998; Williams et al. 1998; cf. section 2.4).

In conclusion, we stress again that behaviours of the selective depletions during collapse must be taken into account in the interpretation of emission profiles to probe the dynamics. The results that we have given point to HCO^+ being a very suitable species to be the focus of observational studies of collapse. However, the results given in Table 7.2 can also be used to infer other species with which collapse

dynamics could be investigated. These species, as mentioned above are: C_3H, C_4H, H_2CO, HC_3N and C_2H. These depend differently on the selective depletions of the elements. Hence, studies of collapse dynamics using these species would also yield information about the rates at which various elements become depleted in the infall regions.

We intend to perform a detailed examination of both the production and removal mechanisms for observationally important species, in an attempt to establish analytical expressions for the behaviour of the fractional abundances with depletion. Such expressions could then be used in the interpretation of observations. However, these observations would need to consist of high sensitivity and high resolution maps, for a number of different species, for sources that have high depletions that increase towards their centres. The work presented here can therefore be considered to be the precursor of a future detailed investigation, to involve both theoretical and observational studies (see Chapter 8).

Chapter 8

Conclusions and future work

Herein we summarise the conclusions presented in the preceding chapters, and outline possible future work.

Chapters 1 and 2 gave a detailed introduction to the current theory of star formation and to the physical and chemical processes that control and regulate the evolution of star forming regions. In these chapters many questions about the star formation process arose; this work has attempted to address some important problems. A theoretical approach has been employed; through the use of physical and chemical models, attempts to interpret existing observational data of star forming regions have been made. The results obtained have been used to infer the physical conditions and evolutionary states of such regions. A key aspect that has been investigated is the role of the gas–dust interaction, and its effects on the physical properties of interstellar gas.

In Chapter 3 the role of the fractional ionization in controlling the turbulent support of translucent clumps in giant molecular clouds was investigated. It was determined that a sharp decline occurs in the fractional ionization at visual extinctions of 2 to 3 magnitudes. This extinction is identified with the critical value for clumps in the Rosette Molecular Cloud: clumps with A_V above $\sim$3 may contain embedded stars, while those with extinction below this value do not. Therefore, it is established that a minimum column density may be a requirement for star formation; when this value, of $N(^{13}\mathrm{CO})\simeq 10^{16}$ cm^{-2}, is exceeded a star may be born. In addition, we found that observations of such objects may provide a way to probe

how the collapse proceeds; in particular to determine the critical density at which the collapse can occur both perpendicular and parallel to the magnetic field lines.

To extend these results our aim is to develop a simple minimal model of the chemistry controlling the fractional ionization in a clump; as a function of incident radiation field, position in the clump and clump density. Such analytic expressions matching the results of the larger models will then be used in time-dependent, one-dimensional and two-dimensional dynamics codes to analyse the dissipation of magnetohydrodynamic (MHD) waves and their role in supporting clumps against collapse. We hope to be able to determine the wave energy input rate required for clump support as a function of central $n(H_2)$ and A_V. Currently, it is not known how the turbulent waves that support the clumps are generated (e.g. see Scalo 1987). We propose to employ a treatment similar to that of Martin et al. (1997) who used the WKB approximation, but did not adopt an ionization structure characteristic of clumps.

In Chapter 4, we have established that in addition to the standard "early-time" HC_3N maximum found for many situations in which elements other than hydrogen are initially in atomic form, a secondary maximum occurs for a variety of conditions after depletion has become significant. The secondary maximum can be sufficiently large and occur for a sufficiently wide range of physical conditions that the assertion that the observed presence of high fractional abundances of cyanopolyynes implies chemical and dynamical youth for the cyanopolyyne emission peak in TMC-1 and other star forming regions may not be secure. HC_3N may therefore be a good species to use in searches for infall signatures. In addition, we attempted to model the very recent observations of TMC-1 by Ohishi & Kaifu (1998). Unfortunately this brief initial attempt was not very successful, yet suggests that furthering the approach adopted may prove to be more fruitful. We aim to explore the various suggestions put forward in Chapter 4 through the use of more sophisticated models in the near future.

We have calculated in Chapter 5 that homonuclear diatomic molecules (which have no pure rotational spectrum), may be detectable in cold, dense cores through their rovibrational emission. We are involved in the preparation of an observing

proposal to search for the 2–1 lines of N_2 and O_2 in cold, dense interstellar clouds. We hope that the various other attempts to detect interstellar O_2 (e.g. by SWAS) will prove successful in the near future. Once accurate measurements of the O_2 and N_2 abundances in dense clouds are available we will review the chemistry of these molecules that the models currently utilize.

In Chapter 6 we considered the sulphur depletion problem and proposed that the fact that much of the sulphur is in S^+ in translucent clumps (n_H<10^3 cm^{-3}) plays a significant role in why it is so depleted in denser sources. Ions collide more rapidly with grains and may stick more efficiently to them than neutrals. As a clump collapses, sulphur may therefore become depleted in it more rapidly than elements which are not primarily ionized in translucent material. Eventually in the collapse, gas phase sulphur will become contained mostly in neutral species, which in our picture leads to a large decrease in its depletion rate and a remnant gas phase elemental fractional abundance high enough for sulphur bearing species in dense cores to be detectable. The nature of the sulphur in the dust will be the subject of future research (see also Klemperer & Scappini 1998). Once the more accurate multifluid MHD collapse models are established (the development of which we described above) we will re-address this problem.

Chapter 7 investigated the dependences of the fractional abundances of a number of species on the selective depletions of elemental carbon, nitrogen, oxygen and sulphur, as well as metals. We determined that HCO^+ has a fractional abundance that is least sensitive to the selective elemental depletions; for this reason it is a particularly appropriate species to study in efforts to diagnose collapse dynamics in star formation from the analysis of infall signatures in spectral line profiles. We also suggested a combination of molecules that could be the focus of observations aimed at the investigation of collapse dynamics; comparisons of the profiles of spectral features of these species would also give insight into the behaviours of the selective depletions of the different elements in the infalling gas. We intend to embark on a joint theoretical and observational study to further these results (see Chapter 7), through an extensive collaboration with both theoreticians and observers. We intend to establish analytical expressions for the behaviours of the fractional abundances

with depletion for the observationally important species that this work has determined. These expressions would then be used to interpret the observations that we propose to also perform; to determine the correlations between the depletions of different elements. An important long-term application is to utilize the results obtained to study the core collapse dynamics from spectral signatures of infall to form stars.

Appendix A

In this section we present further results from Chapter 7. Overleaf are tables which give the values of $x(\mathrm{k})$ for some important species once steady state has been reached, for all 35 of the calculated models. To briefly recap on the notation used (which is described in detail in section 7.2). An element's symbol is given in upper case if the initial fractional abundance used was taken to be the 'standard' value (see Table 7.1). If the element's symbol is given in the lower case, this signifies that the initial fractional abundance used was 1/3 the standard value. In three models we adopted a value for the oxygen abundance that is 1/9 times the 'standard' value. These models are indicated through the use of o_9. To illustrate this, consider the model label CNONAS; this model uses standard values for all the elemental abundances. However, $\mathrm{cnona_s}$ indicates that all the elemental abundances used are 1/3 of the standard value.

Table A.1: Fractional abundances of observable species at steady-state. Results are displayed for all 35 models. The notation $a(-b)$ refers to $a \times 10^{-b}$.

Species	CNONAS	CNONAs	CNOnaS	CNOnas	CNoNAS	CNoNAs	CNonaS
CH	6.0(-12)	6.0(-12)	5.6(-12)	5.6(-12)	4.2(-08)	4.2(-08)	3.3(-08)
CN	1.2(-11)	1.2(-11)	1.0(-11)	1.0(-11)	3.6(-08)	3.6(-08)	3.0(-08)
CO	1.0(-04)	1.0(-04)	1.0(-04)	1.0(-04)	6.6(-05)	6.6(-05)	6.6(-05)
CS	1.6(-08)	5.2(-09)	1.4(-08)	4.7(-09)	1.8(-08)	6.0(-09)	1.8(-08)
NO	2.4(-08)	2.4(-08)	2.5(-08)	2.5(-08)	5.6(-10)	5.6(-10)	8.7(-10)
OH	5.5(-09)	5.5(-09)	5.7(-09)	5.7(-09)	1.3(-09)	1.3(-09)	1.6(-09)
SO	1.6(-09)	5.3(-10)	2.2(-09)	7.2(-10)	1.1(-13)	3.8(-14)	1.8(-13)
C_2H	1.9(-12)	1.9(-12)	2.5(-12)	2.5(-12)	4.9(-08)	4.8(-08)	2.9(-08)
C_2S	3.3(-12)	1.1(-12)	3.6(-12)	1.2(-12)	8.2(-10)	2.7(-10)	8.3(-10)
H_2O	1.8(-06)	1.8(-06)	1.4(-06)	1.4(-06)	9.2(-09)	9.2(-09)	9.3(-09)
H_3^+	2.3(-10)	2.3(-10)	2.4(-10)	2.4(-10)	3.7(-10)	3.7(-10)	3.7(-10)
HCN	2.0(-09)	2.0(-09)	9.4(-10)	9.4(-10)	4.9(-08)	4.9(-08)	4.3(-08)
HCO	3.9(-11)	3.9(-11)	2.1(-11)	2.1(-11)	5.2(-10)	5.2(-10)	4.0(-10)
HCO^+	7.1(-10)	7.1(-10)	1.2(-09)	1.2(-09)	6.1(-10)	6.1(-10)	9.2(-10)
HNC	2.9(-09)	2.9(-09)	1.6(-09)	1.6(-09)	3.4(-08)	3.4(-08)	2.7(-08)
HNO	3.4(-11)	3.4(-11)	3.5(-11)	3.5(-11)	1.5(-09)	1.5(-09)	1.7(-09)
N_2H^+	2.4(-11)	2.4(-11)	3.0(-11)	3.0(-11)	4.9(-11)	4.9(-11)	6.2(-11)
NH_2	2.8(-11)	2.8(-11)	2.9(-11)	2.9(-11)	6.0(-09)	6.0(-09)	6.3(-09)
OCS	1.7(-11)	5.7(-12)	2.0(-11)	6.7(-12)	2.7(-11)	8.9(-12)	2.2(-11)
SO_2	2.2(-09)	7.4(-10)	3.0(-09)	1.0(-09)	7.5(-15)	2.5(-15)	1.5(-14)
C_2H_2	1.5(-09)	1.5(-09)	1.8(-09)	1.8(-09)	2.5(-09)	2.5(-09)	3.1(-09)
C_3H	4.8(-10)	4.9(-10)	5.3(-10)	5.3(-10)	7.8(-07)	7.8(-07)	6.4(-07)
C_3N	6.9(-12)	6.9(-12)	7.3(-12)	7.4(-12)	4.1(-08)	4.1(-08)	3.4(-08)
H_2CO	2.8(-09)	2.8(-09)	2.0(-09)	2.0(-09)	2.1(-07)	2.1(-07)	1.7(-07)
H_2CS	1.0(-11)	3.5(-12)	1.5(-11)	5.0(-12)	9.7(-11)	3.2(-11)	9.1(-11)
H_3O^+	1.5(-10)	1.5(-10)	2.6(-10)	2.6(-10)	8.0(-13)	8.0(-13)	1.4(-12)
NH_3	3.7(-08)	3.7(-08)	2.8(-08)	2.8(-08)	5.8(-09)	5.8(-09)	6.7(-09)
C_3H_2	1.6(-11)	1.6(-11)	1.2(-11)	1.2(-11)	6.6(-08)	6.6(-08)	5.1(-08)
C_4H	1.1(-10)	1.1(-10)	5.7(-11)	5.7(-11)	4.6(-06)	4.6(-06)	4.5(-06)
CH_2CN	3.8(-11)	3.9(-11)	3.0(-11)	3.0(-11)	3.3(-08)	3.3(-08)	3.5(-08)
CH_4	2.5(-08)	2.5(-08)	3.4(-08)	3.4(-08)	1.2(-06)	1.2(-06)	1.4(-06)
HC_3N	2.0(-11)	2.0(-11)	1.4(-11)	1.5(-11)	2.6(-08)	2.6(-08)	2.3(-08)
CH_3OH	1.4(-10)	1.4(-10)	1.4(-10)	1.4(-10)	4.1(-11)	4.1(-11)	4.7(-11)

Table A.1: cont'd

Species	CNonaS	CnONAS	CnONAs	CnOnaS	CnOnaS	CnoNAS	CnoNAs
CH	3.3(-08)	6.2(-12)	6.2(-12)	5.8(-12)	5.8(-12)	4.0(-08)	4.0(-08)
CN	3.0(-08)	7.8(-12)	7.8(-12)	6.9(-12)	6.9(-12)	3.0(-08)	3.0(-08)
CO	6.6(-05)	1.0(-04)	1.0(-04)	1.0(-04)	1.0(-04)	6.6(-05)	6.6(-05)
CS	6.0(-09)	1.5(-08)	5.2(-09)	1.4(-08)	4.7(-09)	1.8(-08)	6.0(-09)
NO	8.7(-10)	2.6(-08)	2.6(-08)	2.6(-08)	2.6(-08)	2.4(-10)	2.4(-10)
OH	1.6(-09)	5.9(-09)	5.9(-09)	6.1(-09)	6.1(-09)	1.2(-09)	1.2(-09)
SO	6.1(-14)	1.7(-09)	5.6(-10)	2.3(-09)	7.6(-10)	1.2(-13)	3.9(-14)
C_2H	2.9(-08)	2.2(-12)	2.2(-12)	3.0(-12)	3.0(-12)	4.1(-08)	4.1(-08)
C_2S	2.8(-10)	4.7(-12)	1.6(-12)	4.5(-12)	1.5(-12)	8.3(-10)	2.8(-10)
H_2O	9.3(-09)	1.8(-06)	1.8(-06)	1.4(-06)	1.4(-06)	9.9(-09)	9.9(-09)
H_3^+	3.7(-10)	2.5(-10)	2.5(-10)	2.5(-10)	2.5(-10)	4.0(-10)	4.0(-10)
HCN	4.3(-08)	6.7(-10)	6.7(-10)	3.2(-10)	3.2(-10)	2.0(-08)	2.0(-08)
HCO	4.0(-10)	4.1(-11)	4.1(-11)	2.2(-11)	2.2(-11)	5.3(-10)	5.3(-10)
HCO^+	9.2(-10)	7.1(-10)	7.1(-10)	1.2(-09)	1.2(-09)	6.3(-10)	6.3(-10)
HNC	2.7(-08)	1.0(-09)	1.0(-09)	5.6(-10)	5.6(-10)	1.3(-08)	1.3(-08)
HNO	1.7(-09)	1.2(-11)	1.2(-11)	1.3(-11)	1.3(-11)	5.7(-10)	5.7(-10)
N_2H^+	6.2(-11)	8.6(-12)	8.6(-12)	1.1(-11)	1.1(-11)	1.8(-11)	1.8(-11)
NH_2	6.3(-09)	1.0(-11)	1.0(-11)	1.1(-11)	1.1(-11)	2.1(-09)	2.1(-09)
OCS	7.5(-12)	1.6(-11)	5.4(-12)	1.9(-11)	6.4(-12)	2.6(-11)	8.7(-12)
SO_2	5.0(-15)	2.3(-09)	7.8(-10)	3.1(-09)	1.0(-09)	6.5(-15)	2.2(-15)
C_2H_2	3.1(-09)	1.6(-09)	1.6(-09)	1.9(-09)	1.9(-09)	2.6(-09)	2.6(-09)
C_3H	6.4(-07)	1.1(-09)	1.1(-09)	1.0(-09)	1.0(-09)	8.1(-07)	8.1(-07)
C_3N	3.4(-08)	5.1(-12)	5.2(-12)	4.9(-12)	4.9(-12)	1.7(-08)	1.7(-08)
H_2CO	1.7(-07)	2.8(-09)	2.8(-09)	2.0(-09)	2.0(-09)	2.0(-07)	2.0(-07)
H_2CS	3.0(-11)	1.1(-11)	3.6(-12)	1.5(-11)	5.1(-12)	8.7(-11)	2.9(-11)
H_3O^+	1.4(-12)	1.5(-10)	1.5(-10)	2.6(-10)	2.6(-10)	9.0(-13)	9.0(-13)
NH_3	6.7(-09)	1.3(-08)	1.3(-08)	1.0(-08)	1.0(-08)	2.4(-09)	2.4(-09)
C_3H_2	5.1(-08)	3.9(-11)	4.0(-11)	2.5(-11)	2.5(-11)	7.2(-08)	7.2(-08)
C_4H	4.5(-06)	2.5(-10)	2.5(-10)	1.1(-10)	1.2(-10)	4.7(-06)	4.8(-06)
CH_2CN	3.5(-08)	1.3(-11)	1.3(-11)	1.0(-11)	1.0(-11)	1.2(-08)	1.2(-08)
CH_4	1.4(-06)	2.5(-08)	2.5(-08)	3.4(-08)	3.4(-08)	1.1(-06)	1.1(-06)
HC_3N	2.3(-08)	1.5(-11)	1.5(-11)	9.7(-12)	9.7(-12)	1.5(-08)	1.5(-08)
CH_3OH	4.7(-11)	1.4(-10)	1.4(-10)	1.4(-10)	1.4(-10)	4.1(-11)	4.1(-11)

Table A.1: cont'd

Species	CnonaS	Cnonas	cNONAS	cNONAs	cNOnaS	cNOnas	cNoNAS
CH	3.1(-08)	3.1(-08)	1.2(-12)	1.2(-12)	1.1(-12)	1.1(-12)	3.7(-11)
CN	2.6(-08)	2.6(-08)	1.1(-12)	1.1(-12)	8.0(-13)	8.0(-13)	4.2(-11)
CO	6.6(-05)	6.6(-05)	3.3(-05)	3.3(-05)	3.3(-05)	3.3(-05)	3.3(-05)
CS	1.8(-08)	6.0(-09)	4.5(-09)	1.5(-09)	3.5(-09)	1.2(-09)	1.4(-08)
NO	3.8(-10)	3.8(-10)	5.6(-08)	5.6(-08)	5.9(-08)	5.9(-08)	9.0(-08)
OH	1.5(-09)	1.5(-09)	1.2(-08)	1.2(-08)	1.2(-08)	1.2(-08)	1.7(-08)
SO	1.9(-13)	6.3(-14)	5.4(-09)	1.8(-09)	5.7(-09)	1.9(-09)	2.9(-09)
C_2H	2.3(-08)	2.3(-08)	8.3(-14)	8.3(-14)	9.2(-14)	9.2(-14)	1.4(-11)
C_2S	8.4(-10)	2.8(-10)	3.1(-14)	1.1(-14)	2.5(-14)	8.4(-15)	1.3(-11)
H_2O	9.9(-09)	9.9(-09)	2.3(-06)	2.3(-06)	1.9(-06)	1.9(-06)	6.4(-07)
H_3^+	4.1(-10)	4.1(-10)	4.7(-10)	4.7(-10)	4.9(-10)	4.9(-10)	6.5(-10)
HCN	1.7(-08)	1.7(-08)	6.6(-10)	6.6(-10)	3.1(-10)	3.1(-10)	2.2(-09)
HCO	4.0(-10)	4.0(-10)	3.4(-11)	3.4(-11)	1.9(-11)	1.9(-11)	1.1(-10)
HCO^+	9.8(-10)	9.8(-10)	4.8(-10)	4.8(-10)	8.5(-10)	8.6(-10)	6.4(-10)
HNC	1.0(-08)	1.0(-08)	6.8(-10)	6.8(-10)	3.7(-10)	3.7(-10)	4.2(-09)
HNO	6.3(-10)	6.3(-10)	7.7(-11)	7.7(-11)	8.1(-11)	8.1(-11)	4.1(-10)
N_2H^+	2.3(-11)	2.3(-11)	7.9(-11)	7.9(-11)	1.1(-10)	1.1(-10)	1.1(-10)
NH_2	2.2(-09)	2.2(-09)	6.3(-11)	6.3(-11)	6.6(-11)	6.6(-11)	3.5(-10)
OCS	2.1(-11)	7.1(-12)	1.4(-12)	4.7(-13)	1.4(-12)	4.5(-13)	8.5(-12)
SO_2	1.3(-14)	4.5(-15)	1.0(-08)	3.4(-09)	1.1(-08)	3.6(-09)	2.7(-09)
C_2H_2	3.3(-09)	3.3(-09)	6.1(-11)	6.1(-11)	6.5(-11)	6.5(-11)	2.5(-09)
C_3H	6.5(-07)	6.5(-07)	3.2(-12)	3.2(-12)	3.0(-12)	3.0(-12)	8.5(-10)
C_3N	1.3(-08)	1.3(-08)	3.2(-14)	3.2(-14)	2.9(-14)	2.9(-14)	2.2(-11)
H_2CO	1.6(-07)	1.6(-07)	6.8(-10)	6.8(-10)	5.2(-10)	5.2(-10)	5.0(-09)
H_2CS	8.0(-11)	2.7(-11)	3.9(-13)	1.3(-13)	4.3(-13)	1.5(-13)	1.1(-11)
H_3O^+	1.6(-12)	1.6(-12)	2.3(-10)	2.3(-10)	4.1(-10)	4.1(-10)	8.5(-11)
NH_3	2.7(-09)	2.7(-09)	5.6(-08)	5.6(-08)	4.3(-08)	4.3(-08)	6.8(-08)
C_3H_2	5.5(-08)	5.5(-08)	2.0(-13)	2.0(-13)	1.3(-13)	1.3(-13)	1.8(-10)
C_4H	4.6(-06)	4.6(-06)	1.6(-13)	1.6(-13)	7.2(-14)	7.2(-14)	7.6(-10)
CH_2CN	1.3(-08)	1.3(-08)	2.4(-12)	2.4(-12)	1.7(-12)	1.7(-12)	2.9(-11)
CH_4	1.3(-06)	1.3(-06)	3.3(-09)	3.3(-09)	4.2(-09)	4.2(-09)	2.0(-08)
HC_3N	1.4(-08)	1.4(-08)	1.3(-13)	1.3(-13)	7.3(-14)	7.3(-14)	6.2(-11)
CH_3OH	4.7(-11)	4.7(-11)	2.8(-11)	2.8(-11)	2.6(-11)	2.6(-11)	5.2(-11)

Table A.1: cont'd

Species	cNoNAs	cNonaS	cNonas	cnONAS	cnONAs	cnOnaS	cnOnas
CH	3.7(-11)	3.6(-11)	3.6(-11)	1.3(-12)	1.3(-12)	1.2(-12)	1.2(-12)
CN	4.2(-11)	3.6(-11)	3.6(-11)	6.0(-13)	6.0(-13)	5.1(-13)	5.1(-13)
CO	3.3(-05)	3.3(-05)	3.3(-05)	3.3(-05)	3.3(-05)	3.3(-05)	3.3(-05)
CS	4.5(-09)	1.3(-08)	4.3(-09)	4.3(-09)	1.5(-09)	3.4(-09)	1.2(-09)
NO	9.0(-08)	9.4(-08)	9.4(-08)	6.0(-08)	6.0(-08)	6.3(-08)	6.3(-08)
OH	1.7(-08)	1.8(-08)	1.8(-08)	1.3(-08)	1.3(-08)	1.4(-08)	1.4(-08)
SO	9.6(-10)	3.1(-09)	1.0(-09)	5.5(-09)	1.8(-09)	5.7(-09)	1.9(-09)
C_2H	1.4(-11)	2.0(-11)	2.0(-11)	9.5(-14)	9.5(-14)	1.1(-13)	1.1(-13)
C_2S	4.3(-12)	1.4(-11)	4.8(-12)	3.5(-14)	1.2(-14)	2.8(-14)	9.5(-15)
H_2O	6.4(-07)	5.3(-07)	5.3(-07)	2.3(-06)	2.3(-06)	1.9(-06)	1.9(-06)
H_3^+	6.5(-10)	6.7(-10)	6.7(-10)	5.3(-10)	5.3(-10)	5.6(-10)	5.6(-10)
HCN	2.2(-09)	1.3(-09)	1.3(-09)	2.2(-10)	2.2(-10)	1.1(-10)	1.1(-10)
HCO	1.1(-10)	6.3(-11)	6.3(-11)	3.8(-11)	3.8(-11)	2.1(-11)	2.1(-11)
HCO^+	6.4(-10)	1.2(-09)	1.2(-09)	5.0(-10)	5.1(-10)	8.9(-10)	8.9(-10)
HNC	4.2(-09)	2.7(-09)	2.7(-09)	2.3(-10)	2.3(-10)	1.3(-10)	1.3(-10)
HNO	4.1(-10)	4.4(-10)	4.4(-10)	3.0(-11)	3.0(-11)	3.2(-11)	3.2(-11)
N_2H^+	1.1(-10)	1.6(-10)	1.6(-10)	2.9(-11)	2.9(-11)	4.2(-11)	4.2(-11)
NH_2	3.5(-10)	3.7(-10)	3.7(-10)	2.5(-11)	2.5(-11)	2.6(-11)	2.6(-11)
OCS	2.8(-12)	8.3(-12)	2.8(-12)	1.4(-12)	4.6(-13)	1.3(-12)	4.4(-13)
SO_2	8.9(-10)	3.0(-09)	9.9(-10)	1.0(-08)	3.4(-09)	1.1(-08)	3.6(-09)
C_2H_2	2.6(-09)	3.5(-09)	3.5(-09)	6.5(-11)	6.5(-11)	7.1(-11)	7.1(-11)
C_3H	8.5(-10)	1.0(-09)	1.0(-09)	6.0(-12)	6.0(-12)	5.1(-12)	5.1(-12)
C_3N	2.2(-11)	2.4(-11)	2.5(-11)	2.1(-14)	2.1(-14)	1.7(-14)	1.7(-14)
H_2CO	5.0(-09)	4.4(-09)	4.4(-09)	7.0(-10)	7.0(-10)	5.5(-10)	5.5(-10)
H_2CS	3.8(-12)	1.6(-11)	5.5(-12)	3.9(-13)	1.3(-13)	4.3(-13)	1.5(-13)
H_3O^+	8.5(-11)	1.5(-10)	1.5(-10)	2.3(-10)	2.3(-10)	4.1(-10)	4.1(-10)
NH_3	6.8(-08)	5.5(-08)	5.5(-08)	2.0(-08)	2.0(-08)	1.5(-08)	1.5(-08)
C_3H_2	1.8(-10)	1.7(-10)	1.7(-10)	4.4(-13)	4.4(-13)	2.4(-13)	2.4(-13)
C_4H	7.7(-10)	5.5(-10)	5.6(-10)	3.3(-13)	3.3(-13)	1.3(-13)	1.3(-13)
CH_2CN	2.9(-11)	2.6(-11)	2.6(-11)	7.8(-13)	7.8(-13)	5.7(-13)	5.7(-13)
CH_4	2.0(-08)	2.8(-08)	2.8(-08)	3.3(-09)	3.3(-09)	4.2(-09)	4.2(-09)
HC_3N	6.2(-11)	5.5(-11)	5.6(-11)	8.4(-14)	8.4(-14)	4.3(-14)	4.3(-14)
CH_3OH	5.2(-11)	5.2(-11)	5.2(-11)	2.6(-11)	2.6(-11)	2.5(-11)	2.5(-11)

Table A.1: cont'd

Species	cnoNAS	cnoNAs	cnonaS	cnonas	cno9nas	Cno9nas	CNo9NAS
CH	4.3(-11)	4.3(-11)	4.1(-11)	4.1(-11)	9.8(-09)	2.7(-08)	3.4(-08)
CN	2.8(-11)	2.8(-11)	2.5(-11)	2.5(-11)	2.0(-08)	5.7(-08)	7.7(-08)
CO	3.3(-05)	3.3(-05)	3.3(-05)	3.3(-05)	2.1(-05)	2.2(-05)	2.2(-05)
CS	1.3(-08)	4.3(-09)	1.2(-08)	4.1(-09)	5.7(-09)	5.7(-09)	1.7(-08)
NO	9.6(-08)	9.6(-08)	9.9(-08)	9.9(-08)	7.3(-09)	1.9(-10)	3.1(-10)
OH	2.0(-08)	2.0(-08)	2.1(-08)	2.1(-08)	1.1(-08)	5.6(-10)	5.6(-10)
SO	3.1(-09)	1.0(-09)	3.3(-09)	1.1(-09)	2.6(-12)	1.4(-14)	3.2(-14)
C_2H	1.7(-11)	1.7(-11)	2.4(-11)	2.4(-11)	3.3(-09)	5.0(-08)	8.3(-08)
C_2S	2.1(-11)	7.2(-12)	2.1(-11)	7.2(-12)	3.9(-10)	4.7(-10)	1.3(-09)
H_2O	6.2(-07)	6.2(-07)	5.2(-07)	5.2(-07)	2.1(-08)	2.7(-09)	2.5(-09)
H_3^+	7.5(-10)	7.5(-10)	7.8(-10)	7.8(-10)	1.1(-09)	6.5(-10)	5.5(-10)
HCN	8.3(-10)	8.4(-10)	5.3(-10)	5.3(-10)	1.7(-08)	4.5(-08)	1.1(-07)
HCO	1.2(-10)	1.2(-10)	6.9(-11)	6.9(-11)	3.6(-10)	3.6(-10)	3.8(-10)
HCO^+	6.7(-10)	6.7(-10)	1.2(-09)	1.2(-09)	9.2(-10)	3.0(-10)	2.2(-10)
HNC	1.5(-09)	1.6(-09)	1.0(-09)	1.0(-09)	8.2(-09)	3.6(-08)	1.0(-07)
HNO	1.7(-10)	1.7(-10)	1.8(-10)	1.8(-10)	2.9(-09)	9.0(-10)	1.9(-09)
N_2H^+	4.1(-11)	4.1(-11)	6.1(-11)	6.1(-11)	9.5(-11)	4.2(-11)	9.0(-11)
NH_2	1.5(-10)	1.5(-10)	1.6(-10)	1.6(-10)	4.6(-09)	1.0(-08)	2.4(-08)
OCS	8.3(-12)	2.8(-12)	8.1(-12)	2.7(-12)	2.9(-12)	2.5(-12)	8.4(-12)
SO_2	3.1(-09)	1.0(-09)	3.4(-09)	1.1(-09)	7.1(-13)	4.8(-16)	1.2(-15)
C_2H_2	2.9(-09)	2.9(-09)	4.0(-09)	4.0(-09)	7.5(-09)	4.3(-09)	3.6(-09)
C_3H	1.4(-09)	1.4(-09)	1.6(-09)	1.6(-09)	2.9(-07)	1.0(-06)	1.1(-06)
C_3N	1.3(-11)	1.3(-11)	1.4(-11)	1.4(-11)	6.8(-09)	1.4(-08)	3.9(-08)
H_2CO	5.1(-09)	5.1(-09)	4.6(-09)	4.6(-09)	9.3(-08)	2.1(-07)	2.2(-07)
H_2CS	1.3(-11)	4.3(-12)	1.8(-11)	6.2(-12)	1.9(-11)	1.1(-10)	3.6(-10)
H_3O^+	8.6(-11)	8.6(-11)	1.6(-10)	1.6(-10)	6.7(-12)	2.3(-13)	1.4(-13)
NH_3	2.5(-08)	2.5(-08)	2.0(-08)	2.1(-08)	8.1(-09)	2.3(-09)	4.5(-09)
C_3H_2	4.0(-10)	4.0(-10)	3.4(-10)	3.4(-10)	4.7(-08)	1.3(-07)	1.4(-07)
C_4H	1.5(-09)	1.5(-09)	1.0(-09)	1.0(-09)	1.9(-06)	1.2(-05)	1.2(-05)
CH_2CN	1.0(-11)	1.1(-11)	1.0(-11)	1.0(-11)	3.2(-09)	2.4(-08)	6.0(-08)
CH_4	2.0(-08)	2.0(-08)	2.8(-08)	2.8(-08)	3.8(-07)	6.9(-07)	7.2(-07)
HC_3N	4.1(-11)	4.2(-11)	3.5(-11)	3.6(-11)	1.3(-08)	4.9(-08)	7.6(-08)
CH_3OH	5.0(-11)	5.0(-11)	5.1(-11)	5.1(-11)	3.6(-11)	7.8(-12)	7.5(-12)

Acknowledgments

Welcome to the section of truths, where I acknowledge the many people who are responsible for making this thesis possible, and for making the time whilst doing it fun! This is one of the hardest sections to write; both to express my gratitude fully and to admit that my time here at UCL is coming to an end. However, on the bright side, it is the part where I can waffle on to my heart's content!

Are you sitting comfortably? I hope so....

Firstly, I must express my profuse thanks to my supervisor David Williams. It has been a pleasure to work with you, and to know that no question (no matter how daft), at any time, would be answered! Thank you for the critical reading of this manuscript, and for getting me to stop running my models and to start writing!

I also owe a huge debt to Tom Hartquist, who has kept me on my toes (slave driver!) and taught me so much about molecular astrophysics. I must also say thanks again for the hospitality in Baltimore and Leeds, and the groovy 'night of shrimp and vodka'!

To my family: Mum, Dad, Peter and William; thank you for all your encouragement and support. Also, huge and profuse thanks for my trips home with the visits to my sanctuaries (Cadbury's World & Alton Towers – even if you did get the ride stopped Peter (oh the shame) and you can't handle the pace William!), the endless supplies of Bacon and Eggs, the rides on motorbikes, and the Baileys 'n' coffee. Ta to my lovely Nan too for the never ending supply of Jammy Dodgers!

Aideen, thank you for so many things; the introduction to Garth, trips to Ireland, Heather movies (and ours to be of course), the long letters (hoho), the future fun in the States and for being a wonderful friend. Rachel, thank you too for being a great friend, for listening to me panic and then giving me great advice, the shopping trips,

drinking binges and tarting it up! To Paul, you are a star; thank you for putting me up in D.C. and for helping me to program with the evil Fortran!. To Neil in TO - huge thanks for showing Canada to me, introducing me to 'Subs' and for being only on the other side of Lake Erie!

More thanks too to Paola Caselli for very useful discussions, answering all my questions and, of course, the fun chats! Also, thanks to Steve Taylor for the programs.

I must also offer 'thanks' to the gang here, for being so much fun to hang out with (lets not forget the great parties (Chris and Kate I owe you one!), trips to Bread & Butter, the groovy time in Edinburgh and the many visits to Gordons, the Houseman Room, the Union and other watering holes) and for helping me out along the way. So a big kiss to: Chris Jomaron (gadget boy and source of general debauchery: ta for help with computers, chocolates and my video); Serena Viti (for remaining sane around this lot and for helping me with my programs and this thesis!); Kaj Siebert (for rides to Mill Hill and lots of programming help); Matthew Pontefract (our 'water-baby'; thanks for the discussions and even more program help); Chris Evans (for his unnerving impression of the Chewitt Monster, chats, coffee, drinks and his never ending attempts to sort his life out!); Nic 'CTQ' Achilleos and Kevin 'CTQ2' (for knowing more celeb trash than me!); Tammay (for fun and gossip - we must do the girlie night out soon!); Phil O'Neill and Tom Stallard (for coffee times and expanding my music collections respectively).

Even more thanks are needed, so 'ta chucks' to: Nish (for lunches, drinks and advice); Rex (for movies, munchies and the endless stream of jokes!); John Deacon (for systems management); Vanessa (for Paris and vegemite); and last, but in no way least, to train-boy for making that trip so much fun!

Thanks again to David, Tom, Serena, Chris E., Chris J., Matthew, Phil and Tom S. for critical readings of the big T – you are all sweeties!

Bibliography

Allan M., 1985, J. Phys. B., 18, 4511

Arons J., Max C.E., 1975, ApJ, 196, L77

Bachiller R., Perez Gutierrez M., 1997, ApJ, 487, L93

Bates D.R., Spitzer L., 1951, ApJ, 113, 441

Bel N., Lafen J.-P.J., Viala Y.P., Loirelux E., 1989, A&A, 208, 331

Bell M.B., Matthews H.E., 1985, ApJ, 291, L63

Benson P.J., Caselli P., Myers P.C., 1998, ApJ, in press

Benson P.J., Myers P.C., 1989, ApJS, 71, 89

Bergin E.A., Langer W.D., 1997, ApJ, 486, 316

Bertoldi F., McKee C.F., 1992, ApJ, 395, 140

Bettens R.P.A., Brown R.D., 1992, MNRAS, 258, 347

Black J.H., Dalgarno A., 1973, Astrophys Letts, 15, 79

Black J.H., Dalgarno A., 1976, ApJ, 203, 132

Blake G.A., van Dishoeck E.F., Jansen D.J., Groesbeck T., Mundy L.G., 1994, ApJ, 428, 680

Cartwright D.C., Dunning T.H., 1974, J. Phys. B., 7, 1776

Caselli P., Hasegawa T.I., Herbst E., 1994, ApJ, 408, 548

Caselli P., Myers P.C., 1995, ApJ, 446, 665

Caselli P., Walmsley C.M., Terzieva R., Herbst E., 1998, ApJ, 499, 234

Chandler C.J., Sargent A.I., 1993, ApJ, 414, L29

Charnley S.B., 1997, ApJ, 481, 396

Charnley S.B., Dyson J.E., Hartquist T.W., Williams D.A., 1988, MNRAS, 235, 1257

Chièze J.P., Pineau des Forêts G., Herbst E., 1991, ApJ, 373, 110

Choi M., Evans II N.J., Gregersen E.M., Wang Y., 1995, ApJ, 448, 742

Ciolek G.E., Mouschovias T.Ch., 1995, ApJ, 454, 194

Crawford I.A., Williams D.A., 1997, MNRAS, 291, L53

Dalgarno A., Allison A.C., Browne J.C., 1969, J. Atmos. Sci, 26, 946

Dalgarno A., McCray R.A., 1972, ARA&A, 10, 375

Dorschner J., Henning T., 1995, in Cutri R.M., Latter W.B., eds, Asp Conf Ser Vol 58 - The first symposium on the infrared cirrus and diffuse interstellar clouds. Astron. Soc. Pac., San Fransisco, p. 227

Draine B.T., 1978, ApJ, 36, 595

Draine B.T., Sutin B., 1987, ApJ, 320, 803.

Duley W.W., Williams D.A., 1984, in Interstellar Chemistry. Academic Press, London.

Duley W.W., Williams D.A., 1992, MNRAS, 257, 13

Duley W.W., Williams D.A., 1993, MNRAS, 260, 37

Elmegreen B.G., 1979, ApJ, 232, 739

Elmegreen B.G., Lada C.J., 1977, ApJ, 214, 725

Encrenaz T., Crovisier J., D'Hendecourt L., Lamy P., Tully J.A., in Encrenaz T., Kessler M.F., 1992, eds, Infrared Astronomy with ISO. Nova Science Publishers, Commack, p. 141

Federman S.R., Sheffer Y., Lambert D., Gilliland R.L., 1993, ApJ, 413, L51

Fiedler R., Mouschovias T.Ch., 1993, ApJ, 415, 680

Flower D.R., Le Bourlot J., Pineau des Forêts G., Roueff E., 1994, A&A, 282, 225

Fuente A., Cernicharo J., Garcia-Burillo S., Tejero J., 1993, A&A, 275, 558

Gail H.-P., Sedylmayr E., 1975, A&A, 41, 359

Gammie T.F., Ostriker E.C., 1996, ApJ, 466, 814

Geballe T.R., Oka T., 1996, Nat, 384, 334

Gerin M., Phillips T.G., Benford D.J., Young K.H., Menten K.M., Frye B., 1997, A&A, 318, 579

Gerlich D., Horning S., 1992, Chem. Rev., 92, 1509

Goldsmith P.F., Langer W.D., Wilson R. 1986, ApJ, 303, L11

Gredel R., Lepp S., Dalgarno A., Herbst E., 1989, ApJ, 347, 289

Gregersen E.M., Evans II N.J., Zhou S., Choi M., 1997, ApJ, 484, 256

Grevesse N., Noels A., 1993, in Pratzos N., et al. , eds, Origins and Evolution of the Elements. CUP, p. 15

Gueth F., Guilloteau S., Dutrey A., Bachiller R., 1997, A&A, 323, 943

Hall P., Williams D.A., 1995, Ap&SS, 229, 49

Hanawa T., Yamamoto S., Hirahara Y., 1994, ApJ, 420, 318

Hartquist T.W., Dyson J.E., 1997. in Reipurth B., Bertout C., eds, IAU Symp. 182 - Herbig-Haro Flows and the Birth of Low-Mass Stars. Kluwer, Dordrecht, p. 537

Hartquist T.W., Oppenheimer M., Dalgarno A., 1980, ApJ, 236, 182

Hartquist T.W., Rawlings J.M.C., Williams D.A., Dalgarno A., 1993, QJRAS, 34, 213

Hartquist T.W., Williams D.A., 1989, MNRAS, 241, 417

Hartquist T.W., Williams D.A., 1995, in The Chemically Controlled Cosmos. CUP.

Hartquist T.W., Williams D.A., 1998, in preparation

Hartquist T.W., Williams D.A., Caselli P., 1996, Ap&SS, 238, 303

Hasegawa T.I., Herbst E., 1993, MNRAS, 263, 589

Hasegawa T.I., Herbst E., Leung C.M., 1992, ApJS, 82, 167

Hatchell J., Thompson M.A., Millar T.J., Macdonald G.H., 1998, A&A, in press

Herbst E., DeFrees D.J., McLean A.D., 1987, ApJ, 321, 898

Herbst E., Green S., Thaddeus P., Klemperer W., 1977, ApJ, 215, 503

Herbst E., Klemperer W., 1973, ApJ, 185, 505

Herzberg G., 1950, Molecular Spectra and Molecular Structure, I Spectra of Diatomic Molecules. van Nostrand, Princeton.

Hirahara Y., Suzuki H., Yamamoto S., Kawaguchi K., Kaifu N., Ohishi M., Takano S., Ishikawa S., Masuda A., 1992, ApJ, 394, 539

Hollenbach D.J., Salpeter E.E., 1971, ApJ, 163, 155

Howe D.A., Taylor S.D., Williams D.A., 1996, MNRAS, 279, 143

Hurt R.L., Barsony M., Wootten A., 1996, ApJ, 456, 686

Irvine W.M., Schloerb F.P., Hjalmarson Å., Herbst E., 1985, in Black D.C., Matthews M.S., eds, Protostars & Planets II. Univ. Arizona, Tucson, p. 579

Irvine W.M., Goldsmith P.F., Hjalmarson Å., 1987, in Hollenbach D.J., Thronsen

H.A. Jr., eds, Interstellar Processes. Reidel, Dordrecht, p. 561

Itikawa Y., 1994, Advan. Atom. Molec. Opt. Phys., 33, 253

James H.M., Coolidge A.S., 1938, ApJ, 87, 438

Jenkins E.B., 1987, in Hollenbach D.J., Thronsen H.A. Jr., eds, Interstellar Processes. Reidel, Dordrecht, p. 533

Kelly M.L., Macdonald G.H., Millar T.J., 1996, MNRAS, 279, 1210

Klemperer W., Scappini F., 1998, in preparation

Krolik J.H., Kallman T.R., 1983, ApJ, 267, 610

Kuiper T.B.H., Langer W.D., Velusamy T., 1996, ApJ, 468, 761

Kulsrud R., Pearce W.A., 1969, ApJ, 156, 445

Langer W.D., Velusamy T., Kuiper T.B.H., Levin S., Olsen E., Migenes V., 1995, ApJ, 453, 293

Le Bourlot J., Pineau des Forêts G., Roueff E., Schilke P., 1993a, ApJ, 416, L87

Le Bourlot J., Pineau des Forêts G., Roueff E., Flower D.R., 1993b, A&A, 267, 233

Leitch-Devlin M.A., Williams D.A., 1985, MNRAS, 213, 295

Lehtinen K., 1997, A&A, 317, L5

Lemme C.M., Walmsley C.M., Wilson T.L., Muders D., 1995, A&A, 302, 509

Leung C.M., Brown R.L., 1977, ApJ, 214, L73

McGonagle D., Irvine W.M., Ohishi M., 1994, ApJ, 422, 621

McCall B.J., Geballe T.R., Hinkle K.H., Oka T., 1998, Sci, 279, 1910

McKee C.F., 1989, ApJ, 345, 782

Mardones D., Myers P.C., Tafalla M., Wilner D.J., Bachiller R., Garay G., 1997, ApJ, 489, 719

Maréchal P., Viala Y.P., Benayoun J.J., 1997, A&A, 324, 221

Martin C.E., Heyvaerts J., Priest E.R., 1997, A&A, 326, 1176

Menten K.M., Serabyn E., Güsten R., Wilson T.L., 1987, A&A, 177, L57

Menten K.M., Walmsley C.M., Krügel E., Ungerechts H., 1984, A&A, 137, 108

Meyer D.M., 1997, in van Dishoeck E.F., ed, IAU Symp. 178 - Molecules in Astrophysics: Probes and Processes. Kluwer, Dordrecht, p. 407

Meyer D.M., Roth K.C., 1991, ApJ, 376, L49

Millar T.J., 1990, in Hartquist T.W., ed, Molecular Astrophysics – A Volume Honouring Alexander Dalgarno. CUP, p. 115

Millar T.J., Farquhar P.R.A., Willacy K., 1997, A&A, 121, 139

Millar T.J., Herbst E., 1990, A&A, 231, 466

Minh Y.C., Ziurys L.M., Irvine W.M., McGonagle D., 1990, ApJ, 360, 136

Mouschovias T.Ch., 1987, in Morfill G.E., Scholer M., eds, Physical Processes in Interstellar Clouds. Reidel, Dordrecht, p. 453 and p. 491

Mouschovias T.Ch., Psaltis D., 1995, ApJ, 444, L105

Myers P.C. 1986., in Peimbert M., Jugaku J., eds, IAU Symp. 115 - Star Forming Regions. D. Reidel Publishing Company, Dordecht, p. 307

Myers P.C., 1990, in Hartquist T.W., ed, Molecular Astrophysics – A Volume Honouring Alexander Dalgarno. CUP, p. 328

Myers P.C., Bachiller R., Caselli P., Fuller G.A., Mardones D., Tafalla M., Wilner D.J., 1995, ApJ, 449, L65

Myers P.C., Benson P.J., 1983, ApJ, 266, 309

Myers P.C., Khersonsky V.K., 1995, ApJ, 442, 186

Myers P.C., Mardones D., Tafalla M., Williams J.P., Wilner D.J., 1996, ApJ, 465, L133

Nejad L.A.M., Hartquist T.W., Williams D.A., 1994, Ap&SS, 220, 261

Norman C.A., Silk J., 1980, ApJ, 238, 158

Ohashi N., Hayashi M., Ho P.T.P., Momose M., 1997, ApJ, 475, 211

Ohishi M., Irvine W.M., Kaifu N., 1992, in Singh P.D., ed, IAU Symp. 178 - Astrochemistry of Cosmic Phenomena. Kluwer, Dordrecht, p. 171

Ohishi M., Kaifu N., 1998, in Faraday Disc. 109 - Chemistry & Physics of Molecules & Grains in Space. p. 205

Oppenheimer M., Dalgarno A., 1974, ApJ, 192, 29

Osterbrock D.E., 1961, ApJ, 134, 270

Pagani L., Langer W.D., Castets A., 1993, A&A, 274, L13

Pickles J.B., Williams D.A., 1977, Ap&SS, 52, 433

Pickles J.B., Williams D.A., 1981, MNRAS, 197, 429

Pineau des Forêts G., Roueff E., Flower D.R., 1992, MNRAS, 258, 45P

Pineau des Forêts G., Roueff E., Schilke P., Flower D.R., 1993, MNRAS, 262, 915

Prasad S.S., Tarafdar S.P., 1983, ApJ, 267, 603

Rawlings J.M.C., 1996, QJRAS, 37, 503

Rawlings J.M.C., Hartquist T.W., Menten K.M., Williams D.A., 1992, MNRAS, 255, 471

Scalo J., 1987, in Hollenbach D.J., Thronsen H.A. Jr., eds, Interstellar Processes. Reidel, Dordrecht, p. 349

Schilke P., Keene J., Le Bourlot J., Pineau des Forêts G., Roueff E., 1995, A&A, 294, L17

Schutte W.A., Greenberg J.M., 1997, A&A, 317, L43

Scott G.B.I., Fairley D.A., Freeman C.G., McEwan M.J., 1997, Chem. Phys. Lett., 269, 88

Scott G.B.I., Freeman C.G., McEwan M.J., 1997, MNRAS, 290, 636

Shalabiea O.M., Greenberg J.M., 1995, A&A, 296, 779

Shu F.H., 1977, ApJ, 214, 488

Shu F.H., Adams F.C., Lizano S., 1987, ARA&A, 25, 84

Sims I., Smith I.W.M., 1995, Ann. Rev. Phys. Chem., 46, 109

Smith I.W.M., 1997, in van Dishoeck E.F., ed, IAU Symp. 178 - Molecules in Astrophysics: Probes and Processes. Kluwer, Dordrecht, p. 253

Smith I.W.M., 1989, ApJ, 347, 282

Snell R.L., Loren R.B., 1976, ApJ, 211, 122

Snow T.P., Witt A.N., 1995, Sci, 270, 1455

Tafalla M., Mardones D., Myers P.C., Caselli P., Bachiller R., Benson P.J., 1998, ApJ, 504, 900

Taylor S.D., Morata O., Williams D.A., 1996, A&A, 313, 269

Terzieva R., Herbst E., 1998, ApJ, 501, 207

Tielens A.G.G.M., Hagen W., 1982, A&A, 114, 245

Tielens A.G.G.M., Whittet D.C.B., 1997, in van Dishoeck E.F., ed, IAU Symp. 178 - Molecules in Astrophysics: Probes and Processes. Kluwer, Dordrecht, in press

van Dishoeck E.F., 1998, in Hartquist T.W., Williams D.A., eds, The Molecular Astrophysics of Stars and Galaxies. OUP, p.